Modelling of All-Optical Devices

Jason J. Beech-Brandt

Doctor of Philosophy
University of Edinburgh
2002

Abstract

Solitons have been proposed as information carriers in next generation fibre optic networks. As the stable waveform in nonlinear optical fibres, solitons are resistant to a wide variety of perturbations from fibre effects, optical devices and other solitons. These fibre effects include fibre loss which is due to scattering and absorption phenomena. This fibre loss must be compensated for by some form of amplification and filtering, preferably all-optical in nature. It is of interest to determine the evolutionary behaviour of solitons in fibre optic networks containing the above mentioned optical devices and fibre properties.

The constituent equation modelling pulse evolution in a nonlinear optical fibre is the nonlinear Schrödinger (NLS) equation. The NLS equation possesses an exact inverse scattering solution. However the evolution to the steady state from an initial pulse is governed by an integral equation and so is difficult to determine. It is this evolutionary behaviour which is of interest. In addition, modelling the above mentioned optical devices and fibre effects requires adding perturbing terms to the NLS equation. These perturbed NLS equations do not possess inverse scattering solutions and so analytical solutions do not exist. Both of these factors lead to the use of approximate and computational techniques to analyse evolutionary pulse behaviour of perturbed NLS equations.

Using conserved quantities of the NLS equation, ordinary differential equations describing pulse parameters can be derived. Key to the use of this method is the choice of trial function substituted into the conservation and moment equations. The trial function used in the present work is based upon a soliton-like pulse with independently varying amplitude and width and a term describing low frequency radiation in the vicinity of the pulse. The effect of dispersive radiation shed by the pulse as it evolves is also coupled to these evolution equations. These approximate evolution equations are solved numerically and compared to numerical solutions of the constituent NLS equation describing the system. Where available, comparisons are also made with previous analytical and computational work. The optical devices and fibre effects modelled in this thesis are fibre loss and amplification, sliding-frequency filters and fibre compressors. Good agreement is obtained using the above analysis technique.

Acknowledgements

I would like to take this opportunity to thank the many people who have helped me get to this point in my education. Their contributions are many and varied. I would first like to thank my supervisor, Noel Smyth, for introducing me to the field of soliton-based fibre optics, and for the help and support over the past three years. To my second supervisor, David Parker, for several valuable suggestions, particularly concerning the sliding-frequency filter work. Thanks to Ken McKinnon for walking me through the optimisation techniques along with providing some of the optimisation code. Also, thank you to Mario Antonioletti for proofreading a large part of the thesis.

On a more personal note, thanks to my parents for their constant support and encouragement. And of course, to my wife Josephine, to whom this thesis is dedicated. It is the least you deserve for putting up with countless late nights, and for steadying frayed nerves.

Table of Contents

List of Figures

List of Tables

Chapter 1

Introduction

The propagation of light in a uniform, monomode, polarisation-preserving, nonlinear optical fibre in the anomalous group-velocity dispersion regime is governed by the nonlinear Schrödinger (NLS) equation [19]. A monomode fibre supports two degenerate fibre modes that are polarised in orthogonal directions. In an ideal, perfectly cylindrical optical fibre, these two modes do not couple. However, in a real fibre, where the geometry is not perfectly cylindrical, the two polarisation states mix, leading to two coupled NLS equations describing pulse evolution. This property is defined as birefringence. Assuming perfect cylindrical symmetry allows us to neglect this birefringence and write the NLS equation governing light in an optical fibre, in a nondimensional form, as the single partial differential equation

$$\mathrm{i}\frac{\partial u}{\partial z} + \frac{1}{2}\frac{\partial^2 u}{\partial t^2} + |u|^2 u = 0 \tag{1.1}$$

[2, 19]. Here u is the complex amplitude of the light, z is the normalised spatial variable along the length of the fibre and t is the normalised time in a frame of reference moving with linear group velocity. The time t has also been normalised by the characteristic time t_0, which is related to the pulse width. The distance z has been normalised by the dispersion distance z_0, which is a length scale over which pulse parameters evolve. The dispersion distance z_0 and the characteristic time t_0 are related by

$$z_0 = -\frac{t_0^2}{k''}, \tag{1.2}$$

where k'' is the group velocity dispersion at the carrier frequency.

The second term in the NLS equation (1.1) represents the dispersion of the group velocity, while the the third term originates from the nonlinear dependence of the refractive index of glass on the strength of the electric field. The refractive index of the glass depends on the amplitude squared of the electric field of the

light, the so-called Kerr nonlinearity. The group velocity dispersion acts to spread a pulse, while the Kerr nonlinearity acts to trap the wave energy in a localised area. Conservation of energy requires that the pulse width contract as the electric field grows in intensity. Under certain circumstances the pulse broadening, due to dispersion, and the pulse contraction, due to the nonlinear effect, balance exactly, forming a stable pulse. This pulse is called a soliton and the NLS equation (1.1) has the exact soliton solution

$$u = \eta \operatorname{sech} \eta(t - \tau_0 - Vt) \exp\left(\frac{1}{2}\mathrm{i}(\eta^2 - V^2)z + \mathrm{i}Vt + \mathrm{i}\theta\right). \tag{1.3}$$

Here η, the soliton amplitude, V, the soliton velocity (which is a deviation from the group velocity), τ_0, the initial time and the phase, θ, are all constant. Setting $\tau_0 = V = 0$ centres the reference frame moving with the soliton.

1.1 Soliton as Information Carrier

Hasegawa and Tappert [18], working with computer simulations of soliton stability, were the first to conjecture that an optical pulse in a nonlinear optical fibre can form a soliton. The previous year Zakharov and Shabat [57] had published a paper on the integrability of the NLS equation (1.1) and showed that the NLS equation possesses an exact inverse scattering solution. This verified the conjecture of Hasegawa and Tappert concerning the propagation of stable, nonlinear waves in optical fibres. However, at the time, experimental validation of soliton transmission in optical fibres was impossible for two reasons. Firstly, fibre dissipation was far too high for the transmission of solitons in an optical fibre, and secondly, and more fundamentally, no method existed for the generation of solitons in optical fibres. It took several years before an optical fibre with low enough fibre loss was developed. Simultaneously, the development of a suitable laser source by Mollenauer and Bloom [40] enabled both of these deficiencies to be remedied. In 1980, Mollenauer *et al.* [43] experimentally verified optical soliton transmission for the first time. With the experimental validation of soliton transmission in optical fibres, it became feasible for their use as information carriers in fibre optic networks. Fibre optic systems based on linear wavetrains exhibit significant distortion owing to dispersion. This pulse broadening is combated by the periodic use of electronic repeaters which reshape the incoming pulse. However repeaters are the major cost in fibre optic systems and are the limiting factor in the transmission rate due to the response time of the electronics. Solitons, however, due to the dispersion being compensated by the nonlinear effects, do not require electronic repeaters and so an all-optical communication system is a

possibility.

However, work still remains to be done before a soliton based fibre optic system can come into widespread use. While solitons are not degraded by the dispersion of the glass, they are still affected by fibre loss. As this is an inherent property of the glass fibre, it must be compensated for. Hasegawa [17] proposed using the Raman gain of the fibre itself for amplification purposes. In Raman amplification, a high frequency amplifying pump wave is transmitted down the fibre simultaneously with the lower frequency carrier wave. Higher frequency photons from the amplifying pump wave are annihilated to create phonons and photons at the lower frequency of the carrier wave. Properly tuned, Raman gain can perfectly compensate for the fibre loss, creating a lossless transmission window for soliton propagation. However Raman gain has drawbacks in that the amplifying Raman pump wave requires large amounts of power. Raman amplification can also lead to difficulties when used with a multi-channel wavelength division multiplexing (WDM) system.

Another problem concerning amplification was discovered by Gordon and Haus [14]. They noticed that amplification of a soliton also amplified the noise in the vicinity of the soliton. This noise amplification can lead to random fluctuations in the soliton position and hence in the arrival time of the solitons, thus degrading system performance. Two discoveries helped to overcome the limitations due to Raman amplification and the random walk of Gordon and Haus. The development of erbium doped fibre amplifiers (EDFA's) [35] overcame the difficulties introduced by Raman amplification. EDFA's, consisting merely of a section of fibre optic cable doped with rare-earth elements, required less power than Raman amplifiers and were suitable for use with multi-channel WDM systems. With the introduction of the concept of sliding-frequency filters (SFF's) [41], which help mitigate the effects of the Gordon-Haus jitter, much of the framework was in place for soliton based optical networks.

In addition to the above devices and fibre effects which are necessary for stable pulse transmission, other fibre optic devices have been proposed for the enhancement of fibre optic system performance. One such device, discussed in the present work, is a fibre compressor. A fibre compressor, in this work, is defined as a section of dispersion decreasing fibre (DDF). DDF is a section of fibre in which the dispersion decreases down the length of the fibre. This decrease may take place in a continuous or discrete fashion. Sections of DDF can be used for two purposes. Firstly, when a sinusoidal input wave is passed into a section of DDF, it evolves into a train of soliton-like pulses. In this manner DDF may be used as a means of soliton generation [31, 54]. Secondly, a pulse train travelling

in a section of DDF will decrease in width due to the decreasing dispersion of the fibre. As a result significant pulse compression, and hence data transfer rate, can be achieved [27, 30].

1.2 Analysing Pulse Behaviour

Work still remains in obtaining an accurate model of pulse evolution in an optical network incorporating various devices and fibre effects, such as those discussed previously. As a pulse evolves in a nonlinear optical fibre, with or without the effects of fibre loss or optical devices, a layer of low frequency radiation accumulates underneath the pulse. As the pulse evolves, attempting to reach the soliton steady state, it sheds dispersive radiation which is fed through the shelf of radiation under the pulse before dispersing from the pulse. This interplay between the pulse and shelf of radiation leads to oscillations in the pulse amplitude and width and the height of the shelf of radiation. These amplitude oscillations are eventually damped by the shedding of dispersive radiation through the shelf. A variety of mathematical and computational techniques have been developed and used to study this evolution. While the NLS equation (1.1) possesses an exact inverse scattering solution, the dynamic, transient evolution of an initial condition to the steady state is complicated and not easily analysed using inverse scattering since this transient behaviour is governed by an integral equation which is difficult to solve. Also, the addition of fibre optic devices, as discussed above, and higher order effects lead to perturbing terms on the right hand side of the NLS equation (1.1). In this case, inverse scattering solutions do not exist and approximate and numerical techniques are generally used to study the effect of these factors.

Perturbed inverse scattering theory [23] has often been used to study the effects of small perturbations on solitons. It has been applied to the study of soliton evolution in lossy fibres with periodic forcing [23] and sliding-frequency filters [6]. However, perturbed inverse scattering theory is based on a slowly varying soliton solution and as such is unable to deal with pulses which do not have the inverse amplitude/width relationship of a soliton (see the soliton solution (1.3)). Furthermore, the inclusion of the effect of the radiation shed by an evolving pulse is difficult via perturbed inverse scattering theory as it is a higher order effect. Burtsev and Kaup [6] found equations describing the shed radiation by extending their perturbation solution to higher order. However, they did not link these equations to those describing pulse parameter evolution, and so did not fully incorporate the effect of this shed radiation.

Approximate evolution equations describing pulse evolution may also be ob-

tained by substituting a trial function into the NLS Lagrangian and taking variations with respect to the trial function parameters. Obviously the choice of trial function is very important as it constrains the future evolution of the pulse. Anderson [3] attempted to include the effects of amplitude-width oscillations by choosing a trial function with independently varying amplitude and width and with a quadratic frequency chirp. This trial solution was an improvement upon previous work as it allowed amplitude oscillations as seen in full numerical solutions of the NLS equation (1.1). However, as the effects of shed radiation were not included, the amplitude oscillations were non-decaying and persistent, so the pulse could not evolve to a steady soliton.

Based upon the work of Anderson [3], Kath and Smyth [22] modified the trial function again, replacing the quadratic frequency chirp with a term representing the low frequency radiation in the vicinity of the pulse. Also, by analysing the linearised NLS equation, expressions were found for the shed radiation and included in the evolution equations obtained from a Lagrangian analysis similar to that of Anderson [3]. When solved, the approximate equations of Kath and Smyth [22] accurately portrayed the dynamic, transient evolution of an initial pulse to a steady soliton. The method of Kath and Smyth, employing a trial function which incorporates independently varying amplitude and width, and the effects of radiation in the vicinity and away from the pulse, has been successfully used in the study of pulse propagation and switching in nonlinear twin-core fibres [53], pulse propagation in non-uniform fibres [52] and pulse propagation in birefringent fibres [51]. As a result of this work, it was found that for an accurate portrayal of pulse evolution in nonlinear optical fibres two things are necessary. Firstly, an independently varying amplitude and width must be assumed. Secondly, some account of dispersive radiation, both in the vicinity of the pulse and away from the pulse, must be included.

1.3 Organisation of Thesis

Taken together, an averaged Lagrangian method based on a trial function with independently varying amplitude and width, to which is added the effect of the dispersive radiation shed by the pulse, provides an accurate and flexible means of analysis for pulse evolution in nonlinear optical fibres. This is the method used in this thesis to analyse pulse evolution in nonlinear optical fibres when various loss processes, amplification, non-uniform fibres, and optical devices are added. Specifically the work of Kath and Smyth [22] will be extended to the study of fibre loss and optical devices such as sliding-frequency filters, amplifiers and fibre com-

pressors. As the work of Kath and Smyth was based upon a Lagrangian analysis [22], which is unsuitable for studying non-conservative systems, an alternative method based upon conservation and moment equations for the NLS equation is used. This conservation and moment equation technique is intimately connected to the Lagrangian method of analysis due to Noether's Theorem for conservative systems. Chapter 2 discusses this conservation and moment equation technique and its relation to the previous Lagrangian method of analysis. Chapter 3 discusses the numerical techniques used in the solution of the approximate equations derived via the conservation and moment equation technique along with the numerical techniques used in the numerical solution of the NLS equation (1.1) and its variations. In Chapter 4 these analysis methods and computational techniques are applied to the study of fibre loss and its compensation by amplification. Much of this work has been done in previous studies and is well documented and so is mainly included to explore the strengths and weaknesses of the solution methods outlined in Chapters 2 and 3. Chapter 5 is concerned with the study of SFF's and their effect on pulse evolution. As discussed earlier, SFF's are used to filter radiation, which left unchecked leads to random fluctuations in the soliton arrival times. As stable pulses do not exist for all values of filter and amplifier strengths, conditions for the existence of stable pulses are also examined. This work is compared to that of Kaup [6], based on perturbed inverse scattering, and the work of Wabnitz, Malomed and Mamyshev [26, 29, 32], based upon a multiple scales analysis. The evolution equations derived using the method outlined above give better agreement with full numerical solutions than those of Kaup [6] and provide a more straight-forward means of analysis. It is shown that this superior agreement is due to the flexibility of the trial function used, along with the inclusion of the effects of dispersive radiation in the pulse parameter evolution equations. Chapter 6 discusses pulse generation and compression using DDF's. This work is based upon that of McKinnon *et al.* [34]. In that work an optimisation procedure was utilised to find the dispersion profile giving maximum pulse compression. The present work extends the work of McKinnon *et al.* [34] to include the effects of fibre loss and the results of the soliton stability study of Chapter 5. The results obtained are in good agreement with full numerical solutions of the governing NLS equation. Chapter 7 concludes by summing up relevant information and suggesting improvements and further work.

Chapter 2

Analysis Method

The NLS equation (1.1) possesses an exact inverse scattering solution [47], which shows that an arbitrary initial condition will evolve into a finite number of solitons plus dispersive radiation. The final soliton state which develops from an initial condition is determined by the solution of an eigenvalue problem, and so its determination is fairly straightforward. However, the evolution to this soliton state is determined by the interaction of the solitons with shed dispersive radiation, which in turn is governed by a linear integral equation. Hence the detailed evolution to the soliton state is difficult to determine in practice. It is this space evolution of the pulse which is of importance in optical applications. The difficulty of determining the interaction of the shed radiation with the evolving solitons via inverse scattering suggests that approximate methods may be useful as an alternative means of analysing the evolutionary behaviour of optical pulses. Another reason for using approximate methods to study pulse behaviour is that perturbed NLS equations do not possess an inverse scattering solutions and so exact solutions do not exist. So approximate methods must be used to get any useful information about pulse evolution for such perturbed equations.

The analysis method used in the work of this thesis is based upon a conservation equation technique linked to linearised equations for the dispersive radiation shed by the evolving pulses. This is closely related to the Lagrangian method of analysis as conserved quantities for the NLS equation are directly associated with symmetries of the NLS Lagrangian via Noether's theorem [13]. The basis of the method is that a suitable trial function can be substituted into these conservation equations to obtain evolution equations for the pulse parameters. To include the effect of the dispersive radiation shed by the pulse the linearised NLS equation is examined, since the radiation is of small amplitude relative to the pulse. The radiation loss determined in this manner is then added to the evolution equations obtained from the conservation equations. The inclusion of the dispersive radiation has the effect of damping the amplitude oscillations of the evolving pulse,

driving it to a steady soliton.

The first section of this chapter introduces the conservation equation technique used in the analysis of a pulse governed by an NLS-type equation. This is followed by a section discussing the analysis of the dispersive radiation and how the results of this analysis are included in the previously obtained evolution equations. As an illustrative example, we analyse the evolution of a pulse for the unperturbed NLS equation (1.1) using the outlined technique. This is the same problem studied by Kath and Smyth [22]. However, their analysis was based upon taking variations of an averaged NLS Lagrangian. It will be shown that both the conservation equation and averaged Lagrangian methods lead to the same equations for the pulse parameters, as required.

2.1 Pulse Evolution Without Shed Radiation

Several approximate methods for describing soliton evolution have been developed. One method closely related to the present work is the Lagrangian method. The Lagrangian density for the NLS equation (1.1) is

$$L = \mathrm{i}(u^* u_z - u u_z^*) - |u_t|^2 + |u|^4, \tag{2.1}$$

where $*$ denotes the complex conjugate, and where u and u^* are treated as separate variables when variations are taken [3]. To apply the Lagrangian method, one must now choose a trial function to substitute into the NLS Lagrangian. Anderson [3] chose a soliton-like pulse with a quadratic phase variation, called chirp, and independently varying amplitude and width

$$u = \eta \operatorname{sech} \frac{t}{w} \exp\left(\mathrm{i}\theta + \frac{\mathrm{i}bt^2}{2w}\right). \tag{2.2}$$

While this trial solution yielded improved results upon previous work, which assumed amplitude and width were inversely proportional, as for an NLS soliton, it was unable to account for the radiation shed by the evolving pulse. Without this shed radiation, the pulse parameters do not evolve to a steady state but undergo oscillations. It is known from both inverse scattering theory and numerical solutions that an initial pulse will evolve to steady solitons.

Later work by Kath and Smyth [22] improved upon the trial function used by Anderson [3] and also showed that inclusion of the effect of the radiation shed as the pulse evolves is necessary in order for the initial pulse to evolve to a steady soliton and to obtain good agreement with numerical solutions. The effect of radiation shed as the pulse evolves was determined by solving the linearised NLS equation. The details of this radiation analysis will be discussed in Section 2.2.

However to return to the systems studied in the present thesis, a Lagrangian only exists for conservative systems, such as the NLS equation (1.1). The modelling of non-conservative systems, such as when fibre loss or filters are added, requires another method. The method used in this work is one utilising conservation equations [23], and is illustrated in this chapter by applying it to the NLS equation (1.1). The NLS equation has three conserved quantities, commonly referred to as mass, momentum, and energy [23]. In this regard the three quantities

$$\rho = |u|^2, \tag{2.3}$$

$$J = \frac{\mathrm{i}}{2}(uu_t^* - u^*u_t), \tag{2.4}$$

$$E = |u_t|^2 - |u|^4, \tag{2.5}$$

are defined, which are referred to as mass density, momentum density and energy density, respectively [19]. With these definitions, the following conservation equations can be derived from the NLS equation (1.1)

$$\frac{\partial \rho}{\partial z} + \frac{\partial J}{\partial t} = 0, \tag{2.6}$$

$$\frac{\partial J}{\partial z} + \frac{\partial}{\partial t}\left[E + \frac{1}{2}\rho^2 - \frac{1}{4}\rho_{tt}\right] = 0, \tag{2.7}$$

$$\frac{\partial E}{\partial z} + \frac{\partial}{\partial t}\left[\frac{\mathrm{i}}{2}\left(u_t u_{tt}^* - u_t^* u_{tt}\right) - 2\rho J\right] = 0. \tag{2.8}$$

Integrating these conservation laws with respect to t we obtain

$$\frac{\mathrm{d}}{\mathrm{d}z}\int_{-\infty}^{\infty} \rho \,\mathrm{d}t = 0, \tag{2.9}$$

$$\frac{\mathrm{d}}{\mathrm{d}z}\int_{-\infty}^{\infty} J \,\mathrm{d}t = 0, \tag{2.10}$$

$$\frac{\mathrm{d}}{\mathrm{d}z}\int_{-\infty}^{\infty} E \,\mathrm{d}t = 0. \tag{2.11}$$

The NLS equation also possesses moment equations. The moment equation of interest in the present work is the moment of momentum equation, which can also be derived directly from the NLS equation (1.1)

$$\frac{\partial}{\partial z}(tJ) + \frac{\partial}{\partial t}\left[\frac{1}{2}tE - \frac{1}{4}t\left(u^*u_{tt} + uu_{tt}^*\right) + \frac{1}{4}\left(u^*u_t + uu_t^*\right)\right] = E + \frac{1}{2}\rho^2. \tag{2.12}$$

Integrating this moment equation with respect to t then gives

$$\frac{\mathrm{d}}{\mathrm{d}z}\int_{-\infty}^{\infty} tJ \,\mathrm{d}t = \int_{-\infty}^{\infty}\left[E + \frac{1}{2}\rho^2\right] \mathrm{d}t. \tag{2.13}$$

An approximate solution consisting of a soliton with varying parameters is then substituted into these conservation and moment equations so that ODE's for the

soliton parameters are determined. These ODE's for the pulse parameters are the same as those derived from the averaged Lagrangian for the NLS equation (1.1) by Kath and Smyth [22], as required.

It should be mentioned that the phase of the pulse is not determined by the conservation or moment equations as they are all independent of the phase. An equation for the phase can be derived from an extension of Noether's theorem [13, 56] based on scale invariance of the NLS equation [22]. However the equations for the other parameters are independent of the phase and so the phase equation is not dealt with in this work.

The trial solution used in the above conservation and moment equations is [22]

$$u = \left(\eta \operatorname{sech} \frac{t}{w} + \mathrm{i}g\right) \exp(\mathrm{i}\theta), \tag{2.14}$$

where the amplitude η, width w, phase θ, and g are functions of z. Variations based on this particular trial function will be used for the particular optical device being modelled and will be discussed in the relevant sections. The first term in the trial function (2.14) represents a soliton-like pulse with independently varying amplitude and width. The second term in g, which is independent of t, represents the low frequency radiation in the vicinity of the pulse. The reason for this long wavelength radiation can be seen from the following argument. The group velocity for the linearised NLS equation is $c_g = -2\kappa$, so that low frequency radiation has low group velocity and so stays in the vicinity of the pulse, creating a shelf on which the soliton sits. This shelf of low frequency radiation, referred to as a pedestal in the experimental literature, can be seen in Figure 2.1. The radiation cannot continue to be flat away from the pulse however, as otherwise it would contain infinite mass. It is therefore assumed that the radiation is flat in the region $-\ell/2 < t < \ell/2$ about the pulse. Furthermore, numerical solutions show that the radiation is of small amplitude, so that $|g| \ll \eta$.

To illustrate the method in action, we will now analyse the solution of the NLS equation (1.1). This is the same equation studied in Kath and Smyth [22], the difference here being that the conservation and moment equation technique will be used rather than the averaged Lagrangian.

Substituting the trial function (2.14) into the conservation and moment equa-

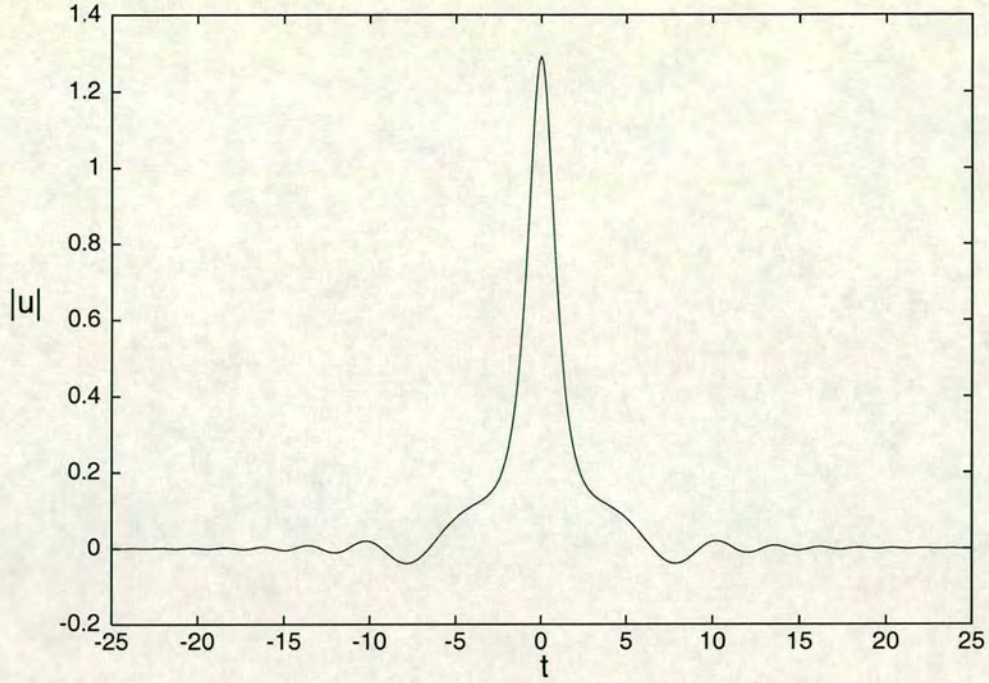

Figure 2.1: Full numerical solution of the NLS equation (1.1) with boundary condition $u(0,t) = 1.25\,\mathrm{sech}\,t$ showing the formation of the shelf.

tions (2.9)–(2.11) and (2.13), we obtain the following three equations

$$\frac{\mathrm{d}}{\mathrm{d}z}\left(2\eta^2 w + \ell g^2\right) = 0, \tag{2.15}$$

$$\frac{\mathrm{d}}{\mathrm{d}z}\left(\frac{\eta^2}{w} - 2\eta^4 w\right) = 0, \tag{2.16}$$

$$\frac{\mathrm{d}}{\mathrm{d}z}\left(\pi g \eta w\right) = \frac{2\eta^2}{3w} - \frac{2}{3}\eta^4 w, \tag{2.17}$$

the first two being mass and energy conservation for the pulse. By Galilean invariance, the pulse can be centred in a reference frame moving with the group velocity. In this frame of reference the momentum of the pulse is zero by symmetry, so that the momentum conservation equation (2.10) is identically satisfied by the trial solution (2.14). By manipulating the equations (2.15)–(2.17) and removing higher order terms in g that do not contribute to mass conservation these equations can be simplified to

$$\frac{\mathrm{d}g}{\mathrm{d}z} = -\frac{2\eta}{3\pi}\left(\eta^2 - w^{-2}\right), \tag{2.18}$$

$$\frac{\mathrm{d}}{\mathrm{d}z}(\eta w) = \frac{\ell g}{\pi}\left(\eta^2 - \frac{1}{2}w^{-2}\right), \tag{2.19}$$

$$\frac{\mathrm{d}}{\mathrm{d}z}\left(\frac{\eta^2}{w} - 2\eta^4 w\right) = 0. \tag{2.20}$$

These approximate equations are the same as those formed by Kath and Smyth [22].

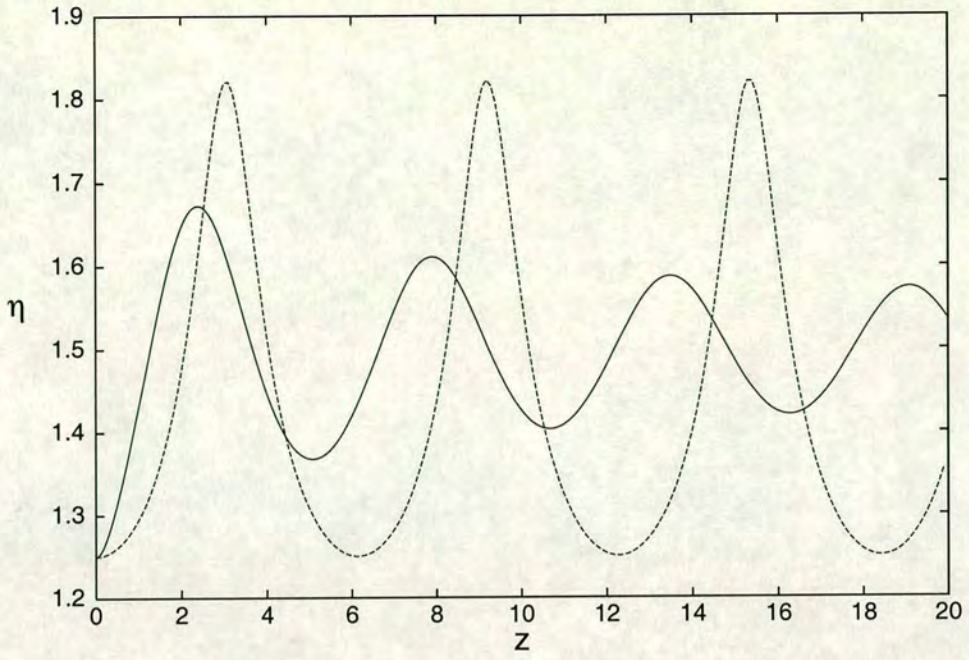

Figure 2.2: Pulse amplitude η as a function of distance z with boundary condition $u(0,t) = 1.25\,\mathrm{sech}\,t$. Full numerical solution of (1.1): — ; solution of approximate equations (2.18)–(2.20): - - -

Kath and Smyth [22] found the length ℓ of the shelf by matching the frequency of oscillations of the solution of the approximate equations (2.18)–(2.20) near the fixed point $\eta = \hat{\kappa}$ and $w = 1/\hat{\kappa}$ to the steady soliton oscillation frequency $\hat{\kappa}^2/2$, obtaining

$$\ell = \frac{3\pi^2}{8\hat{\kappa}}. \tag{2.21}$$

Finally, the steady amplitude $\hat{\kappa}$ was found from the energy conservation equation (2.20) as

$$\hat{\kappa} = \left[2\eta^4 w - \frac{\eta^2}{w}\right]^{1/3}. \tag{2.22}$$

The analysis is not yet complete as the effect of dispersive radiation shed from the pulse has not been included. Without the dispersive radiation loss the pulse will oscillate about the steady state given by equation (2.22) without ever settling to it. Figure 2.2 shows just such a comparison between the solution of the approximate equations (2.18)–(2.20), which neglect shed dispersive radiation, and the full numerical solution of (1.1). The dispersive radiation acts to damp the oscillations of the approximate solution. The form of this shed dispersive radiation is the subject of the next section.

2.2 Radiation Analysis

Following the example in the last section, we will now discuss the analysis of the radiation shed from the pulse in the context of the NLS equation (1.1) based on the work of Kath and Smyth [22]. The extension to the perturbed NLS equations (4.1), (5.1) and (6.1) will be discussed in their respective chapters.

Numerical solutions show that outside of the region of length ℓ centred about the pulse the radiation is of small amplitude. As such, the nonlinear term in the NLS equation (1.1) is negligible and can be ignored giving

$$\mathrm{i}\frac{\partial u}{\partial z} + \frac{1}{2}\frac{\partial^2 u}{\partial t^2} = 0 \tag{2.23}$$

as the equation governing the shed dispersive radiation. This equation, being linear, can of course be solved exactly to give the form of the radiation leaving the pulse. However the functional form the radiation is not of importance in this analysis. What is important is the flux, or flow, of radiation away from the pulse. Knowing the amount of radiation leaving the pulse, one can then modify the evolution equations (2.18)–(2.20) to take account of this loss.

Keeping this desire for flux information in mind, we note that the conservation of mass equation for the linearised NLS equation (2.23) is the same as the mass conservation equation (2.6). Integrating this equation from the edge of the shelf at $t = \ell/2$ to $t = \infty$ gives the mass flowing to the right away from the pulse as

$$\frac{\mathrm{d}}{\mathrm{d}z}\int_{\ell/2}^{\infty} |u|^2 \,\mathrm{d}t = \mathrm{Im}(u^* u_t)|_{t=\ell/2}. \tag{2.24}$$

By symmetry, this is the same as the mass flowing to the left. The objective is to now find expressions for u and u_t at the edge of the shelf in order to calculate this mass flux to radiation.

Taking the Laplace transform of the linearised NLS equation (2.23), we obtain

$$\mathrm{i}s\bar{u} + \frac{1}{2}\frac{\mathrm{d}^2\bar{u}}{\mathrm{d}t^2} = 0, \tag{2.25}$$

where

$$\bar{u} = \mathcal{L}\{u\} = \int_0^{\infty} \mathrm{e}^{-sz} u \,\mathrm{d}z \tag{2.26}$$

is the Laplace transform of u in z. Equation (2.25) is an ordinary differential equation, in Laplace space, which can be solved for $\bar{u}$. Doing this, we obtain

$$\bar{u} = A\mathrm{e}^{-\sqrt{-2\mathrm{i}s}\,t} \quad \text{for } t > \ell/2. \tag{2.27}$$

Differentiating this expression with respect to t one then obtains

$$\frac{\mathrm{d}\bar{u}}{\mathrm{d}t} = -\sqrt{2}\mathrm{e}^{-\mathrm{i}\pi/4}\sqrt{s}\,\bar{u}, \tag{2.28}$$

where we have used the principal root. This can also be written

$$\frac{\mathrm{d}\bar{u}}{\mathrm{d}t} = -\sqrt{2}\mathrm{e}^{-\mathrm{i}\pi/4}\frac{s}{\sqrt{s}}\,\bar{u}. \tag{2.29}$$

Inverting the Laplace transform, using the convolution theorem, the relation

$$u_t = -\sqrt{2}\mathrm{e}^{-\mathrm{i}\pi/4}\frac{\mathrm{d}}{\mathrm{d}z}\int_0^z \frac{u(\ell/2,\tau)}{\sqrt{\pi(z-\tau)}}\,\mathrm{d}\tau. \tag{2.30}$$

between u and u_t is obtained.

The relation (2.30) between u and u_t can now be substituted into the mass conservation equation (2.24) to give

$$\frac{\mathrm{d}}{\mathrm{d}z}\int_{\ell/2}^{\infty}|u|^2\,\mathrm{d}t = -\sqrt{2}\,\mathrm{Im}\left[\mathrm{e}^{-\mathrm{i}\pi/4}u^*(\ell/2,z)\frac{\mathrm{d}}{\mathrm{d}z}\int_0^z \frac{u(\ell/2,\tau)}{\sqrt{\pi(z-\tau)}}\,\mathrm{d}\tau\right] \tag{2.31}$$

for the mass radiated to the right away from the pulse. Taking into account the symmetric mass radiated to the left away from the pulse, and noticing that the mass lost via this dispersive radiation must come from the pulse contained in $-\ell/2 \le t \le \ell/2$, the mass conservation equation (2.15) for the pulse is modified to

$$\frac{\mathrm{d}}{\mathrm{d}z}\int_{-\infty}^{\infty}\rho\,\mathrm{d}t = 2\sqrt{2}\,\mathrm{Im}\left(\mathrm{e}^{-\mathrm{i}\pi/4}u^*(\ell/2,z)\frac{\mathrm{d}}{\mathrm{d}z}\int_0^z \frac{u(\ell/2,\tau)}{\sqrt{\pi(z-\tau)}}\,\mathrm{d}\tau\right). \tag{2.32}$$

to take account of the mass shed from the pulse to dispersive radiation.

The expression $u(\ell/2,z)$ is the radiation at the edge of the shelf. To find an expression for this radiation, Kath and Smyth [22] noticed that the phase of the low frequency radiation in the vicinity of the pulse, seen in Figure 2.1, is nearly constant. As such, the above mass conservation equation is then nearly independent of the phase and so $u(\ell/2,z)$ and $u^*(\ell/2,z)$ can both be replaced by $r = |u(\ell/2,z)|$, which will be called the radiation height. An expression for r was found by doing a perturbation analysis on the mass conservation equation (2.15) near the fixed point (2.22) and comparing the difference in the mass between the pulse and an exact NLS soliton (the fixed point) to find

$$r^2 = \frac{3\hat{\kappa}}{8}\left(2\eta^2 w - 2\hat{\kappa} + \frac{3\pi^2}{8\hat{\kappa}}g^2\right). \tag{2.33}$$

We note that at the fixed point (2.22) $g = 0$ and $r = 0$ as required since there is no radiation.

With this expression for r (the radiation at the edge of the shelf), the pulse mass conservation equation (2.32) simplifies to

$$\frac{\mathrm{d}}{\mathrm{d}z}\left(2\eta^2 w + \frac{3\pi^2}{8\hat{\kappa}}g^2\right) = -2r\frac{\mathrm{d}}{\mathrm{d}z}\int_0^z \frac{r}{\sqrt{\pi(z-\tau)}}\,\mathrm{d}\tau. \tag{2.34}$$

This mass loss rate must now be included in the pulse parameter evolution equations (2.18)–(2.20) derived from the conservation and moment equations. The mass loss in the mass equation (2.34) can be added to either of (2.18) and (2.19) or distributed between both. Kath and Smyth found it more natural to place the mass loss in equation (2.18) for g since the shelf drives the mass loss to radiation. In addition Kath and Smyth found that solutions of the resulting equations were very insensitive to the distribution of the mass loss between (2.18) and (2.19). Doing this, equation (2.18) for g is modified to

$$\frac{\mathrm{d}g}{\mathrm{d}z} = \frac{2}{3\pi}\left(\frac{\eta}{w^2} - \eta^3\right) - 2\alpha g, \tag{2.35}$$

where

$$\alpha = \frac{3\hat{\kappa}}{8}\frac{1}{r}\frac{\mathrm{d}}{\mathrm{d}z}\int_0^z \frac{r}{\sqrt{\pi(z-\tau)}}\,\mathrm{d}\tau. \tag{2.36}$$

The coefficient of α was found by requiring that an appropriate combination of (2.35), (2.19) and (2.20) reduces to the mass equation (2.34).

From this analysis we now have a full set of evolution equations for the pulse that includes loss from the pulse to dispersive radiation. These equations are

$$\frac{\mathrm{d}g}{\mathrm{d}z} = -\frac{2\eta}{3\pi}\left(\eta^2 - w^{-2}\right) - 2\alpha g, \tag{2.37}$$

$$\frac{\mathrm{d}}{\mathrm{d}z}(\eta w) = \frac{\ell g}{\pi}\left(\eta^2 - \frac{1}{2}w^{-2}\right), \tag{2.38}$$

$$\frac{\mathrm{d}}{\mathrm{d}z}\left(\frac{\eta^2}{w} - 2\eta^4 w\right) = 0, \tag{2.39}$$

$$\alpha = \frac{3\hat{\kappa}}{8}\frac{1}{r}\frac{\mathrm{d}}{\mathrm{d}z}\int_0^z \frac{r}{\sqrt{\pi(z-\tau)}}\,\mathrm{d}\tau, \tag{2.40}$$

$$r^2 = \frac{3\hat{\kappa}}{8}\left(2\eta^2 w - 2\hat{\kappa} + \frac{3\pi^2}{8\hat{\kappa}}g^2\right). \tag{2.41}$$

Figure 2.3 shows the effect of adding radiation damping to the approximate equation (2.18)–(2.20). As can be seen from the figure the agreement between the solution of the approximate equations and the full numerical solution of (1.1) is much better when the effect of dispersive radiation is included. The comparison figures of this chapter are merely included to demonstrate the motivation for using the current analysis technique. More detailed comparisons and analysis can be found in [22].

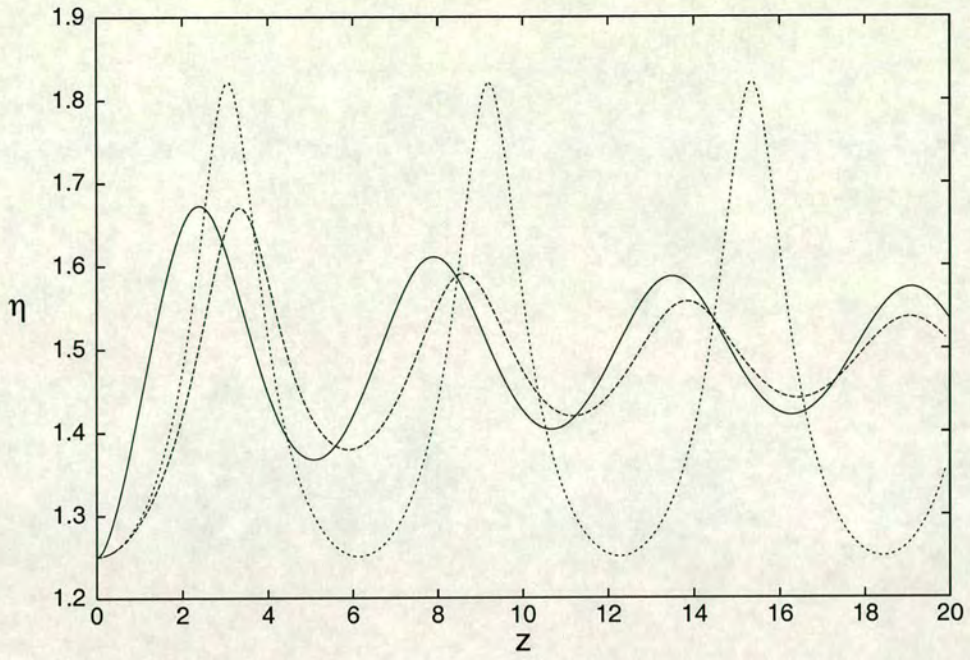

Figure 2.3: Pulse amplitude η as a function of distance z with boundary condition $u(0,t) = 1.25\,\mathrm{sech}\,t$. Full numerical solution of (1.1): — ; solution of approximate equations (2.37)–(2.41): – – – ; solution of approximate equations (2.18)–(2.20): - - -

A variety of numerical techniques have been used to find the solutions shown in Figures 2.1, 2.2 and 2.3. The full numerical solution of the NLS equation (1.1) is obtained using a pseudo-spectral method similar to that of Fornberg and Whitham [11]. The solution of the approximate equations (2.37)–(2.41), obtained from the conservation and moment equations and radiation analysis, was obtained using a fourth-order Runge-Kutta method along with a numerical method for dealing with the singular integrand in the radiation integral (2.40). These numerical techniques are the subject of the next chapter.

Chapter 3

Numerical Methods

This section will describe the various numerical methods used in this thesis and will be split into three sections. Firstly, we shall discuss the numerical techniques used for the full numerical solution of the NLS (1.1) and perturbed NLS equations (4.1), (5.1) and (6.1). Secondly, we shall discuss the numerical techniques used for numerically solving the approximate equations derived via the perturbation technique discussed in Chapter 2. Lastly, we shall then discuss the numerical techniques used for the optimisation of the dispersion profile (see Chapter 6).

3.1 Numerical Method for NLS Equation

To numerically solve the NLS equation (1.1) a pseudospectral method similar to that of Fornberg and Whitham [11] was used. The main idea is to calculate t derivatives using discrete Fourier transforms and then integrate in space using Runge-Kutta methods. This method is also known as the integrating factor, or linearly exact, method for reasons which will become obvious shortly. The integrating factor method has been widely used in a variety of contexts ranging from free-surface flows in geophysics [38] to optical soliton propagation [4, 22, 34]. Fornberg and Driscoll [12] compared a variety of numerical techniques applied to the NLS equation, including the split-step Fourier method [2, 48], the method of Chan and Kerkhoven [7] and the integrating factor method. Their comparison showed the integrating factor method to be highly competitive and accurate.

To describe the integrating factor method, we first define the Fourier transform of $u(t, z)$ in the standard fashion as

$$\hat{u}(\omega, z) = F\{u\} = \int_{-\infty}^{\infty} u(t, z) \mathrm{e}^{\mathrm{i}\omega t} \mathrm{d}t \tag{3.1}$$

and the inverse transform of $\hat{u}(\omega, z)$ as,

$$u(t, z) = F^{-1}\{\hat{u}\} = \frac{1}{2\pi} \int_{-\infty}^{\infty} \hat{u}(\omega, z) \mathrm{e}^{-\mathrm{i}\omega t} \mathrm{d}\omega. \tag{3.2}$$

Now taking the Fourier transform of the NLS equation (1.1), remembering that the Fourier transform of t-derivatives are

$$F\left\{\frac{\mathrm{d}^{(n)}u}{\mathrm{d}t^{(n)}}\right\} = (-\mathrm{i}\omega)^{(n)}\hat{u}, \tag{3.3}$$

we obtain

$$\frac{\mathrm{d}\hat{u}}{\mathrm{d}z} + \frac{\mathrm{i}}{2}\omega^2\hat{u} = \mathrm{i}F\left\{|u|^2u\right\}. \tag{3.4}$$

Multiplying by the integrating factor $\mathrm{e}^{\mathrm{i}\omega^2 z/2}$, equation (3.4) can be written as a first order ordinary differential equation in space

$$\frac{\mathrm{d}}{\mathrm{d}z}(\hat{u}\mathrm{e}^{\mathrm{i}\omega^2 z/2}) = \mathrm{i}F\left\{|u|^2u\right\}\mathrm{e}^{\mathrm{i}\omega^2 z/2}. \tag{3.5}$$

We must now replace these continuous Fourier transforms with discrete Fourier transforms (DFT) suitable for numerical calculation. In doing so, we take u on some interval $-L/2 \leq t \leq L/2$, with u periodically extended outside of this interval. In applying the DFT, the interval is discretised over N points with spacing $\Delta t = L/N$, with N chosen large enough for the required accuracy. Introducing periodicity into the problem is an artificial condition as an NLS soliton with radiation should be allowed to extend to an arbitrary distance. With the periodicity, radiation cannot escape the system and over time will build up and compromise the soliton. However, as periodicity must be imposed in order to use the pseudo-spectral technique we must minimise its impact. This is done by two methods. Firstly, Fornberg and Whitham [11] recommended that L is chosen large enough so that u is negligible at the boundaries $t = -L/2$ and $t = L/2$. However in doing so, one must make a corresponding increase in N, the number of points over which the interval is discretised. This places a practical limit on the size of L as larger N means longer computation times.

In order to avoid inordinately long simulation times dictated by a large N, If *et al.* [21] suggested another method for dealing with the boundaries. They introduced an absorption profile at the boundaries $t = \pm L/2$ with the intent of absorbing any radiation leaving the cell bounded by $t = \pm L/2$. Doing so would simulate dispersive radiation radiating away from the soliton indefinitely. Towards this end the NLS equation (1.1) was modified to

$$\mathrm{i}u_z + \frac{1}{2}u_{tt} + |u|^2u + \mathrm{i}\theta(t)u = 0 \tag{3.6}$$

where $\theta(t)$ is the absorbing function,

$$\theta(t) = \theta_0\left(\mathrm{sech}^2\left[\alpha\left(t - L/2\right)\right] + \mathrm{sech}^2\left[\alpha\left(t + L/2\right)\right]\right). \tag{3.7}$$

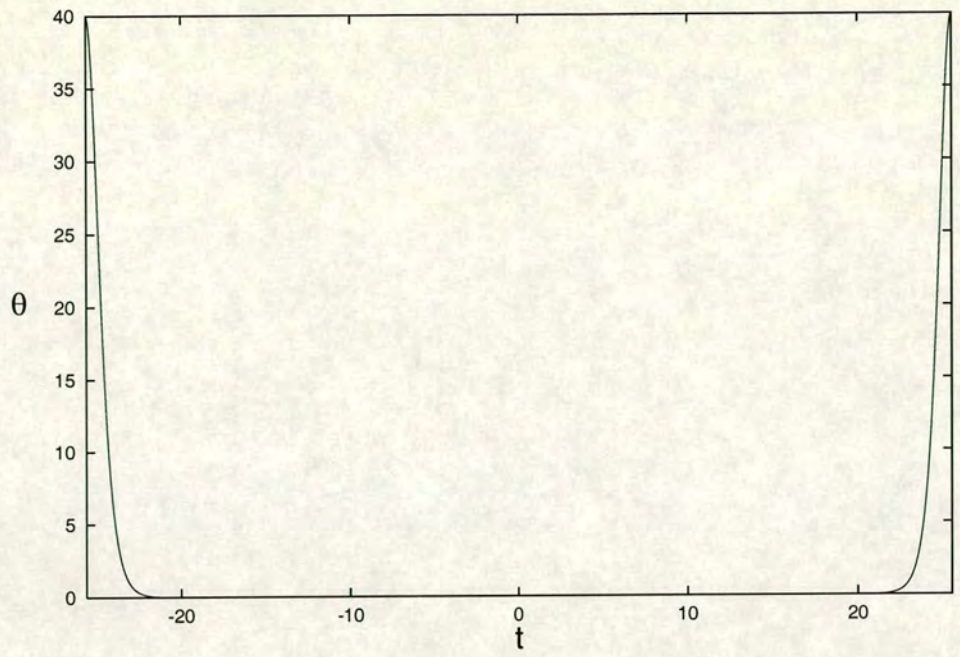

Figure 3.1: Absorbing boundaries obtained from equation (3.7) with $\theta_0 = 40.0$, $\alpha = 1.0$ and $L = 51.2$.

Here θ_0 is the strength of the absorbing layer and α is its inverse width. Figure 3.1 shows an example boundary created using equation (3.7).

Using the procedure outlined above we may incorporate the absorbing boundary into the numerical procedure. By taking the Fourier transform of equation (3.6) and using an integrating factor, (3.6) may be rewritten in Fourier space as,

$$\frac{\mathrm{d}}{\mathrm{d}z}(\hat{u}\mathrm{e}^{\mathrm{i}\omega^2 z/2}) = \left(\mathrm{i}F\left\{|u|^2 u\right\} - F\{\theta(t)u\}\right)\mathrm{e}^{\mathrm{i}\omega^2 z/2}. \tag{3.8}$$

For numerical calculations the Fourier transforms (3.1) and (3.2) are now replaced by their discrete analogues

$$\hat{u}_k = \sum_{j=-N/2+1}^{N/2} u_j \exp\left(\frac{2\pi \mathrm{i}kj}{N}\right), \; u_j = u(j\Delta t, z) \tag{3.9}$$

$$u_j = u(j\Delta t, z) = \frac{1}{N}\sum_{k=-N/2+1}^{N/2} \hat{u}_k \exp\left(\frac{-2\pi \mathrm{i}kj}{N}\right). \tag{3.10}$$

Then the ordinary differential equation (3.8) in discrete Fourier space becomes,

$$\frac{\mathrm{d}}{\mathrm{d}z}\left(\hat{u}_j \exp\left(\frac{\mathrm{i}\omega_j^2 z}{2}\right)\right) = \left(\mathrm{i}F\left\{|u|^2 u\right\} - F\left\{\theta(t)u\right\}\right)\exp\left(\frac{\mathrm{i}\omega_j^2 z}{2}\right) \tag{3.11}$$

with

$$\omega_j = \frac{2\pi j}{L}, \quad j = -N/2+1, \ldots, N/2 \tag{3.12}$$

In the numerical procedure, the Fourier transforms are calculated using the Fast Fourier Transform (FFT) algorithm [49]. The first order ordinary differential equation (3.11) can then be solved using Runge-Kutta methods [49]. A standard fourth-order Runge-Kutta method was used with the understanding that the space propagation takes place in Fourier space and an integrating factor is present. As at each space step Runge-Kutta routines calculate the right hand side at the points z, $z+\Delta z/2$ and $z+\Delta z$, estimates of u at $z+\Delta z/2$ and $z+\Delta z$ are needed. Since space steps of size $\Delta z/2$ are required, the integrating factor in (3.11) can have z replaced by $\Delta z/2$ upon suitable choice of the lower limit of integration for the integrating factor. Hence

$$\frac{\mathrm{d}}{\mathrm{d}z}(w_j) = f(u_j)\exp\left(\frac{\mathrm{i}\omega_j^2\Delta z}{4}\right) = G(u,z), \tag{3.13}$$

where $f(u) = \mathrm{i}F\{|u|^2u\} - F\{\theta u\}$ and $w_j = \hat{u}_j(n\Delta z)\exp\left(\mathrm{i}\omega_j^2\Delta z/4\right)$.

Now to progress from the n to the $n+1$ space-step, the fourth-order Runge-Kutta algorithm, in Fourier space, is

$$\begin{aligned}
U_1 &= w_j^n + \frac{\Delta z}{2}G(u,z)\\
U_2 &= w_j^n + \frac{\Delta z}{2}G\left(F^{-1}\{U_1\}, z+\frac{\Delta z}{2}\right)\\
U_3 &= w_j^n + \Delta z G\left(F^{-1}\{U_2\}, z+\frac{\Delta z}{2}\right)\\
U_4 &= -w_j^n + \frac{\Delta z}{2}G\left(F^{-1}\{U_3\}, z+\Delta z\right)
\end{aligned}$$

with the solution at $(n+1)\Delta z$ begin given by

$$w_j^{n+1} = \frac{1}{3}U_1 + \frac{2}{3}U_2 + \frac{1}{3}U_3 + \frac{1}{3}U_4.$$

The solution u at $z = (n+1)\Delta z$ is then obtained by multiplying w_j^{n+1} by the inverse integrating factor and inverting $\hat{u}$ using the FFT algorithm. The Runge-Kutta algorithm now works in the following fashion:

1. As G is evaluated at z in U_1 and u is known at this point

$$U_1 = w_j^n + \frac{\Delta z}{2}G(u,z). \tag{3.14}$$

2. As U_2 requires u at $z+\Delta z/2$ we need to propagate a distance $\Delta z/2$ forward to estimate u at this point. The calculation of U_1 is a Euler step of length $\Delta z/2$ and so gives an estimate of w at $z+\Delta z/2$. Multiplying U_1 by the inverse integrating factor $\exp\left(-\mathrm{i}\omega_j^2\Delta z/4\right)$ and inverting the Fourier transform then gives an estimate of u at $z+\Delta z/2$. Hence U_2 may be calculated.

3. U_3 requires U_2, and hence u, calculated at $z + \Delta z/2$. Since u is already estimated at $z + \Delta z/2$, U_3 can be calculated.

4. U_4 requires u at $z+\Delta z$. Now U_3 is a Euler step of length Δz from z, so that U_3 gives an estimate of w at $z + \Delta z$. Multiplying U_3 twice by the inverse integrating factor $\exp\left(-\mathrm{i}\omega_j^2 \Delta z/4\right)$ then gives an estimate of $\hat{u}$ at $z + \Delta z$. Inverting the Fourier transform finally gives an estimate of u at $z+\Delta z$ and so U_4 may be calculated.

The final solution $F\{u_{n+1}\}$ is now just the Runge-Kutta sum of the above four components after multiplication by the inverse integrating factor. The solution u_{n+1} at $z + \Delta z$ can finally be obtained using the inverse FFT algorithm to get u in physical space. Notice that at each Runge-Kutta step the nonlinear part of (3.11) is calculated in physical space exactly and then converted to Fourier space numerically using Fast Fourier Transforms. This is standard practice in pseudospectral methods for the NLS and related equations.

Equations which are perturbations of the NLS equation (1.1) can be solved in a similar fashion. The perturbing terms are incorporated into the integrating factor of equation (3.11) or included in the nonlinear terms on the right hand side. The equation is then solved numerically using the Runge-Kutta method outlined above. The form of these changes will be discussed in the relevant chapters.

3.2 Numerical Technique for Approximate Equations

This section discusses the numerical solution of the approximate ordinary differential equations obtained from the Lagrangian or Conservation/Moment method applied to the various forms of the NLS equation as discussed in Chapter 2.

First we write the set of ODE's as the matrix equation

$$\mathsf{A}\boldsymbol{x}' = \boldsymbol{b}. \tag{3.15}$$

Here $\boldsymbol{x}'$ is the vector of the derivatives of the soliton parameters, A is the matrix of coefficients of these derivatives and $\boldsymbol{b}$ is the inhomogeneous part of the differential equation.

As a set of first order ODE's, equation (3.15) can be solved using Runge-Kutta methods. However, it must first be put in the form $\boldsymbol{x}' = \mathsf{A}^{-1}\boldsymbol{b}$. This was done using LU decomposition on the matrix A. That is, the matrix A was numerically factored into a lower triangular matrix L and an upper triangular matrix U [49]. Using a numerical forward and backward substitution routine [49], the matrix

equation (3.15) was then solved for $\boldsymbol{x}'$. Standard Runge-Kutta techniques [49] could then be used to calculate $\boldsymbol{x}$.

In calculating the solution of the approximate ODE's describing the pulse parameters, another numerical technique had to be used. This was for calculating the effect of the dispersive radiation propagating away from the pulse. As was discussed in Section 2.2, the equation governing the dispersive radiation is given by an integral of the form

$$M = \int_0^z \frac{r(\tau)}{\sqrt{z-\tau}} \mathrm{d}\tau. \tag{3.16}$$

The difficulty in evaluating this integral is that the integrand is singular at the upper limit.

To numerically evaluate this integral, the second order method of Miksis and Ting [37] was used. Following their method, we decompose the integral (3.16) into the sum

$$M = M_1 + M_2, \tag{3.17}$$

where

$$M_1 = \int_0^m \frac{r(\tau)}{\sqrt{z-\tau}} \mathrm{d}\tau \tag{3.18}$$

and

$$M_2 = \int_m^z \frac{r(\tau)}{\sqrt{z-\tau}} \mathrm{d}\tau. \tag{3.19}$$

The integral change-over point, m, is chosen far enough away from z to make the integrand in M_1 smooth. As the integrand of M_1 is not singular over the range of integration, M_1 can be calculated directly, in this case using the Trapezoidal Rule.

To evaluate M_2, we rewrite the integral as the sum of many small integrals

$$M_2 = \sum_{i=k}^{n} M_2^i = \sum_{i=k}^{n} \int_{z_i}^{z_{i+1}} \frac{r(\tau)}{\sqrt{z-\tau}} \mathrm{d}\tau, \tag{3.20}$$

where $z_k = m$ and $z_{n+1} = z$. In the interval $z_i < \tau < z_{i+1}$ we approximate r with the linear polynomial

$$r(\tau) = r(z_i) + (\tau - z_i) r', \tag{3.21}$$

where

$$r' = \frac{r(z_{i+1}) - r(z_i)}{z_{i+1} - z_i}. \tag{3.22}$$

We now replace r in the integral (3.20) with the linear approximation (3.21) to obtain

$$M_2^i = \int_{z_i}^{z_{i+1}} \frac{r(z_i) + r'(\tau - z_i)}{\sqrt{z-\tau}}\, \mathrm{d}\tau. \tag{3.23}$$

By re-writing $r'(\tau - z_i) = r'(z - z_i) - r'(z - \tau)$, the integral (3.23) can be written as

$$M_2^i = \int_{z_i}^{z_{i+1}} \frac{r(z_i) + r'(z - z_i) - r'(z - \tau)}{\sqrt{z-\tau}}\, \mathrm{d}\tau. \tag{3.24}$$

This integral can be integrated exactly as

$$M_2^i = -2(r(z_i) + r'(z - z_i))\sqrt{z-\tau}\Big|_{z_i}^{z_{i+1}} + \frac{2}{3}r'(z-\tau)^{3/2}\Big|_{z_i}^{z_{i+1}}. \tag{3.25}$$

Evaluating this expression at the upper and lower limits, we obtain

$$\begin{aligned} M_2^i = 2(r(z_i) + r'(z - z_i))\left(\sqrt{z - z_i} - \sqrt{z - z_{i+1}}\right) \\ + \frac{2}{3}r'\left((z - z_{i+1})^{3/2} - (z - z_i)^{3/2}\right), \end{aligned} \tag{3.26}$$

giving for the integral M_2

$$\begin{aligned} M_2 = \sum_{i=k}^{n} \Big(2\left(r_i + r'(z - z_i)\right)\left(\sqrt{z - z_i} - \sqrt{z - z_{i+1}}\right) \\ + \frac{2}{3}r'\left((z - z_{i+1})^{3/2} - (z - z_i)^{3/2}\right)\Big). \end{aligned} \tag{3.27}$$

If $z < m$, splitting of the integral is not necessary. In this case $M_1 = 0$ and M_2 is evaluated over the entire range of integration. Once $z > m$, both integrals are necessary for the evaluation of the total loss integral (3.16).

The choice of m is an issue which would appear to affect the accuracy of the numerical scheme. This point is discussed in [37], but not in great detail, beyond saying that m should be chosen far enough away from z to ensure the integrand of M_1 is smooth. This was the criterion for choosing the value of m used in these calculations. Different values of m were chosen to examine the effect on the final integral, but as long as reasonable values were taken, no significant difference resulted.

The primary reason for splitting the integral in the original work [37], as in equation (3.17), was to take advantage of the smooth nature of M_1. Assuming M_1 is smooth means that a larger integration step size could be used when evaluating it. As M_2 is evaluated near a singularity, a smaller step size could then be used to account for this. In this way, variable step sizes could be used to minimise calculation time and maximise accuracy. However in the integral being considered

(3.16), r is only known in discrete steps in z of length Δz. Therefore we cannot take smaller step lengths in evaluating M_2 as we do not know r at steps of less than Δz. However, with the speed of modern computers, and considering the specific problem of calculating (3.16), this is not a major limitation. As we are not dealing with particularly long integration times, the integral (3.16) can be evaluated with a small integration time step without too much difficultly. However, given this information, there is still justification for performing the integration using this integral-splitting method. The error associated with using the Trapezoidal Rule, used in evaluating integral (3.18), is $O(\Delta z^3 r'')$. The error associated with evaluating integral (3.19) is $O(\Delta z^2 r'')$, or a factor h less accurate. So to obtain good numerical results, it is advisable to keep m as close as possible to z, without compromising the smooth nature of the integrand in M_1.

3.3 Numerical Optimisation Technique

In multidimensional optimisation, one must choose between two different techniques. The first is based upon using evaluations of the function at the point in question, whereas the second also uses local gradient information at the point. Generally methods using gradient information are more powerful in that this extra information can "point" the algorithm in the right direction. However gradient-dependent algorithms can be complicated and are not always the best choice for certain problems. Also for problems where the objective function, i.e. the function to be optimised, may contain discontinuities, gradient-based methods will not work.

The optimisation problem of this thesis was to determine the dispersion profile in a fibre in order to maximise pulse compression. This consists of splitting the fibre into a number of sections and varying the length and dispersion over each section to maximise compression. Keeping the above comments regarding optimisation techniques in mind, one can examine the compressor at hand and use a method best suited to it. In the present work the function to be maximised, f, equivalent to minimising $-f$, is comprised of the steady-state amplitude, η_f, of the soliton, minus various penalties. As was reported in McKinnon *et al.* [34], η_f is not a differentiable function of the dispersion parameters. In fact, η_f contains small discontinuities, which make finding gradient information impossible. As a similar objective function was used in the present work, the same difficultly is present. For this reason it was decided to use an optimisation method which was an extension of the method used in [34], which in turn was based on the method of [49]. This method is a variation of the downhill simplex method of Nelder and

Mead [46]. While no gradient information is required by this method, it can be extremely slow. However, if time is not a restriction, and an easily implementable optimisation method is required, the Nelder-Mead simplex method can work well.

The method requires $N + 1$ initial points to form an initial N-dimensional simplex. Here N is the number of variables in the minimisation procedure. The $N+1$ initial points are obtained by making a starting guess, say $\boldsymbol{p}_0$, and creating the other N points via the equation

$$\boldsymbol{p}_i = \boldsymbol{p}_0 + \lambda_i \boldsymbol{e}_i \tag{3.28}$$

where $\boldsymbol{e}_i$ are N unit vectors and λ_i are N constants which are estimates of the problem's characteristic length scales. Taking a $\lambda_i = 0$ would indicate a stationary point in the optimisation, i.e. it will remain constant. The simplex formed by the above points moves about the N-dimensional space in the manner recommended by Nelder and Mead [46], which can be summarised as follows [55]. Firstly define

$\boldsymbol{p}_h$: vertex with the highest function value

$\boldsymbol{p}_s$: vertex with the second highest function value

$\boldsymbol{p}_l$: vertex with the lowest function value

$\boldsymbol{p}_c$: centroid of all vertices except $\boldsymbol{p}_h$, i.e.

$$\boldsymbol{p}_c = \frac{1}{N} \sum_{\substack{j=1 \\ j \neq h}}^{N+1} \boldsymbol{p}_j.$$

Also, let $y = f(\boldsymbol{p})$, $y_h = f(\boldsymbol{p}_h)$, and so on. Then the Nelder-Mead method proceeds as follows:

1. Evaluate $f(\boldsymbol{p})$ at all N vertices.

2. **Reflection** Reflect $\boldsymbol{p}_h$ using a reflection factor α to find a new point $\boldsymbol{p}_0$ defined as

$$\boldsymbol{p}_0 = (1 + \alpha)\boldsymbol{p}_c - \alpha \boldsymbol{p}_h.$$

3. If $y_l \leq y_0 \leq y_s$, replace the point $\boldsymbol{p}_h$ by $\boldsymbol{p}_0$ and go to step 2.

4. **Expansion** If $y_0 \leq y_l$, expand the simplex using an expansion factor γ to obtain a new point $\boldsymbol{p}_{00}$ defined by

$$\boldsymbol{p}_{00} = \gamma \boldsymbol{p}_0 + (1 - \gamma)\boldsymbol{p}_c.$$

   In other words, for a particularly small vertex, the algorithm expands the simplex further in that direction.

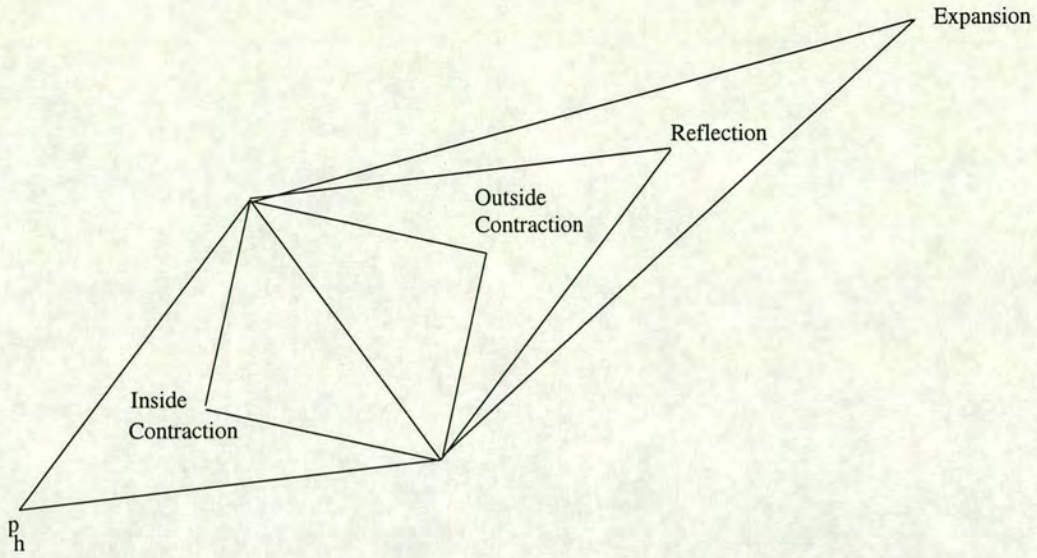

Figure 3.2: Reflections, expansions and contractions in the Nelder-Mead algorithm.

(a) If $y_{00} < y_l$, replace $\boldsymbol{p}_h$ by $\boldsymbol{p}_{00}$ and go to step 2.

(b) If $y_{00} \geq y_l$, replace $\boldsymbol{p}_h$ by $\boldsymbol{p}_0$ and go to step 2.

5. **Contraction** If $y_0 > y_s$, contract the simplex using a contraction factor. This is analogous to the Expansion step 4 and there are two cases to consider.

   (a) **Outside Contraction** If $y_0 < y_h$, calculate $\boldsymbol{p}_{00}$ by

   $$\boldsymbol{p}_{00} = \beta \boldsymbol{p}_0 + (1 - \beta)\boldsymbol{p}_c.$$

   (b) **Inside Contraction** If $y_0 \geq y_h$, calculate $\boldsymbol{p}_{00}$ by

   $$\boldsymbol{p}_{00} = \beta \boldsymbol{p}_h + (1 - \beta)\boldsymbol{p}_c.$$

   Whichever of the two cases occur, there are then two further cases to consider

   (c) If $y_{00} < y_h$ and $y_{00} < y_0$, replace $\boldsymbol{p}_h$ by $\boldsymbol{p}_{00}$ and go to step 2.

   (d) **Shrink** If $y_{00} \geq y_h$ or $y_{00} > y_0$ reduce the size of the simplex by halving the distances from $\boldsymbol{p}_l$ using $\boldsymbol{p}_j = \boldsymbol{p}_l - (\boldsymbol{p}_j - \boldsymbol{p}_l)/2$ for $1 \leq j \leq N + 1$ and $j \neq l$. Go to step 2.

Figure 3.2 shows the possible movement, bar the shrink step 5(d), of the Nelder-Mead algorithm in two dimensions. Nelder and Mead [46] set the expansion and contraction parameters as $\alpha = 1$, $\beta = \frac{1}{2}$ and $\gamma = 2$.

In this way the simplex, moving simply by reflections, contractions and expansions, moves about the N-dimensional space, hopefully bracketing and homing in on a minimum.

Knowing when to stop the minimisation once a local minimum is found is difficult to define. In this thesis, we use the same minimisation criterion as used in the Nelder-Mead algorithm of [49]. Namely, minimisation is deemed complete once a cycle through the Nelder-Mead algorithm produces no appreciable change in the difference between the highest and lowest function values. Defining this change as

$$\text{rtol} = \frac{|y_h - y_l|}{|y_h + y_l|}, \tag{3.29}$$

a minimum was "found" when rtol $<$ ftol, where ftol is a user-defined tolerance. This minimum is not necessarily a global minimum, but probably one of many local minima. To verify this, the Nelder-Mead method was modified in [34] in order to restart the optimisation procedure with a small perturbation from the claimed minimum as an initial point. In this fashion, one can obtain a family of local minima from which a "global" minimum can be chosen.

One weakness of the Nelder-Mead method is that it is not guaranteed to converge to a minimum. However, ignoring the possibility of a shrink step (5(d) in the algorithm above), which indicates a failure of the simplex to find a value lower than y_h through simple reflections, expansions or contractions, the Nelder-Mead method will reduce the average of the function values at the simplex vertices [25]. That is

$$\bar{f} = \frac{1}{N+1} \sum_{i=1}^{N+1} y_i \tag{3.30}$$

will be reduced at the end of a Nelder-Mead cycle.

The Nelder-Mead method is not guaranteed to converge even for smooth functions [33]. When the Nelder-Mead method converges on a point which is not a local minimum, this is defined as stagnation. Stagnation can be remedied by reinitialising the simplex and beginning the optimisation from the stagnation point. Towards this end, we define the following quantities as in [24, 25]. Assume the vertices of the simplex $\boldsymbol{p}_i$ are ordered

$$y_1 \leq y_2 \leq \cdots \leq y_{N+1} \tag{3.31}$$

from the smallest function value to the largest. Now let V denote the $N \times N$ matrix of simplex directions for a simplex S defined by

$$\mathsf{V}(S) = (\boldsymbol{p}_2 - \boldsymbol{p}_1, \boldsymbol{p}_3 - \boldsymbol{p}_1, \cdots, \boldsymbol{p}_{N+1} - \boldsymbol{p}_1). \tag{3.32}$$

We now let $\boldsymbol{\delta}(f : S)$ denote the vector of objective function differences

$$\boldsymbol{\delta}(f : S) = (y_2 - y_1, y_3 - y_1, \ldots, y_{N+1} - y_1)^{\mathrm{T}}. \tag{3.33}$$

Kelley [24] also defined two oriented lengths as

$$\sigma_+(S) = \max_{2 \le j \le N+1} \|\boldsymbol{p}_1 - \boldsymbol{p}_j\| \text{ and } \sigma_-(S) = \min_{2 \le j \le N+1} \|\boldsymbol{p}_1 - \boldsymbol{p}_j\|. \tag{3.34}$$

With the above definitions (3.32)–(3.34), Kelley [24] defined a simplex gradient $\boldsymbol{D}(f : S)$ as

$$\boldsymbol{D}(f : S) = \left(\mathsf{V}^{\mathrm{T}}\right)^{-1} \boldsymbol{\delta}(f : S). \tag{3.35}$$

While the simplex gradient defined in (3.35) is not a traditional gradient in the continuous sense (f may be discontinuous), it does provide some information about the directional dependence of f, the objective function, on $\boldsymbol{p}$, the simplex vertices. If we denote the simplex S at the kth iteration as S^k we may simplify the above notation as

$$\mathsf{V}^k = \mathsf{V}(S^k) \text{ and } \boldsymbol{D}^k f = \boldsymbol{D}(f : S^k).$$

The criterion for stagnation in [24] was taken to be the failure of

$$\bar{f}^{k+1} - \bar{f}^k < -\alpha \|\boldsymbol{D}^k f\|^2, \tag{3.36}$$

but $\bar{f}^{k+1} - \bar{f}^k < 0$, which is satisfied by the Nelder-Mead method assuming no shrink steps take place and the initial simplex vertices are linearly independent, which they are by (3.28). Here α is a small positive parameter. When stagnation takes place, Kelley [24] suggests replacing the original stagnated simplex with a new, smaller simplex having vertices $\boldsymbol{r}_j$ with $\boldsymbol{r}_1 = \boldsymbol{p}_1$ and

$$\boldsymbol{r}_j = \boldsymbol{r}_1 + \beta_{j-1} \boldsymbol{e}_{j-1} \text{ for } 2 \le j \le N + 1. \tag{3.37}$$

Here $\boldsymbol{e}_i$ is the ith coordinate vector as in (3.28) and

$$\beta_i = \frac{1}{2} \begin{cases} \sigma_-(S^k) \operatorname{sign}((\boldsymbol{D}^k f)_i), & (\boldsymbol{D}^k f)_i \neq 0, \\ \sigma_-(S^k), & (\boldsymbol{D}^k f)_i = 0 \end{cases} \tag{3.38}$$

and $(\boldsymbol{D}^k f)_i$ is the ith component of $\boldsymbol{D}^k f$. By shrinking the simplex and making the simplex edges orthogonal, individual simplex reflections take smaller steps in many more directions, making it more likely that (3.36) is satisfied. While the above reorientation will not eliminate stagnation in the Nelder-Mead method, Kelley [24] found it to be a significant improvement upon the original method.

Chapter 4

Soliton Evolution in Lossy Fibres with Amplifiers

Previous work [22] has shown that for an accurate model of pulse evolution in a fibre without loss it is necessary to include the radiation shed as the pulse evolves. Without radiation loss the equations describing pulse evolution show that it oscillates about a fixed point without ever actually decaying to this fixed point. So for an accurate model of pulse evolution in a fibre, radiation loss must be accounted for. It is of interest to determine how the inclusion of intrinsic fibre loss affects the evolution of a propagating pulse, this being the subject of the present chapter.

This intrinsic fibre loss comes from two distinct causes, namely absorption and scattering. The scattering phenomenon, known as Rayleigh scattering, results from random density variations in the fibre material. These density variations result in local variations in the index of refraction causing light to scatter. Rayleigh scattering is a fundamental effect in glass fibres. The absorption phenomenon is due to the fibre material absorbing photons. Pure silica glass absorbs in the infrared region beyond wavelengths of 2μm, well beyond the optimum transmission wavelength. However, a very small amount of impurity can lower the absorption band to anywhere between wavelengths of $0.5 - 2\mu$m, thus affecting transmission of optical pulses. Absorption can be controlled to a certain extent by ensuring the purity of the glass. Taking both of these types of fibre loss into consideration, the minimum fibre loss is approximately 0.2 dB/km at a wavelength of 1.55μm, the loss being dominated by Rayleigh scattering. It is therefore of practical interest to determine how the inclusion of this loss in the fibre affects the evolution of a pulse.

4.1 Fibre Loss

The propagation of light in a uniform, monomode, polarisation-preserving, nonlinear optical fibre in the anomalous group-velocity dispersion regime is governed by the nonlinear Schrödinger (NLS) equation (1.1). When the effect of fibre loss is added, the governing equation is the perturbed NLS equation

$$\mathrm{i}\frac{\partial u}{\partial z} + \frac{1}{2}\frac{\partial^2 u}{\partial t^2} + |u|^2 u = -\mathrm{i}\sigma u, \tag{4.1}$$

where σ is the normalised damping rate [2, 19]. The distance z and time t have been normalised as in Chapter 1. The normalised damping rate σ is defined as damping rate per dispersion distance by

$$\sigma = 0.115\delta z_0 \tag{4.2}$$

where δ is the fibre loss rate in dB/km and z_0 is the dispersion distance in km given by equation (1.2). Hence a constant fibre loss rate δ can result in different values for the normalised damping rate depending on the dispersion distance z_0.

For the perturbed NLS equation (4.1) the conservation and moment equations (2.6)–(2.8) and (2.12) are modified to

$$\frac{\partial \rho}{\partial z} + \frac{\partial J}{\partial t} = -2\sigma\rho, \tag{4.3}$$

$$\frac{\partial J}{\partial z} + \frac{\partial}{\partial t}\left[E + \frac{1}{2}\rho^2 - \frac{1}{4}\rho_{tt}\right] = -2\sigma J, \tag{4.4}$$

$$\frac{\partial E}{\partial z} + \frac{\partial}{\partial t}\left[\frac{\mathrm{i}}{2}\left(u_t u_{tt}^* - u_t^* u_{tt}\right) - 2\rho J\right] = 2\sigma(\rho^2 - E), \tag{4.5}$$

$$\begin{aligned}\frac{\partial}{\partial z}tJ + \frac{\partial}{\partial t}&\left(\frac{1}{2}tE - \frac{1}{4}t\left(u^* u_{tt} + u u_{tt}^*\right) + \frac{1}{4}\left(u^* u_t + u u_t^*\right)\right)\\ &= E + \frac{1}{2}\rho^2 - 2\sigma t J,\end{aligned} \tag{4.6}$$

where $*$ denotes the complex conjugate. Integrating these conservation and moment equations with respect to t then gives the integrated conservation and moment equations

$$\frac{\mathrm{d}}{\mathrm{d}z}\int_{-\infty}^{\infty} \rho \,\mathrm{d}t = -2\sigma \int_{-\infty}^{\infty} \rho \,\mathrm{d}t, \tag{4.7}$$

$$\frac{\mathrm{d}}{\mathrm{d}z}\int_{-\infty}^{\infty} J \,\mathrm{d}t = -2\sigma \int_{-\infty}^{\infty} J \,\mathrm{d}t, \tag{4.8}$$

$$\frac{\mathrm{d}}{\mathrm{d}z}\int_{-\infty}^{\infty} E \,\mathrm{d}t = 2\sigma \int_{-\infty}^{\infty} \left(\rho^2 - E\right) \mathrm{d}t, \tag{4.9}$$

$$\frac{\mathrm{d}}{\mathrm{d}z}\int_{-\infty}^{\infty} tJ \,\mathrm{d}t = \int_{-\infty}^{\infty} \left[E + \frac{1}{2}\rho^2\right] \mathrm{d}t - 2\sigma \int_{-\infty}^{\infty} tJ \,\mathrm{d}t. \tag{4.10}$$

Substituting the trial function (2.14) into the integrated conservation and moment equations (4.7)–(4.10) yields the approximate equations

$$\frac{\mathrm{d}}{\mathrm{d}z}\left(2\eta^2 w + \ell g^2\right) = -2\sigma\left(2\eta^2 w + \ell g^2\right), \tag{4.11}$$

$$\frac{\mathrm{d}}{\mathrm{d}z}\left(\frac{\eta^2}{w} - 2\eta^4 w\right) = 8\sigma\eta^4 w - 2\sigma\frac{\eta^2}{w}, \tag{4.12}$$

$$\frac{\mathrm{d}}{\mathrm{d}z}(\pi g\eta w) = \frac{2}{3}\frac{\eta^2}{w} - \frac{2}{3}\eta^4 w - 2\sigma\pi g\eta w, \tag{4.13}$$

for the pulse parameters. The conservation of momentum equation (4.8) is identically satisfied by symmetry after the trial function is inserted into it. This is because the pulse is centred in a reference frame moving with the group velocity, and as such, has no momentum relative to this reference frame.

After some manipulation, which involves discarding $O(g^2)$ terms, the above equations can be written in the simplified form

$$\frac{\mathrm{d}}{\mathrm{d}z}(\eta w) = \frac{\ell g}{\pi}\left(\eta^2 - \frac{1}{2}w^{-2}\right) - \sigma\eta w, \tag{4.14}$$

$$\frac{\mathrm{d}g}{\mathrm{d}z} = -\frac{2\eta}{3\pi}\left(\eta^2 - w^{-2}\right) - \sigma g, \tag{4.15}$$

$$\frac{\mathrm{d}}{\mathrm{d}z}\left(\frac{\eta^2}{w} - 2\eta^4 w\right) = 2\sigma\left(4\eta^4 w - \frac{\eta^2}{w}\right). \tag{4.16}$$

Notice also that setting the loss parameter, σ, to zero will return the equations to those derived for the unperturbed NLS equation (2.18)–(2.20), as required.

As was discussed in Section 2.1, in the absence of fibre loss the shelf length, ℓ, is given by equation (2.21), where $\hat{\kappa}$, the steady amplitude, is given by equation (2.22). We shall use the same expressions for ℓ and $\hat{\kappa}$ when fibre loss is present with the following justification. The only fixed point of the approximate equations (4.14)–(4.16) is $\hat{\kappa} = 0$, so the method used by Kath and Smyth to determine ℓ for the NLS equation (1.1) will not work when fibre loss is included. When there is no loss, $\hat{\kappa}$ is constant; loss causes $\hat{\kappa}$ to decrease (ultimately to zero). Taking ℓ to be given by (2.21) will then be valid when $\hat{\kappa}$ is slowly varying, which will be the case for small loss σ. The method used here to calculate the shelf length ℓ then gives the local value of amplitude $\hat{\kappa}$ that the pulse would achieve if the fibre loss were turned off at some point. Also with this value of ℓ, setting $\sigma = 0$ in (4.14)–(4.16) reduces the approximate equations to those derived from the averaged Lagrangian of Kath and Smyth [22].

4.2 Radiation Analysis

As the radiation outside of the region $-\ell/2 \leq t \leq \ell/2$ has small amplitude, the nonlinear term in the perturbed NLS equation (4.1) is negligible there and can be

ignored. Therefore, the equation governing radiation away from the neighbourhood of the pulse is

$$\mathrm{i}u_z + \frac{1}{2}u_{tt} = -\mathrm{i}\sigma u. \tag{4.17}$$

Making the substitution $u = U\mathrm{e}^{-\sigma z}$, the linearised NLS equation (4.17) becomes

$$\mathrm{i}U_z + \frac{1}{2}U_{tt} = 0, \tag{4.18}$$

which is the same equation, in the variable U, as used in the radiation analysis of Kath and Smyth and discussed in Section 2.2. The conservation of mass equation for the linearised NLS equation (4.18) is

$$\mathrm{i}\frac{\partial}{\partial z}|U|^2 + \frac{1}{2}\frac{\partial}{\partial t}\left(U^*U_t - UU_t^*\right) = 0. \tag{4.19}$$

Integrating this conservation equation from the edge of the shelf at $t = \ell/2$ to $t = \infty$ yields an expression for the mass radiated to the right away from the pulse as

$$\frac{\mathrm{d}}{\mathrm{d}z}\int_{\ell/2}^{\infty}|U|^2\,\mathrm{d}t = \mathrm{Im}\left(U^*U_t\right)|_{t=\ell/2}. \tag{4.20}$$

As in Section 2.2, taking the Laplace transform of the linearised NLS equation (4.18) yields the convolution relation

$$U_t = -\sqrt{2}\mathrm{e}^{-\mathrm{i}\pi/4}\frac{\mathrm{d}}{\mathrm{d}z}\int_0^z \frac{U(\ell/2,\tau)}{\sqrt{\pi(z-\tau)}}\,\mathrm{d}\tau \tag{4.21}$$

between U and U_t at $t = \ell/2$. Using this convolution relation, the radiation expression (4.20) becomes

$$\frac{\mathrm{d}}{\mathrm{d}z}\int_{\ell/2}^{\infty}|U|^2\,\mathrm{d}t = -\sqrt{2}\,\mathrm{Im}\left(\mathrm{e}^{-\mathrm{i}\pi/4}U^*(\ell/2,z)\frac{\mathrm{d}}{\mathrm{d}z}\int_0^z \frac{U(\ell/2,\tau)}{\sqrt{\pi(z-\tau)}}\,\mathrm{d}\tau\right). \tag{4.22}$$

Changing back to the original variables via the transformation $U = u\mathrm{e}^{\sigma z}$, the radiation expression (4.22) becomes

$$\frac{\mathrm{d}}{\mathrm{d}z}\int_{\ell/2}^{\infty}\mathrm{e}^{2\sigma z}|u|^2\,\mathrm{d}t = -\sqrt{2}\,\mathrm{Im}\left(\mathrm{e}^{-\mathrm{i}\pi/4}\mathrm{e}^{\sigma z}u^*(\ell/2,z)\frac{\mathrm{d}}{\mathrm{d}z}\int_0^z \frac{\mathrm{e}^{\sigma\tau}u(\ell/2,\tau)}{\sqrt{\pi(z-\tau)}}\,\mathrm{d}\tau\right). \tag{4.23}$$

Carrying out the differentiation on the left hand side and simplifying the right hand side, the radiation expression becomes

$$\frac{\mathrm{d}}{\mathrm{d}z}\int_{\ell/2}^{\infty}|u|^2\,\mathrm{d}t = \mathrm{e}^{-\sigma z}u^*(\ell/2,z)\frac{\mathrm{d}}{\mathrm{d}z}\int_0^z \frac{u(\ell/2,\tau)\mathrm{e}^{\sigma\tau}}{\sqrt{\pi(z-\tau)}}\,\mathrm{d}\tau, \tag{4.24}$$

which gives the total mass radiated to the right away from the pulse. In deriving this final expression, a term proportional to σ, the loss parameter, was left out as it has already been included via the original mass conservation equation (4.7) and so does not contribute to the extra mass radiated away from the pulse.

Combining this expression for mass radiated to the right away from the pulse with an analogous expression for mass radiated to the left, and remembering that this shed radiation must come from the pulse, via mass conservation, the original mass conservation equation (4.11) is modified to

$$\frac{\mathrm{d}}{\mathrm{d}z}\int_{-\infty}^{\infty}\rho\,\mathrm{d}t = -2\sigma\left(2\eta^2 w + \ell g^2\right) - 2\mathrm{e}^{-\sigma z} r\frac{\mathrm{d}}{\mathrm{d}z}\int_0^z \frac{r\mathrm{e}^{\sigma(\tau)}}{\sqrt{\pi(z-\tau)}}\,\mathrm{d}\tau. \tag{4.25}$$

This modified mass conservation relation then includes the extra mass loss from the pulse due to shed dispersive radiation. Here $r = |u(\ell/2, z)|$ is the height of the shelf at its edges $t = \pm\ell/2$. As above, where the expressions for shelf width, ℓ, and the steady state amplitude, $\hat{\kappa}$, were assumed to be the same as in Kath and Smyth [22], the shelf height r is assumed to be the same as for the lossless case $\sigma = 0$, for similar reasons. Taking r to be the same as for the lossless case $\sigma = 0$ is valid in the slowly varying limit when loss σ is small. So in the current work, for small fibre loss σ, the shelf height will be the same as that discussed earlier, namely

$$r^2 = \frac{3\hat{\kappa}}{8}\left(2\eta^2 w - 2\hat{\kappa} + \frac{3\pi^2}{8\hat{\kappa}}g^2\right). \tag{4.26}$$

As in Section 2.2, the modified mass conservation equation (4.25) must be incorporated into the evolution equations (4.14)–(4.16). As the variable g is linked to the radiation under the evolving pulse, it is the equation for g which is modified to include loss to dispersive radiation. In this manner equation (4.15) for g becomes

$$\frac{\mathrm{d}g}{\mathrm{d}z} = -\frac{2\eta}{3\pi}\left(\eta^2 - w^{-2}\right) - \sigma g - 2\alpha g, \tag{4.27}$$

where the equation for α is

$$\alpha = \frac{3\hat{\kappa}}{8}\frac{1}{r}\mathrm{e}^{-\sigma z}\frac{\mathrm{d}}{\mathrm{d}z}\int_0^z \frac{r\mathrm{e}^{\sigma\tau}}{\sqrt{\pi(z-\tau)}}\,\mathrm{d}\tau. \tag{4.28}$$

Setting $\sigma = 0$ in the equation for g will reproduce the equation of Kath and Smyth [22] as discussed in Section 2.2, as required.

The full set of approximate equations describing pulse evolution in the pres-

ence of fibre loss is given by

$$\frac{\mathrm{d}g}{\mathrm{d}z} = -\frac{2\eta}{3\pi}\left(\eta^2 - w^{-2}\right) - \sigma g - 2\alpha g, \tag{4.29}$$

$$\frac{\mathrm{d}}{\mathrm{d}z}(\eta w) = \frac{\ell g}{\pi}\left(\eta^2 - \frac{1}{2}w^{-2}\right) - \sigma\eta w, \tag{4.30}$$

$$\frac{\mathrm{d}}{\mathrm{d}z}\left(\frac{\eta^2}{w} - 2\eta^4 w\right) = 2\sigma\left(4\eta^4 w - \frac{\eta^2}{w}\right), \tag{4.31}$$

$$\alpha = \frac{3\hat{\kappa}}{8}\frac{1}{r}\mathrm{e}^{-\sigma z}\frac{\mathrm{d}}{\mathrm{d}z}\int_0^z \frac{r\mathrm{e}^{\sigma\tau}}{\sqrt{\pi(z-\tau)}}\,\mathrm{d}\tau, \tag{4.32}$$

$$r^2 = \frac{3\hat{\kappa}}{8}\left(2\eta^2 w - 2\hat{\kappa} + \frac{3\pi^2}{8\hat{\kappa}}g^2\right). \tag{4.33}$$

4.3 Amplification of Pulse

In a fibre with loss, the pulse will have to be periodically amplified and reshaped if it is to travel any useful distance. One method of amplification is to use the Raman gain of the fibre itself. A light wave incident on the fibre material can excite the resonance. In doing so an incident photon is annihilated to create a photon at a downshifted frequency along with a phonon which conserves energy and momentum. This is known as Raman scattering and plays an important part in light wave propagation in nonlinear optics. In Raman amplification a pump wave with a frequency higher than the soliton frequency is passed through the fibre simultaneously with the carrier wave. The pump wave excites the Raman effect in the fibre stimulating photon creation at the lower soliton frequency. When properly tuned, this will cancel the fibre loss. This is known as Raman amplification and was first proposed by Hasegawa [17]. It has been shown to successfully amplify the soliton and aid in the long-distance transmission of solitons [42, 44]. However, Raman amplification has a drawback in that it can lead to crosstalk between different channels in wavelength-division multiplexing (WDM) systems which can seriously degrade performance. Also the pump wave which is responsible for the Raman amplification requires relatively large amounts of power.

An alternative to Raman amplification is to use another type of all-optical amplifier known as a doped fibre amplifier. These are simple, highly efficient devices and, being all-optical, they are very fast. In addition, they are easily implemented in a fibre optic system as they merely involve doping sections of the fibre with rare-earth metals. A small, low-power diode laser is used to excite the rare-earth metal ions in the doped section of the fibre. The carrier wave then stimulates photon emission from the excited rare-earth metal ions. In particular,

the erbium-doped fibre amplifier (EDFA) [35] is of special interest as it operates near the 1.5μm wavelength region where the optical fibre assumes minimum loss. It has been demonstrated that EDFA's successfully reshape solitons in fibre optic systems [45] and current amplification of fibre optic cables involve EDFA's for amplification.

In optical applications if the dispersion distance is much longer than the amplifier spacing, the amplifiers can be treated as continuous. This is known as the distributed-amplifier approximation. At this point it would be useful to define the soliton width and its relation to dispersion distance. We define the width in the standard fashion as the width which corresponds to half the peak power of the soliton (FWHM). So the soliton width of an optical soliton which has an amplitude of $\text{sech}(\tau/t_0)$ is given by

$$\tau_s = 1.76 t_0. \tag{4.34}$$

The pulse width τ_s can be related to the dispersion distance by equation (1.2) as

$$z_0 = -\left(\frac{\tau_s}{1.76}\right)^2 \frac{1}{k''}. \tag{4.35}$$

According to Malomed [29], solitons with widths of 10 picoseconds (ps) or greater typically satisfy the distributed-amplifier approximation. Solitons intended for use in long-distance telecommunications generally have widths that range from 10 to 20 ps. In this width range the amplifiers can be taken to balance loss on a continuous basis, which is equivalent to setting $\sigma = 0$. However, for narrow solitons, where the dispersion distance may be less than the amplifier spacing, amplifiers have to be treated as discrete. However making the solitons too narrow presents its own set of difficulties. The smaller the pulse width, the more important higher order effects become in the NLS equation. In general for solitons with widths less than 0.1 ps higher order effects must be accounted for [2]. For the present amplifier analysis, a balance was chosen between narrow pulses which satisfy the discrete amplifier approximation, but wide enough so that we can neglect higher order effects.

To model the effect of discrete amplifiers, at each amplifier the amplitude, η, and shelf height, g, are simultaneously multiplied by a factor of $(1 + \zeta)$, where ζ is the amplifier coefficient. The modified pulse plus shelf is then treated as a new initial condition. At each amplifier the shelf is incorporated into the pulse by adding the shelf mass to its mass and adjusting the width of the pulse to reflect this. Mass conservation then gives the new width, w_1, of the pulse as

$$2\eta^2 w + \ell g^2 = 2\eta^2 w_1 \tag{4.36}$$

so that,

$$w_1 = w + \frac{\ell g^2}{2\eta^2}. \tag{4.37}$$

Here η is the amplitude of the pulse after amplification. At this point we now have a new initial value problem with initial conditions η for the amplitude and w_1 for the width. The pulse then propagates along the new section of fibre to the next amplifier according to the approximate equations (4.29)–(4.33) or the perturbed NLS equation (4.1).

4.4 Results

Full numerical solutions of the perturbed NLS equation (4.1) were compared with numerical solutions of the approximate equations (4.29)–(4.33). The nondimensionalised fibre loss term σ is defined as damping rate per distance and is wavelength dependent. So for a given wavelength, changing the scaling of the NLS equation will alter the fibre loss σ. As was discussed at the beginning of the chapter, the minimum fibre loss is $\delta = 0.2$ dB/km at a wavelength of 1.55μm. Using this value of fibre loss, a normalised fibre loss of $\sigma = 0.3$ will correspond to a dispersion distance of $z_0 = 12.5$ km.

4.4.1 Modifications to Full Numerical Code

As was discussed in Section 3.1 perturbed NLS equations can be solved using the integrating factor method. The perturbations due to loss to the NLS equation (1.1) can be incorporated into the integrating factor. The perturbed NLS equation incorporating fibre loss and damping at boundaries is

$$\mathrm{i}u_z + \frac{1}{2}u_{tt} + |u|^2 u + \mathrm{i}\theta(t)u = -\mathrm{i}\sigma u. \tag{4.38}$$

Fourier transforming this equation gives

$$\frac{\mathrm{d}\hat{u}}{\mathrm{d}z} + \frac{\mathrm{i}}{2}\omega^2\hat{u} = \mathrm{i}F\left\{|u|^2u\right\} - F\left\{\theta(t)u\right\} - \sigma\hat{u}, \tag{4.39}$$

where σ is the fibre loss. This loss term can now be incorporated into the integrating factor of equation (3.5) as

$$\frac{\mathrm{d}}{\mathrm{d}z}\left[\hat{u}\exp\left(\frac{\mathrm{i}\omega^2 z}{2} + \sigma z\right)\right] = \left[\mathrm{i}F\left\{|u|^2u\right\} - F\left\{\theta(t)u\right\}\right]\exp\left(\frac{\mathrm{i}\omega^2 z}{2} + \sigma z\right). \tag{4.40}$$

This equation is now solved numerically using the Runge-Kutta procedure outlined in Section 3.1.

4.4.2 Modification to Approximate Numerical Code

To numerically evaluate the radiation loss integral (4.28) a modification to the method of Section 3.2 is necessary. The radiation integral is now of the form

$$M = \int_0^z \frac{r\mathrm{e}^{\sigma\tau}}{\sqrt{\pi(z-\tau)}}\,\mathrm{d}\tau. \tag{4.41}$$

Following the method of [37] outlined in Section 3.2, the integral (4.41) is written as the sum of two integrals

$$M = M_1 + M_2, \tag{4.42}$$

where

$$M_1 = \int_0^m \frac{r(\tau)\mathrm{e}^{\sigma\tau}}{\sqrt{z-\tau}}\,\mathrm{d}\tau \tag{4.43}$$

and

$$M_2 = \int_m^z \frac{r(\tau)\mathrm{e}^{\sigma\tau}}{\sqrt{z-\tau}}\,\mathrm{d}\tau. \tag{4.44}$$

Again, as M_1 does not contain a singularity, it can be evaluated directly using the Trapezoidal Rule.

The integral M_2 is evaluated by dividing it into the sum of many small integrals as

$$M_2 = \sum_{i=k}^{n} M_2^i = \sum_{i=k}^{n} \int_{z_i}^{z_{i+1}} \frac{r\mathrm{e}^{\sigma\tau}}{\sqrt{z-\tau}}\,\mathrm{d}\tau, \tag{4.45}$$

where $z_k = m$ and $z_{n+1} = z$. In the region $z_i < \tau < z_{i+1}$ of integration the numerator of (4.45) is approximated by a linear function as

$$r(\tau)\mathrm{e}^{\sigma\tau} = r(z_i)\mathrm{e}^{\sigma z_i} + (\tau - z_i)r', \tag{4.46}$$

where the derivative r' is

$$r' = \frac{r(z_{i+1})\mathrm{e}^{\sigma z_{i+1}} - r(z_i)\mathrm{e}^{\sigma z_i}}{z_{i+1} - z_i}. \tag{4.47}$$

Placing this expression for $r(\tau)\mathrm{e}^{\sigma\tau}$ in equation (4.45) gives

$$M_2^i = \int_{z_i}^{z_{i+1}} \frac{r(z_i)\mathrm{e}^{\sigma z_i} + r'(\tau - z_i)}{\sqrt{z-\tau}}\,\mathrm{d}\tau. \tag{4.48}$$

After rearranging the numerator as in (3.24) this integral can be evaluated exactly as

$$\begin{aligned} M_2^i = {} & 2\left(r(z_i)\mathrm{e}^{\sigma z_i} + r'(z - z_i)\right)\left(\sqrt{z-z_i} - \sqrt{z-z_{i+1}}\right) \\ & + \frac{2}{3}r'\left((z-z_{i+1})^{3/2} - (z-z_i)^{3/2}\right). \end{aligned} \tag{4.49}$$

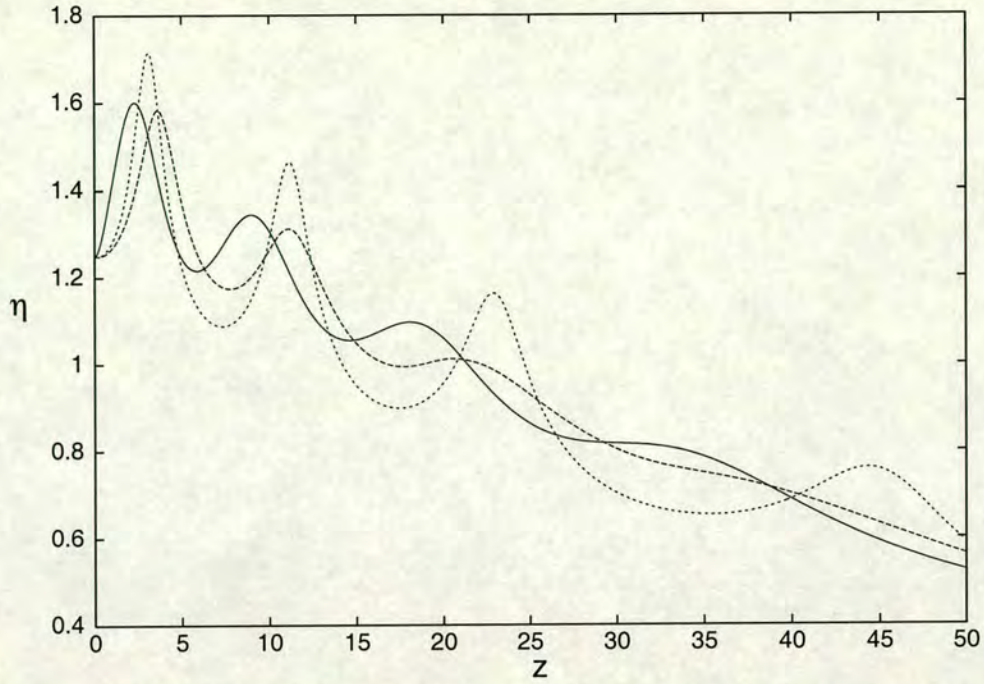

Figure 4.1: Pulse amplitude η as a function of distance z with $\sigma = 0.01$ and boundary condition $u(0,t) = 1.25\,\mathrm{sech}\,t$. Approximate solution with radiation: – – –; without radiation: - - -; full numerical solution: —.

4.4.3 Numerical Results

Figure 4.1 shows a comparison between the solutions of the approximate equations (4.29)–(4.33), with and without radiation loss, and the full numerical solution of the perturbed NLS equation (4.1). The loss parameter is set to $\sigma = 0.01$ and the boundary condition is a non-NLS soliton pulse with $\eta = 1.25$ and $w = 1$. As can be seen in Figure 4.1, for low values of fibre loss σ the inclusion of radiation loss gives approximate solutions in much better agreement with full numerical solutions. This shows that for low fibre loss it is necessary to include radiation loss to adequately describe the evolution of a pulse in a lossy fibre. The phase shift between the numerical and approximate solutions apparent in this figure is a result of assuming the instantaneous formation of the shelf [22]. However, as mentioned above, an accurate determination of the phase is not necessary in the present work and so this phase difference is not critical.

Figure 4.1 shows a comparison for a non-soliton boundary condition. It is of interest to see how a pulse would evolve under the same conditions, but with a soliton boundary condition. Figure 4.2 shows such a comparison between the solutions of the approximate equations (4.29)–(4.33), again both with and without radiation loss, and the full numerical solution of the perturbed NLS equation (4.1). The loss is the same as in Figure 4.1, $\sigma = 0.01$, but the boundary condition is an NLS soliton with $\eta = w = 1.0$. As can be seen in Figure 4.2, there is little

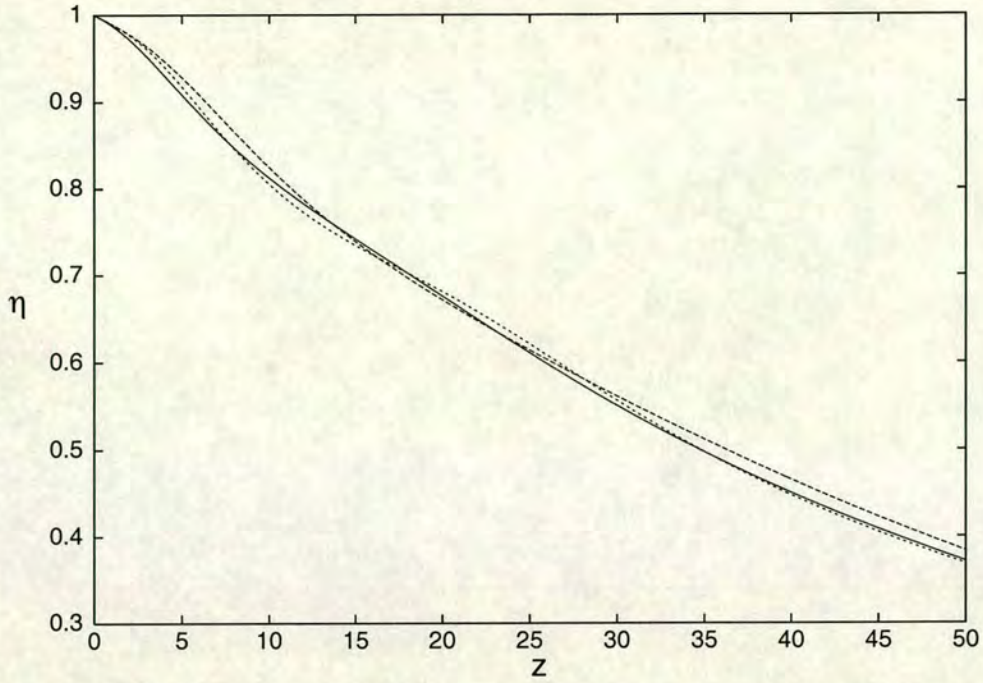

Figure 4.2: Pulse amplitude η as a function of distance z with $\sigma = 0.01$ and boundary condition $u(0,t) = \operatorname{sech} t$. Approximate solution with radiation: – – –; without radiation: - - -; full numerical solution: —.

radiation shed by the pulse as it evolves and including radiation loss yields no improvement in the agreement with the full numerical solution. This is because optical pulses mainly shed radiation in an attempt to become a soliton. Once this state is achieved, or nearly achieved, the amount of shed radiation drops dramatically, so that at this point the radiation loss is less important. This can be seen in equation (4.25) for conservation of mass. The pulse loses mass at a rate proportional to r. As was discussed in Section 2.2, r is found by examining the relation between the amount of mass present in the pulse at a given value of z and the amount of mass present at the fixed point. When these are nearly equal, r, the shelf height, will become very small, decreasing the rate of mass loss due to radiation.

For loss values approximately equal to the real loss value of $\sigma = 0.3$ the picture is more ambiguous. Figure 4.3 shows a comparison between the solutions of the approximate equations (4.29)–(4.33), both with and without radiation loss, and the full numerical solution of the perturbed NLS equation (4.1). As mentioned above, the real fibre loss is $\sigma = 0.3$. The boundary condition chosen was a non-NLS soliton pulse with $\eta = 1.25$ and $w = 1$. As can be seen in Figure 4.3, the approximate solutions are virtually identical while the full numerical solution slowly oscillates. For this value of fibre loss it appears that including radiation loss may not be necessary, but it is difficult to draw any firm conclusions.

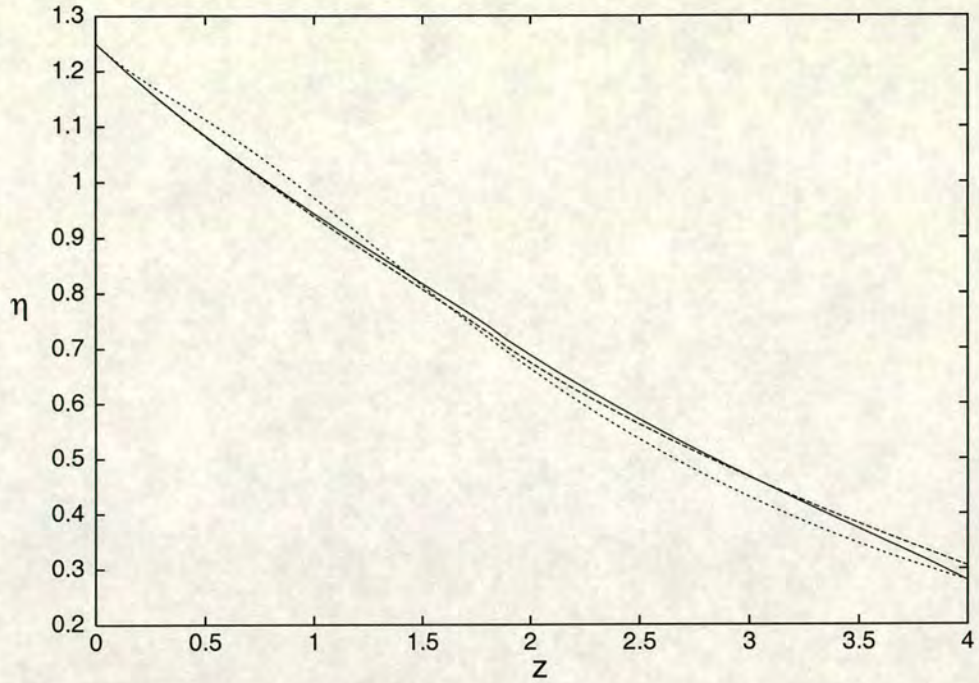

Figure 4.3: Pulse amplitude η as a function of distance z with $\sigma = 0.3$ and boundary condition $u(0,t) = 1.25\,\mathrm{sech}\,t$. Approximate solution with radiation: – – –; without radiation: - - -; full numerical solution: —.

For large values of fibre loss σ, radiation loss plays little part in pulse evolution. Figure 4.4 shows a comparison between the solution of the approximate equations (4.29)–(4.33), both with and without radiation loss, and the full numerical solution of the perturbed NLS equation (4.1). The fibre loss parameter is $\sigma = 0.5$ and the boundary condition is a non-NLS soliton with $\eta = 1.25$ and $w = 1$. As can be seen from Figure 4.4, the large fibre loss completely dominates the evolution of the pulse, so that radiation losses are negligible by comparison. This value of fibre loss is well above real values for this scaling and is only included to test the model.

In a potential soliton-based communication systems using EDFA's for pulse amplification, the optical amplifiers would be spaced anywhere from 30–100 km apart, depending on implementation. To reflect this, a different scaling was used with $z = 1$ corresponding to a dispersion distance of $z_0 = 60$ km, which gives a normalised fibre loss of $\sigma = 1.5$. Taking the amplifiers to be 60 km apart then means that the discrete amplifier approximation is correct as the dispersion length is roughly equal to the amplifier spacing. In analysing the effects of dispersive radiation in Section 4.2 it was assumed that the fibre loss σ would be small. However with the scaling being used this is no longer the case. As a result the radiation analysis of Section 4.2 may not strictly be applicable. Figure 4.5 shows a comparison between the solution of the approximate equations (4.29)–(4.33) with

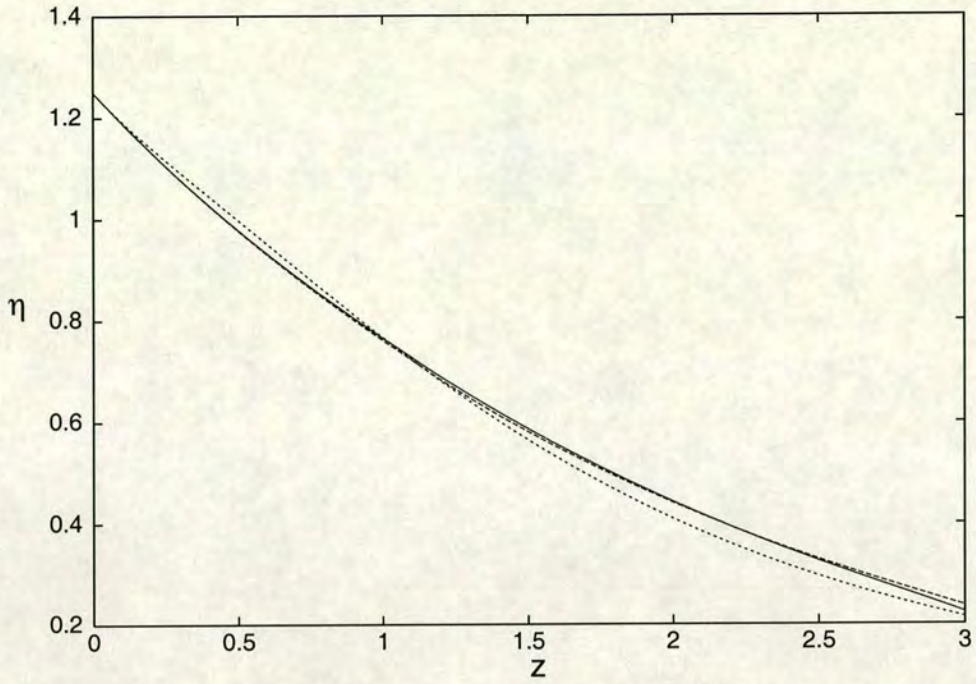

Figure 4.4: Pulse amplitude η as a function of distance z with $\sigma = 0.5$ and boundary condition $u(0,t) = 1.25\,\mathrm{sech}\,t$. Approximate solution with radiation: – – –; without radiation: - - -; full numerical solution: —.

radiation loss, and the full numerical solution of the perturbed NLS equation (4.1) travelling a distance of almost 1000 km. The fibre loss is $\sigma = 1.5$ and the boundary condition is an NLS soliton with $\eta = w = 1.0$. It can be seen in Figure 4.5 that the full numerical and approximate solution diverge over time. This is because small differences between the two solutions are magnified at each amplifier, leading to growing errors. Also, as mentioned above, the radiation analysis is no longer strictly valid for such a large value of fibre loss. However, initially at least, the comparison is very good and divergence only sets in after a significant distance has been travelled.

While the comparison in all of the above figures was good, the approximate equations gave the best agreement for small fibre loss σ. As will be seen in the next chapter, modelling sliding frequency filters with fibre loss greatly benefits from the analysis of the present chapter of fibre loss. The most important effects included in this analysis are the independently varying amplitude and width of the pulse and the inclusion of the radiation propagating away from the pulse. As will be shown, inclusion of both of these effects proves essential for an accurate model of pulse evolution when filters, fibre loss and amplification are included.

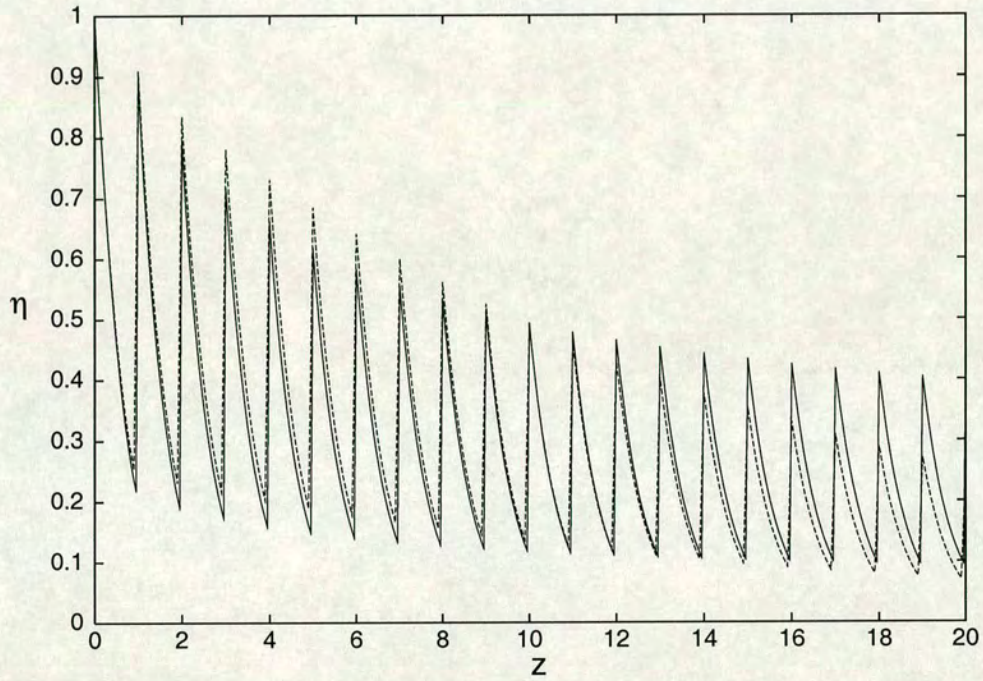

Figure 4.5: Pulse amplitude η as a function of distance z with $\sigma = 1.5$ and periodic amplification at each distance unit z. Boundary condition $u(0,t) = \operatorname{sech} t$. Full numerical solution: —; Approximate solution with radiation: $- - -$.

Chapter 5

Sliding-Frequency Filters

Sliding-frequency filters (SFF's) are used to suppress the effect of the spontaneous noise generated by erbium doped fibre amplifiers (EDFA's) (see Section 4.3) in optical communication systems [20, 41]. These all-optical amplifiers are used to counteract the loss inherent in fibre optic cables. However, while the EDFA's amplify the signal, they also amplify the noise in the system. In a soliton based communication system, this noise amplification causes a shift in the soliton parameters, most importantly in its amplitude and frequency. As the soliton frequency is coupled to its velocity, this then causes random fluctuations in the soliton velocity and thus in the arrival time of the soliton. This negative effect of amplification is known as Gordon-Haus (GH) jitter [14].

To reduce the effect of noise, optical filters are used [36]. A fixed-frequency filter can reduce GH jitter by creating an attractive value of soliton frequency, and thus velocity. Random noise will therefore not drive the soliton too far from its preferred velocity, reducing fluctuations in the soliton arrival time. However, a fixed-frequency filter is unable to reduce radiation within the filter's passband. To reduce this noise, an SFF is employed [41]. An SFF allows the central frequency of the filter to change along the length of the fibre. As the filter passband changes, the nonlinear soliton re-adjusts to this new frequency, while the linear radiation underneath does not. In this way radiation around and under the soliton is filtered out, reducing GH jitter.

There is no exact solution of the perturbed NLS equation which results when the effect of SFF's are added. Therefore it is a perfect candidate for approximate and numerical analysis methods. As mentioned above, to counteract the pulse damping due to the filtering and the inherent fibre loss, periodically spaced optical amplifiers are used, which in the limit of the amplifier spacing being much smaller than the dispersion length of the soliton, can be modelled by a continuous system of amplifiers [20]. In an experimental and numerical study, Mamyshev and Mollenauer [32] showed that stable soliton propagation was possible with am-

plification for a range of filter sliding rates and strengths. In particular it was found that there are upper and lower bounds on the soliton energy for which stable propagation is possible. For energies below the lower bound, the pulse decays into dispersive radiation due to excessive filtering and for energies above the upper bound, a second soliton is formed, as may be expected from inverse scattering theory [50]. Kodama and Wabnitz [26] used a multiple scales analysis based on a slowly varying NLS soliton to derive ordinary differential equations governing the parameters of a soliton propagating in the presence of SFF's and amplification. It was shown that these equations possessed two fixed points, one of which was stable and the other unstable. It was further shown that the fixed point existed for energies above a certain threshold, in agreement with Mamyshev and Mollenauer [32]. However, the multiple scales analysis did not predict the upper energy bound. Burtsev and Kaup [6] used perturbed inverse scattering theory to derive the same approximate equations governing the soliton parameters as Kodama and Wabnitz [26]. Now, as a perturbed soliton propagates, it sheds dispersive radiation. Burtsev and Kaup [6] deduced that it was this radiation that gave rise to the second soliton. By extending their perturbation analysis to higher order, Burtsev and Kaup [6] obtained estimates on this radiation which enabled them to find an approximation to the upper energy bound. This deduced upper bound was found to be in good agreement with that found from numerical results by Mamyshev and Mollenauer [32]. Soliton propagation in the presence of SFF's was also studied by Malomed and Tasgal [29] using the same multiple scales method of Kodoma and Wabnitz [26], but for ultra-short pulses for which the amplifiers must be taken as discrete.

All of the previous analytical work on pulse propagation in the presence of SFF's was based on a slowly varying soliton. However, the choice of a slowly-varying NLS soliton as the approximate solution of the perturbed NLS equation has drawbacks. Firstly, the evolution equations obtained using this assumption monotonically evolve to a steady state in the presence of amplification and filtering. However this is not reflected in full numerical solutions of the perturbed NLS equation (5.1) where amplitude oscillations are present. These oscillations are due to variations in the amplitude/width relation and oscillations of mass and energy between the pulse and shelf of radiation on which the pulse sits. Both of these factors lead to oscillations in the evolving pulse which are seen in full numerical solutions. The present work takes both of these factors into account. Furthermore, radiation is shed by the pulse. The effect of this shed radiation is to damp the amplitude oscillations, driving the pulse to a steady soliton. Again, this behaviour is seen in full numerical solutions of (5.1) and is included in the

present analysis. While the second order perturbed inverse scattering work of [6] does find equations for this shed radiation, it does not include the coupling of this radiation to the evolving pulse and the equations for the soliton amplitude and velocity are the same as those of [26, 29]. Again, there is no need to take into account this dispersive radiation away from the pulse as there are no amplitude oscillations to damp due to the monotonic evolution.

In this chapter the analysis method of Chapter 2 will be extended to study the evolution of pulses under the action of SFF's, fibre loss and amplification. It is found that the approximate equations of this chapter give solutions in better agreement with numerical solutions than those of [6, 26, 29]. The main reason for this is that the amplitude and width oscillations of the pulse are now independent. The present approximate equations also give the same lower energy bound for stable pulse propagation as [6, 26]. However, in addition by using mass and energy conservation, an approximation to the upper energy bound due to the formation of a second soliton is also found. This new upper bound is found to be in good agreement with numerical results.

5.1 Approximate Equations

Light propagating in a monomode, polarisation-preserving, nonlinear optical fibre operating in the anomalous group-velocity dispersion regime is described by the NLS equation [19]. When the effects of fibre loss and an SFF are added, the governing equation is the perturbed NLS equation

$$\mathrm{i}\frac{\partial u}{\partial z} + \frac{1}{2}\frac{\partial^2 u}{\partial t^2} + |u|^2 u = -\mathrm{i}\sigma u + \mathrm{i}\gamma\left(\frac{\partial}{\partial t} + \mathrm{i}\Omega z\right)^2 u \tag{5.1}$$

in nondimensional form [20]. Equation (5.1) is valid when the dispersion length is longer than the amplifier/filter spacing. Here u is the complex-valued envelope of the pulse, z is the normalised spatial variable along the length of the fibre and t is the normalised time in a frame moving with the linear group velocity. The first term on the right hand side represents uniform fibre loss, where σ is the loss parameter [19]. The second term represents an SFF with filter strength γ and frequency sliding rate Ω [20]. When the amplifier spacing is much smaller than the dispersion length scale of the soliton, the term $-\mathrm{i}\sigma u$ on the right hand side of (5.1) represents the excess gain over loss for $\sigma < 0$ [19, 20].

The dimensionless filter and loss parameters, γ, Ω and σ can be related to physical parameters, assuming that one uses Fabry-Perot filters with mirror re-

flectivity r, via

$$\gamma = \frac{1}{2}\frac{z_0}{z_a}\frac{1}{(\mathrm{FSR}\, t_0)^2}\frac{r}{(1-r)^2} \tag{5.2}$$

$$\Omega = 2\pi f' t_0 z_0 \tag{5.3}$$

$$|\sigma| = \frac{1}{2}\sigma_r z_0 \tag{5.4}$$

where z_0 is the dispersion length (1.2). z_a is the spacing between amplifier/filter points. FSR is the free spectral range of the filter and f' is the sliding rate of the filter, measured in frequency per distance. σ_r is the dimensional excess gain, measured in units of inverse distance. Taking typical values of the dimensional parameters to be [6, 32] $k'' = -2.2$ ps^2/km, $t_0 = 16$ ps, $z_a = 39$ km, $\sigma_r = 1.5$ Mm^{-1} and $f' = 13$ GHz/Mm gives $z_0 = 116$ km, $\gamma = 0.2$, $\Omega = 0.15$ and $\sigma = 0.085$. As the dispersion length z_0 is longer than the filter/amplifier spacing z_a the perturbed NLS equation (5.1) is valid.

For this perturbed NLS equation (5.1), the conservation and moment equations (2.9)–(2.11) and (2.13) are modified to

$$\frac{\mathrm{d}}{\mathrm{d}z}\int_{-\infty}^{\infty}\rho\,\mathrm{d}t = -\int_{-\infty}^{\infty}\left[\left(2\sigma+2\gamma\Omega^2z^2\right)\rho+4\gamma\Omega zJ+2\gamma\left(E+\rho^2\right)\right]\mathrm{d}t, \tag{5.5}$$

$$\begin{aligned}\frac{\mathrm{d}}{\mathrm{d}z}\int_{-\infty}^{\infty}J\,\mathrm{d}t = &-\int_{-\infty}^{\infty}\left[\left(2\sigma+2\gamma\Omega^2z^2\right)J+4\gamma\Omega z\left(E+\rho^2\right)\right.\\ &\left.+\mathrm{i}\gamma\left(u_tu_{tt}^*-u_t^*u_{tt}\right)\right]\mathrm{d}t,\end{aligned} \tag{5.6}$$

$$\begin{aligned}\frac{\mathrm{d}}{\mathrm{d}z}\int_{-\infty}^{\infty}E\,\mathrm{d}t = &\int_{-\infty}^{\infty}\left[\left(2\sigma+2\gamma\Omega^2z^2\right)\left(\rho^2-E\right)\right.\\ &+2\gamma\left(4|u_t|^2|u|^2+(u^*)^2u_t^2+u^2(u_t^*)^2-|u_{tt}|^2\right)\\ &\left.+2\mathrm{i}\gamma\Omega z\left(u_t^*u_{tt}-u_tu_{tt}^*+2|u|^2uu_t^*-2|u|^2u^*u_t\right)\right]\mathrm{d}t,\end{aligned} \tag{5.7}$$

$$\begin{aligned}\frac{\mathrm{d}}{\mathrm{d}z}\int_{-\infty}^{\infty}tJ\,\mathrm{d}t = &\int_{-\infty}^{\infty}\left[E+\frac{1}{2}\rho^2-\left(2\sigma+2\gamma\Omega^2z^2\right)tJ+\mathrm{i}\gamma t\left(u_t^*u_{tt}-u_tu_{tt}^*\right)\right.\\ &\left.-4\gamma\Omega zt\left(E+\rho^2\right)\right]\mathrm{d}t.\end{aligned} \tag{5.8}$$

The trial solution (2.14) needs to be extended in order to account for two phenomena that are present here. The first is that the pulse no longer travels with a constant group velocity. Also, connected with this, the reference frame is no longer centred at the soliton, but rather at a mean position y. Incorporating these two changes into a trial solution, (2.14) becomes

$$u = \left(\eta\,\mathrm{sech}\,\frac{t-y}{w}+\mathrm{i}g\right)\exp\left[\mathrm{i}\theta+\mathrm{i}V\left(t-y\right)\right], \tag{5.9}$$

where V is the deviation from the group velocity. Substituting this new trial

solution (5.9) into the conservation and moment equations (5.5)–(5.8) yields

$$\left(2\eta^2 w + \ell g^2\right)\frac{\mathrm{d}V}{\mathrm{d}z} = -\frac{8}{3}\gamma\left(\Omega z + V\right)\frac{\eta^2}{w}, \tag{5.10}$$

$$\begin{aligned}\frac{\mathrm{d}}{\mathrm{d}z}\left(\frac{\eta^2}{w} - 2\eta^4 w\right) &= 2\left(\sigma + \gamma\Omega^2 z^2 + \gamma V^2 + 2\gamma\Omega z V\right)\left(4\eta^4 w - \frac{\eta^2}{w}\right) \\ &\quad + \gamma\left(\frac{24\eta^4 w^2 - 14\eta^2}{5w^3}\right),\end{aligned} \tag{5.11}$$

$$\begin{aligned}\frac{\mathrm{d}}{\mathrm{d}z}\left(\pi\eta g w\right) &= \frac{2}{3}\left(\frac{\eta^2}{w} - \eta^4 w\right) \\ &\quad - 2\left(\sigma + \gamma\Omega^2 z^2 + 3\gamma V^2 + 4V\gamma\Omega z\right)\pi\eta g w,\end{aligned} \tag{5.12}$$

$$\begin{aligned}\frac{\mathrm{d}}{\mathrm{d}z}\left(2\eta^2 w + \ell g^2\right) &= -2\left(\sigma + \gamma\Omega^2 z^2 + \gamma V^2 + 2\gamma\Omega z V\right)\left(2\eta^2 w + \ell g^2\right) \\ &\quad - \frac{4}{3}\gamma\frac{\eta^2}{w}.\end{aligned} \tag{5.13}$$

The last equation is

$$\frac{\mathrm{d}y}{\mathrm{d}z} = V, \tag{5.14}$$

which links the soliton centre position to the velocity. After some manipulation, the conservation and moment equations (5.10)–(5.13) become

$$\left(2\eta^2 w + \ell g^2\right)\frac{\mathrm{d}V}{\mathrm{d}z} = -\frac{8}{3}\gamma\left(\Omega z + V\right)\frac{\eta^2}{w}, \tag{5.15}$$

$$\begin{aligned}\frac{\mathrm{d}}{\mathrm{d}z}\left(\frac{\eta^2}{w} - 2\eta^4 w\right) &= 2\left(\sigma + \gamma\Omega^2 z^2 + \gamma V^2 + 2\gamma\Omega z V\right)\left(4\eta^4 w - \frac{\eta^2}{w}\right) \\ &\quad + \gamma\left(\frac{24\eta^4 w^2 - 14\eta^2}{5w^3}\right),\end{aligned} \tag{5.16}$$

$$\begin{aligned}\frac{\mathrm{d}}{\mathrm{d}z}\left(\eta w\right) &= -\left(\sigma + \gamma\Omega^2 z^2 + \gamma V^2 + 2\gamma\Omega z V\right)\eta w - \frac{\ell g}{2\pi}\frac{1 - 2\left(\eta w\right)^2}{w^2} \\ &\quad + \frac{\gamma}{5}\frac{\eta}{w},\end{aligned} \tag{5.17}$$

$$\begin{aligned}\frac{\mathrm{d}g}{\mathrm{d}z} &= \frac{2}{3\pi}\frac{\eta}{w^2}\left[1 - \left(\eta w\right)^2\right] - \left(\sigma + \gamma\Omega^2 z^2 + 5\gamma V^2 + 6\gamma\Omega z V\right)g \\ &\quad - \frac{\gamma}{5}\frac{g}{w^2}.\end{aligned} \tag{5.18}$$

In deriving these equations, terms of $O(g^2)$ and higher have been dropped, except for the quadratic term in g proportional to ℓ, since this term is important in mass conservation [22].

For the case of the NLS equation (1.1) and as discussed in Section 2.1, Kath and Smyth [22] found the length ℓ of the shelf by matching the frequency of oscillation of the solution of the NLS approximate equations near the fixed point $\eta = \hat{\kappa}$, $w = 1/\hat{\kappa}$ to the steady NLS soliton oscillation frequency $\hat{\kappa}^2/2$, obtaining equation (2.21), where $\hat{\kappa}$ was given by (2.22). However, the situation for the

perturbed NLS equation (5.1) is the same as that of Section 4.1. The only fixed point of the present approximate equations (5.14)–(5.18) in the absence of amplification is $\eta = 0$ due to the loss terms. Therefore the method of [22] cannot be used to determine ℓ. If the loss parameters σ and γ are small, then a slowly varying approximation to ℓ is (2.21). In a similar vein, since the fixed point of the present approximate equations (5.14)–(5.18) (in the absence of amplification) is $\eta = \hat{\kappa} = 0$, the NLS fixed point (2.22) will be used to determine ℓ via (2.21). For σ and γ small, $\hat{\kappa}$ given by (2.22) is not constant, but slowly varying in z. This slowly varying approximation gives the local value of amplitude $\hat{\kappa}$ that the pulse would achieve if the fibre loss and filter strength were set instantaneously to zero. Furthermore, with this value of ℓ, setting $\sigma = \gamma = 0$ in the present approximate equations (5.15)–(5.18) reduces the equations to those derived from an averaged Lagrangian by Kath and Smyth [22]. However, as will be discussed in Section 5.3.3, steady state solutions of (5.14)–(5.18) do exist when the amplification ($\sigma < 0$) is sufficient to compensate for the filtering. The form of that fixed point will be discussed in Section 5.3.3.

Kodama and Wabnitz [26] and Malomed and Tasgal [29] derived another set of approximate equations for the pulse amplitude and velocity based on another trial function. Their method uses a trial solution in the form of an NLS soliton with variable parameters

$$u = \eta \operatorname{sech}(\eta(t-y)) \exp(-\mathrm{i}\theta - \mathrm{i}V(t-y)). \tag{5.19}$$

This trial solution assumes that the amplitude η and width η^{-1} of the pulse are inversely related. The pulse phase is θ and the pulse velocity is V. Finally the parameters are all functions of t. Based on this trial solution, Kodama and Wabnitz [26] used the method of multiple scales and Malomed and Tasgal [29] used the balance-equation technique [28] to derive the following approximate equations for the pulse parameters of (5.19)

$$\frac{\mathrm{d}\eta}{\mathrm{d}z} = -2\eta\left\{\sigma + \gamma\left[\frac{\eta^2}{w} + (V-\Omega z)^2\right]\right\}, \tag{5.20}$$

$$\frac{\mathrm{d}V}{\mathrm{d}z} = -\frac{4}{3}\eta^2\gamma(V-\Omega z). \tag{5.21}$$

Notice that setting $\eta = 1/w$ and $g = 0$ in the present approximate equations (5.15)–(5.18) give these equations, as expected.

The approximate equations (5.14)-(5.18) along with (2.21) and (2.22) for ℓ and $\hat{\kappa}$ are not yet complete as they do not incorporate the effect of the dispersive radiation shed by the evolving pulse. This shed radiation is the subject of the next section.

5.2 Radiation Loss

Following the method of Section 2.2 and that of Kath and Smyth [22], the effect of the shed radiation on the evolution of the pulse will be analysed.

As the shed radiation has small amplitude, the nonlinear term in the perturbed NLS equation (5.1) is negligible away from the pulse. Therefore, the equation governing the shed radiation is

$$\mathrm{i}u_z + \frac{1}{2}u_{tt} = -\mathrm{i}\sigma u + \mathrm{i}\gamma u_{tt} - 2\Omega z\gamma u_t - \mathrm{i}\gamma\Omega^2 z^2 u. \tag{5.22}$$

The substitution

$$u = U(t,z)\exp\left(-\sigma z - \frac{1}{3}\gamma\Omega^2 z^3\right) \tag{5.23}$$

transforms the linearised equation (5.22) to

$$\mathrm{i}U_z + \left(\frac{1}{2} - \mathrm{i}\gamma\right)U_{tt} = -2\Omega z\gamma U_t. \tag{5.24}$$

Now the conservation of mass equation for this transformed radiation equation (5.24) is

$$\begin{aligned}\frac{\partial}{\partial z}|U|^2 =& \frac{\mathrm{i}}{2}\frac{\partial}{\partial t}\left(U^*U_t - UU_t^*\right) + \gamma\frac{\partial}{\partial t}\left(U^*U_t + UU_t^*\right) - 2\gamma|U_t|^2 \\ &- 2\mathrm{i}\Omega z\gamma\left(UU_t^* - U^*U_t\right).\end{aligned} \tag{5.25}$$

Integrating this mass equation from the edge of the shelf $t = y+\ell/2$ to $t = \infty$, and noticing that the last two terms on the right hand side in (5.25) do not represent radiation shed from the pulse, yields an expression for the mass radiated to the right away from the pulse as

$$\begin{aligned}\frac{\mathrm{d}}{\mathrm{d}z}\int_{y+\ell/2}^{\infty}|U|^2\,\mathrm{d}t =& -V|U|^2_{t=y+\ell/2} + \mathrm{Im}\left(U^*U_t\right)|_{t=y+\ell/2} \\ &- 2\gamma\,\mathrm{Re}\left(U^*U_t\right)|_{t=y+\ell/2}.\end{aligned} \tag{5.26}$$

Kath and Smyth [22] used Laplace transforms to solve the linearised NLS equation and thus determined an expression for the mass radiated by the evolving pulse. It was this method that was outlined in Section 2.2 and utilised to study the dispersive radiation with fibre loss in Section 4.2. However the linearised equation (5.24) has non-constant coefficients and so Laplace transforms are not really useful for its analysis. If we assume that the frequency sliding rate, Ω, is small, the non-constant coefficient Ωz in the linearised equation (5.24) is slowly varying, and so may be taken to be constant on the fast scale z. This is equivalent to saying that the filter's central frequency, Ωz, changes slowly over the length

scale z, which is governed by the dispersion length. There is another, related complication in solving (5.24) for which the assumption of small Ω will be needed. The radiation equation (5.24) is a moving boundary problem with an unknown moving boundary since a boundary condition will be imposed at the edge of the shelf $t = y + \ell/2$. The location of the moving boundary is determined by the approximate equations (5.15)–(5.18). Because of this coupling, the radiation equation (5.24) could not be solved even if it had constant coefficients. However if the frequency sliding rate Ω is again taken to be small, the velocity V is then slowly varying on the scale z and so can be taken to be constant. The moving boundary is therefore known and the radiation equation (5.24) can be solved. Once this slowly varying assumption is made, Laplace transforms may then be used to solve the linearised equation (5.24). Doing this, it is found that

$$\left(\frac{1}{2} - \mathrm{i}\gamma\right)\bar{U}_{tt} + 2\Omega z\gamma\bar{U}_t + \mathrm{i}s\bar{U} = 0, \tag{5.27}$$

where an overbar denotes a Laplace transform and s is the Laplace transform variable. The solution of this equation is of the form

$$\bar{U} = \exp(\lambda t) \tag{5.28}$$

with λ given by

$$\lambda = \frac{-2\Omega z\gamma \pm \sqrt{4\Omega^2 z^2\gamma^2 - 4\left(\frac{1}{2} - \mathrm{i}\gamma\right)\mathrm{i}s}}{1 - 2\mathrm{i}\gamma}. \tag{5.29}$$

Neglecting the quadratic term in Ω and using the Taylor series expansion

$$\sqrt{1 - 2\mathrm{i}\gamma} = 1 - \mathrm{i}\gamma + O\left(\gamma^2\right). \tag{5.30}$$

Assuming the filter strength, γ, is small, which was already done to derive an expression for ℓ, the shelf length, the equation for the roots of the characteristic polynomial (5.29) becomes

$$\lambda_\pm = -2\Omega z\gamma \pm \left[\exp\left(-\frac{\mathrm{i}\pi}{4}\right)\sqrt{2s} + \gamma\exp\left(\frac{\mathrm{i}\pi}{4}\right)\sqrt{2s}\right]. \tag{5.31}$$

The root λ_- corresponds to a decaying solution as $t \to \infty$ and the root λ_+ to a growing solution as $t \to \infty$. Choosing the decaying solution, we have

$$\bar{U}_t = \left[-2\Omega z\gamma - \exp\left(-\frac{\mathrm{i}\pi}{4}\right)\sqrt{2s} - \gamma\exp\left(\frac{\mathrm{i}\pi}{4}\right)\sqrt{2s}\right]\bar{U}. \tag{5.32}$$

Inverting using the convolution theorem then gives

$$\begin{aligned} U_t = &-2\Omega z\gamma U - \sqrt{2}\left[\exp\left(-\frac{\mathrm{i}\pi}{4}\right) + \gamma\exp\left(\frac{\mathrm{i}\pi}{4}\right)\right] \\ &\times \left(\frac{\mathrm{d}}{\mathrm{d}z}\int_0^z \frac{U}{\sqrt{\pi(z-\tau)}}\,\mathrm{d}\tau\right). \end{aligned} \tag{5.33}$$

Substituting this expression into the radiated mass equation (5.26) and ignoring quadratic terms in γ, we obtain

$$\frac{\mathrm{d}}{\mathrm{d}z}\int_{y+\ell/2}^{\infty}|U|^2\,\mathrm{d}t = -V|U|^2_{t=y+\ell/2} + (1+\gamma)U^*\frac{\mathrm{d}}{\mathrm{d}z}\int_0^z \frac{u}{\sqrt{\pi(z-\tau)}}\,\mathrm{d}\tau \qquad (5.34)$$

for the mass radiated to the right of the pulse (i.e. into $t > y + \ell/2$). An expression for the mass radiated to the left of the pulse (i.e. into $t < y - \ell/2$) may be obtained in a similar manner, the only difference to the mass expression (5.34) being that the sign of the $V|U|^2$ term is reversed. Then inverting the transformation (5.23) and substituting the right and left mass loss expressions into the mass conservation equation (5.5) for the pulse results in the modified mass conservation equation for the pulse

$$\begin{aligned}\frac{\mathrm{d}}{\mathrm{d}z}\int_{-\infty}^{\infty}\rho\,\mathrm{d}t = -\int_{-\infty}^{\infty}&\left[\left(2\sigma + 2\gamma\Omega^2z^2\right)\rho + 4\gamma\Omega z J + 2\gamma\left(E+\rho^2\right)\right]\,\mathrm{d}t \\ &- 2(1+\gamma)r\exp\left(-\sigma z - \frac{1}{3}\gamma\Omega^2z^3\right) \\ &\times\frac{\mathrm{d}}{\mathrm{d}z}\int_0^z\frac{r\exp\left(\sigma\tau+\frac{1}{3}\gamma\Omega^2\tau^3\right)}{\sqrt{\pi(z-\tau)}}\,\mathrm{d}\tau \qquad (5.35)\end{aligned}$$

which incorporates mass lost to shed dispersive radiation. Again $r = |u(y+\ell/2)|$ is the height of the shelf at its edge. The second term on the right hand side of (5.35) is the mass shed by the pulse in the form of dispersive radiation. When σ and γ are small, the height of the shelf is given by the same expression, to first order, as that in Kath and Smyth [22] and discussed in Section 2.2. Therefore,

$$r^2 = \frac{3\hat{\kappa}}{8}\left(2\eta^2 w - 2\hat{\kappa} + \ell g^2\right). \qquad (5.36)$$

The extra mass loss term in the mass conservation equation (5.35) is incorporated into the approximate equations (5.14)–(5.18) by modifying the equation for g to

$$\begin{aligned}\frac{\mathrm{d}g}{\mathrm{d}z} =& \frac{2}{3\pi}\frac{\eta}{w^2}\left[1-(\eta w)^2\right] - \left(\sigma + \gamma\Omega^2z^2 + 5\gamma V^2 + 6\gamma\Omega z V\right)g \\ &- \frac{\gamma}{5}\frac{g}{w^2} - 2\alpha(1+\gamma)g,\end{aligned} \qquad (5.37)$$

where

$$\alpha = \frac{3\hat{\kappa}}{8}\frac{1}{r}\exp\left(-\sigma z - \frac{1}{3}\gamma\Omega^2z^3\right)\frac{\mathrm{d}}{\mathrm{d}z}\int_0^z\frac{r\exp\left(\sigma\tau+\frac{1}{3}\gamma\Omega^2\tau^3\right)}{\sqrt{\pi(z-\tau)}}\,\mathrm{d}\tau. \qquad (5.38)$$

In a similar manner, the momentum lost to shed dispersive radiation can be added to the momentum conservation equation (5.6). However it is found that

the same momentum equation (5.6) results since V is taken to be constant for small γ. The energy lost to shed dispersive radiation is of higher order than the lost mass and momentum, and so can be neglected. Hence the full set of equations governing pulse evolution with fibre loss and SFF's, including radiation loss, is

$$\left(2\eta^2 w + \ell g^2\right)\frac{\mathrm{d}V}{\mathrm{d}z} = -\frac{8}{3}\gamma\left(\Omega z + V\right)\frac{\eta^2}{w}, \tag{5.39}$$

$$\begin{aligned}\frac{\mathrm{d}}{\mathrm{d}z}\left(\frac{\eta^2}{w} - 2\eta^4 w\right) &= 2\left(\sigma + \gamma\Omega^2 z^2 + \gamma V^2 + 2\gamma\Omega z V\right)\left(4\eta^4 w - \frac{\eta^2}{w}\right) \\ &\quad + \gamma\left(\frac{24\eta^4 w^2 - 14\eta^2}{5w^3}\right),\end{aligned} \tag{5.40}$$

$$\begin{aligned}\frac{\mathrm{d}}{\mathrm{d}z}\left(\eta w\right) &= -\left(\sigma + \gamma\Omega^2 z^2 + \gamma V^2 + 2\gamma\Omega z V\right)\eta w - \frac{\ell g}{2\pi}\frac{1 - 2\left(\eta w\right)^2}{w^2} \\ &\quad + \frac{\gamma}{5}\frac{\eta}{w^2},\end{aligned} \tag{5.41}$$

$$\begin{aligned}\frac{\mathrm{d}g}{\mathrm{d}z} &= \frac{2}{3\pi}\frac{\eta}{w^2}\left[1 - \left(\eta w\right)^2\right] - \left(\sigma + \gamma\Omega^2 z^2 + 5\gamma V^2 + 6\gamma\Omega z V\right) g \\ &\quad - \frac{\gamma}{5}\frac{g}{w^2} - 2\alpha(1+\gamma)g,\end{aligned} \tag{5.42}$$

$$\frac{\mathrm{d}y}{\mathrm{d}z} = V, \tag{5.43}$$

with

$$\alpha = \frac{3\hat{\kappa}}{8}\frac{1}{r}\exp\left(-\sigma z - \frac{1}{3}\gamma\Omega^2 z^3\right)\frac{\mathrm{d}}{\mathrm{d}z}\int_0^z \frac{r\exp\left(\sigma\tau + \frac{1}{3}\gamma\Omega^2\tau^3\right)}{\sqrt{\pi(z-\tau)}}\,\mathrm{d}\tau, \tag{5.44}$$

$$r^2 = \frac{3\hat{\kappa}}{8}\left(2\eta^2 w - 2\hat{\kappa} + \ell g^2\right). \tag{5.45}$$

5.3 Results

In this section, solutions of the approximate equations (5.39)–(5.45) and the equations (5.20)–(5.21) of [6, 26, 29] will be compared with full numerical solutions of the governing perturbed NLS equation (5.1). The approximate ODE's (5.39)–(5.45) and (5.20)–(5.21) were solved using the method described in Section 3.2. The perturbed NLS equation (5.1) was solved numerically using the method described in Section 3.1.

5.3.1 Modifications to Full Numerical Code

The procedure for numerically solving the NLS equation with sliding-frequency filters (5.1) is similar to that for the original unperturbed case as discussed in Section 3.1. However the integrating factor is no longer constant in distance z. Notice that in the case of the unperturbed NLS equation (3.5), and for NLS

incorporating fibre loss (4.40), the z-coefficient in the integrating factor is a constant, being comprised of the Fourier frequency and loss. This is not the case for variable coefficient equations, such as those for sliding-frequency filters (5.1) or for variable dispersion fibre (6.1).

To modify the numerical procedure to account for variable-coefficient equations, we write the NLS equation incorporating SFF's and fibre loss, along with absorbing boundaries, as

$$\mathrm{i}\frac{\partial u}{\partial z} + \frac{1}{2}\frac{\partial^2 u}{\partial t^2} + |u|^2 u + \mathrm{i}\theta(t)u = -\mathrm{i}\sigma u + \mathrm{i}\gamma\left(\frac{\partial}{\partial t} + \mathrm{i}\Omega z\right)^2 u. \tag{5.46}$$

Taking Fourier transforms, this equation becomes

$$\frac{\mathrm{d}\hat{u}}{\mathrm{d}z} + \frac{\mathrm{i}}{2}\omega^2\hat{u} + \sigma\hat{u} + \gamma\omega^2\hat{u} + 2\gamma\Omega z\omega\hat{u} + \gamma\Omega^2 z^2\hat{u} = \mathrm{i}F\left\{|u|^2 u\right\} - F\left\{\theta(t)u\right\}. \tag{5.47}$$

Taking the lower limit of integration as the previous space point z for the calculation of u at $z + \Delta z$, the integrating factor for the half space step $\Delta z/2$ is then $\exp(\lambda\Delta z/2)$ where

$$\lambda = \frac{\mathrm{i}}{2}\omega^2 + \sigma + \gamma\omega^2 + 2\gamma z\Omega\omega + \gamma\Omega^2 z^2. \tag{5.48}$$

5.3.2 Modifications to Approximate Code

Numerically evaluating the radiation integral (5.38) requires a modification to the numerical method as in the case of fibre loss as outlined in Section 4.4.2. The current radiation integral is

$$\int_0^z \frac{r\exp\left(\sigma\tau + \frac{1}{3}\gamma\Omega^2\tau^3\right)}{\sqrt{(z-\tau)}}\,\mathrm{d}\tau. \tag{5.49}$$

This integral can again be decomposed into the sum of two integrals

$$M = M_1 + M_2, \tag{5.50}$$

where

$$M_1 = \int_0^m \frac{r(\tau)\exp\left(\sigma\tau + \frac{1}{3}\gamma\Omega^2\tau^3\right)}{\sqrt{z-\tau}}\,\mathrm{d}\tau \tag{5.51}$$

and

$$M_2 = \int_m^z \frac{r(\tau)\exp\left(\sigma\tau + \frac{1}{3}\gamma\Omega^2\tau^3\right)}{\sqrt{z-\tau}}\,\mathrm{d}\tau. \tag{5.52}$$

Again the integral M_1 does not have a singular integrand and so is evaluated directly using the Trapezoidal Rule. To evaluate M_2, whose integrand is singular at $\tau = z$, M_2 is written as the sum of many small integrals

$$M_2 = \sum_{i=k}^{n} M_2^i = \sum_{i=k}^{n} \int_{z_i}^{z_{i+1}} \frac{r \exp\left(\sigma\tau + \frac{1}{3}\gamma\Omega^2\tau^3\right)}{\sqrt{z-\tau}}\, \mathrm{d}\tau, \tag{5.53}$$

where $z_k = m$ and $z_{n+1} = z$. In the region $z_i < \tau < z_{i+1}$ of integration, the numerator of (5.53) is assumed linear and approximated as

$$r(\tau)\exp\left(\sigma\tau + \frac{1}{3}\gamma\Omega^2\tau^3\right) = r(z_i)\exp\left(\sigma z_i + \frac{1}{3}\gamma\Omega^2 z_i^3\right) + (\tau - z_i)r', \tag{5.54}$$

where

$$r' = \frac{r(z_{i+1})\exp\left(\sigma z_{i+1} + \frac{1}{3}\gamma\Omega^2 z_{i+1}^3\right) - r(z_i)\exp\left(\sigma z_i + \frac{1}{3}\gamma\Omega^2 z_i^3\right)}{z_{i+1} - z_i}. \tag{5.55}$$

Substituting this approximation for $r(\tau)\exp\left(\sigma\tau + \frac{1}{3}\gamma\Omega^2\tau^3\right)$ into equation (5.53) gives

$$M_2^i = \int_{z_i}^{z_{i+1}} \frac{r(z_i)\exp\left(\sigma z_i + \frac{1}{3}\gamma\Omega^2 z_i^3\right) + r'(\tau - z_i)}{\sqrt{z-\tau}}\, \mathrm{d}\tau. \tag{5.56}$$

After rearranging the numerator as for the similar integral (3.24), this integral can be evaluated exactly as

$$\begin{aligned} M_2^i = 2\left[r(z_i)\exp\left(\sigma z_i + \frac{1}{3}\gamma\Omega^2 z_i^3\right) + r'(z - z_i)\right]\left(\sqrt{z-z_i} - \sqrt{z-z_{i+1}}\right) \\ + \frac{2}{3}r'\left((z-z_{i+1})^{3/2} - (z-z_i)^{3/2}\right). \end{aligned} \tag{5.57}$$

5.3.3 Numerical Results

When the effect of amplification is added, the parameter σ in the perturbed NLS equation (5.1) is negative. In this case, the approximate equations (5.39)–(5.45), which include the effect of radiation loss, possess a steady state. This steady state corresponds to a pulse with a steady profile that travels with constant acceleration. The requirement of constant acceleration means that

$$V = az + b, \tag{5.58}$$

where a is a constant, denoting the constant acceleration. Taking the approximate equation derived from momentum conservation (5.10) and seeking a solution with constant acceleration, we find

$$\left(2\eta^2 w\right) a = -\frac{8}{3}\gamma\left(\Omega z + az + b\right)\frac{\eta^2}{w} \tag{5.59}$$

to first order in g. It should be noted that for the steady state, in the presence of amplification and filtering, $g \neq 0$ and $g = O(\gamma)$. The shelf variable g is non-zero at the steady state because the shelf of radiation, which moves with the pulse, is being amplified by the amplifiers and filtered by the SFF's and the balance of these two effects results in a steady, non-zero shelf under the pulse. Since the filter strength γ has been assumed to be small, g is small at the steady state. For a steady pulse, the right hand side of (5.59) must be independent of z. This gives $a = -\Omega$ which in turn implies

$$b = \frac{3}{4}\frac{\Omega}{\gamma}w^2. \tag{5.60}$$

Equation (5.58) for the velocity in the steady state now becomes

$$V = -\Omega z + \frac{3}{4}\frac{\Omega}{\gamma}w^2. \tag{5.61}$$

To first order in γ equation (5.18) for g gives $\eta = 1/w = \hat{\kappa}$ at the steady state, where $\hat{\kappa}$ is the steady amplitude of the soliton, as expected for an NLS soliton. Taking this inverse width-amplitude relation for an NLS soliton and the velocity steady state (5.61) and substituting these into the conservation of energy equation (5.16) produces

$$f(\hat{\kappa}) = \gamma\hat{\kappa}^6 + 3\sigma\hat{\kappa}^4 + \frac{27}{16}\frac{\Omega^2}{\gamma} = 0 \tag{5.62}$$

for the steady amplitude $\hat{\kappa}$. This steady state equation for $\hat{\kappa}$ is the same as that found by [6, 26] from a multiple scales analysis and from perturbed inverse scattering. The question now remains as to when equation (5.62) possesses real, positive solutions. In other words, what parameter combinations (σ, γ, Ω) will produce steady pulses. A further question is then the stability of these steady pulses.

Differentiating the function f in equation (5.62) with respect to $\hat{\kappa}$ we find

$$\frac{\mathrm{d}f}{\mathrm{d}\hat{\kappa}} = 6\hat{\kappa}^3\left(\gamma\hat{\kappa}^2 + 2\sigma\right). \tag{5.63}$$

So f has stationary points at $\hat{\kappa} = 0$ and $\hat{\kappa} = \pm\sqrt{2|\sigma|/\gamma}$. The absolute values around σ are due to σ now being negative since this is amplification. As we are interested in positive solutions, let us examine the positive critical point. The second derivative with respect to $\hat{\kappa}$ of f is

$$\frac{\mathrm{d}^2 f}{\mathrm{d}\hat{\kappa}^2} = 30\gamma\hat{\kappa}^4 + 36\sigma\hat{\kappa}^2. \tag{5.64}$$

Evaluating this derivative at the critical point of interest, $\hat{\kappa} = \sqrt{2|\sigma|/\gamma}$, shows that $\hat{\kappa} = \sqrt{2|\sigma|/\gamma}$ is a minimum of f. Now

$$f\left(\sqrt{\frac{2|\sigma|}{\gamma}}\right) = \frac{1}{\gamma}\left(\frac{27}{16}\Omega^2 - \frac{4|\sigma|^3}{\gamma}\right). \tag{5.65}$$

Therefore, if

$$|\sigma| > \frac{3}{4}\Omega^{\frac{2}{3}}\gamma^{\frac{1}{3}} \tag{5.66}$$

f is negative at $\hat{\kappa} = \sqrt{2|\sigma|/\gamma}$, so that equation (5.62) possesses two positive solutions as $f(0) = 27\Omega^2/(16\gamma) > 0$.

From numerical results it was found that the larger of the two critical points is stable, the other being unstable, in agreement with the previous work of [26]. Examining equation (5.41) for ηw about the fixed point $\hat{\kappa}w = 1$, we find

$$g = \frac{2\pi}{\ell}\left(\frac{\sigma}{\hat{\kappa}^2} + \frac{9}{16}\frac{\Omega^2}{\gamma\hat{\kappa}^6} - \frac{\gamma}{5}\right) \tag{5.67}$$

for the fixed point of g. Using equation (5.62) for the fixed point amplitude $\hat{\kappa}$ to eliminate σ, equation (5.67) becomes

$$g = -\frac{16\pi}{15\ell}\gamma. \tag{5.68}$$

Hence $g = O(\gamma)$ at the fixed point as stated above and the analysis above for the fixed point is valid for small γ. The solution of the present approximate equations does not evolve to a steady-state in the absence of loss to dispersive radiation. Without radiative loss, numerical solutions show that the stable fixed point is absent and an amplitude-width-shelf oscillation is set up with mass and energy oscillating between the pulse and the shelf.

To perform a full stability analysis on our approximate filter equations including the effect of shed dispersive radiation one would have to linearise equations (5.39)–(5.42) about the steady state $\eta = 1/w = \hat{\kappa}$ and $g = g_0$,

$$\eta = \hat{\kappa} + \tilde{\eta}, \tag{5.69}$$

$$w = \frac{1}{\hat{\kappa}} + \tilde{w}, \tag{5.70}$$

$$g = -\frac{16\pi}{15\ell}\gamma + \tilde{g}, \tag{5.71}$$

$$V = -\Omega z + \frac{3}{4}\frac{\Omega}{\gamma\hat{\kappa}^2} + \tilde{V}. \tag{5.72}$$

Doing this stability analysis however would also require linearising the radiation integral (5.38) about the steady state. However this is impossible as the integral

requires the details of the pulse behaviour back to $z = 0$, remembering that the present approximate equations do not evolve to a steady state in the absence of radiative loss. This stability analysis is not possible. However numerical solutions of the approximate equations (5.39)–(5.43) show that the pulse evolves to a steady state critical point whose amplitude is the larger root of (5.62). In this context it should be noted that the approximate equations (5.39)–(5.43) give oscillatory evolution to the steady state, in agreement with full numerical solutions, whereas previous work [6, 26] gave monotonic evolution to the steady state. Hence the present approximate equations correctly determine the nature of the fixed point, whereas the previous work did not. The fixed point obtained from the analysis is then used in the calculation of the shelf length ℓ given by equation (2.21). In the absence of a steady state the slowly varying approximation to ℓ is still (2.21) with the fixed point $\hat{\kappa}$ given by (2.22) as discussed in Section 5.1.

The inequality (5.66) determines the lower energy bound on the existence of stable pulse propagation in the presence of SFF's and amplification [6, 26]. In other words, the amplification $|\sigma|$ has to be large enough to compensate for the losses associated with filtering. As for the converse of (5.66),

$$|\sigma| < \frac{3}{4}\Omega^{\frac{2}{3}}\gamma^{\frac{1}{3}}, \tag{5.73}$$

equation (5.62) possesses no real solutions and so no steady state pulse exists.

For a given value of the filter strength γ, a sufficiently high value of the amplification $|\sigma|$ amplifies the dispersive radiation to the point at which a second soliton can form out of it. This formation of a second soliton is obviously undesirable in applications and was termed instability by [6, 32]. However, this is not instability in the sense that the evolving pulse loses its coherence. The parameter values for which a second soliton will form were determined by [6] via the perturbed inverse scattering solution of the perturbed NLS equation (5.1). In the present work equations for mass and energy will be used to determine when a second soliton will form.

From equations (2.5) and (5.11) it can be seen that the energy of a pulse is

$$E = \frac{\eta^2}{w} - 2\eta^4 w. \tag{5.74}$$

If there is no filtering and amplification, then an initial pulse will evolve to a steady soliton for which $\eta = \hat{\kappa}$ and $w = 1/\hat{\kappa}$ and whose energy is $E = -\hat{\kappa}^3$. Hence an initial pulse can evolve to a steady soliton only if its initial energy is negative. If its initial energy is positive, then it will decay into dispersive radiation alone. The borderline case is then an initial pulse with energy $E = 0$. From the

energy expression (5.74) we see that for this borderline case, the pulse amplitude and width are related by

$$\eta w = \frac{1}{\sqrt{2}}. \tag{5.75}$$

Let us now consider a pulse of amplitude η and width w which has just enough mass and energy to break up into two solitons. At the boundary between one and two solitons forming, the second soliton will have zero energy. Let us take the final steady amplitude and width of the first soliton to be $\eta = \hat{\kappa}$ and $w = 1/\hat{\kappa}$. Then the total energy is

$$E = \frac{\eta^2}{w} - 2\eta^4 w = -\hat{\kappa}^3, \tag{5.76}$$

since the second soliton has zero energy. From (2.3) and (5.13) it can be seen that the total mass of the two solitons is

$$M = 2\eta^2 w = \sqrt{2}\eta + 2\hat{\kappa}. \tag{5.77}$$

The term $2\eta^2 w$ is the mass of the pulse which is about to split into two solitons. The first term on the right is the mass of a pulse with zero energy, for which the amplitude-width relation (5.75) holds. The second term on the right is the mass of the final steady soliton with amplitude $\hat{\kappa}$. In making this division of the mass and energy, it has been assumed that in the borderline case no mass and energy are taken away by dispersive radiation. On eliminating $\hat{\kappa}$ between the energy conservation result (5.76) and the mass relation (5.77), it is found that

$$(\eta w)^6 - \frac{7}{2}(\eta w)^4 + \frac{7}{4}(\eta w)^2 - \frac{1}{8} = 0, \tag{5.78}$$

so that $\eta w = 1.702\ldots$. Therefore for $\eta w > 1.702$ an initial pulse will break up into two solitons, both of non-trivial final amplitude. In the preceding analysis for the generation of a second soliton, the effects of amplification and filtering have been ignored. However the condition $\eta w > 1.702$ at some point in the evolution of a pulse for a second soliton to form will still be valid if it is assumed that when there is sufficient mass and energy for a second pulse to form, it will do so, and it will then evolve under the influence of amplification and filtering. Much the same assumption was made by [6] based on their perturbed inverse scattering solution. Their condition for a second soliton to form was based on the fact that the NLS equation (1.1) possesses an inverse scattering solution. Using this solution, [50] showed that for a boundary condition of the form $u = \eta \operatorname{sech} t$, a second soliton will form for the NLS equation when $\eta w > 1.5$, which is in good agreement with the value $\eta w > 1.702$ found from the present mass and energy argument. However

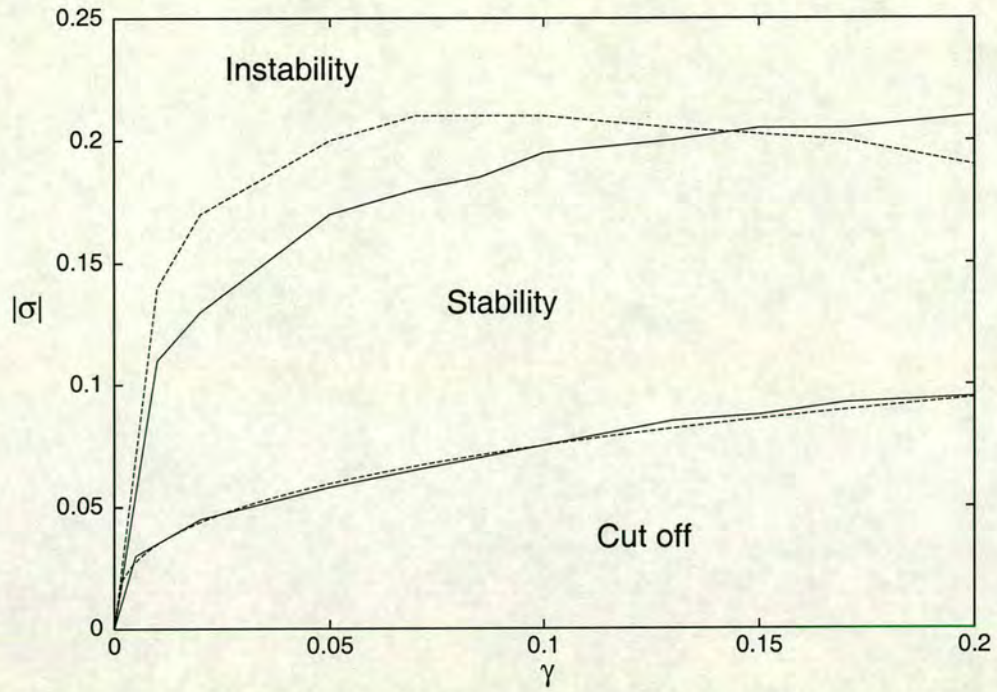

Figure 5.1: Number of stable pulses in the $|\sigma| - \gamma$ plane as given by the approximate and full numerical solutions for the soliton boundary condition $\eta = 1$, $w = 1$, and $V = 1$ for the filter sliding rate $\Omega = 0.1$. Boundaries from full numerical solution: — ; boundaries from approximate equations (5.39)–(5.45): – – – – .

the present mass and energy argument is applicable to equations for which there are no inverse-scattering solutions.

The approximate equations (5.39)–(5.45) can now be used to determine when a second soliton will form during the evolution of an initial pulse. The combination ηw is calculated as the pulse evolves and a second soliton is said to form when $\eta w > 1.702$ at some distance z. Figure 5.1 shows a comparison in the $|\sigma| - \gamma$ plane of the boundary between the regions of one and two solitons as given by the approximate and full numerical solutions. Also shown is a similar comparison for the region (5.73) for no stable pulse, labelled cut off in the figure. It can be seen that there is excellent agreement for the region of no stable pulse, as was also found by [6]. The agreement between the numerical and approximate solutions for the region of two solitons is good in view of the approximations made to derive the boundary $\eta w = 1.702$. It can further be seen that the agreement for the region of two solitons decreases as γ increases. This is to be expected as the analysis of Section 5.2 for the calculation of the effect of the shed dispersive radiation was based upon assuming that γ is small. The overall comparison for the region of two solitons is similar to that obtained by Burtsev and Kaup [6] from perturbed inverse scattering.

If the effect of the dispersive radiation shed as the pulse evolves was neglected,

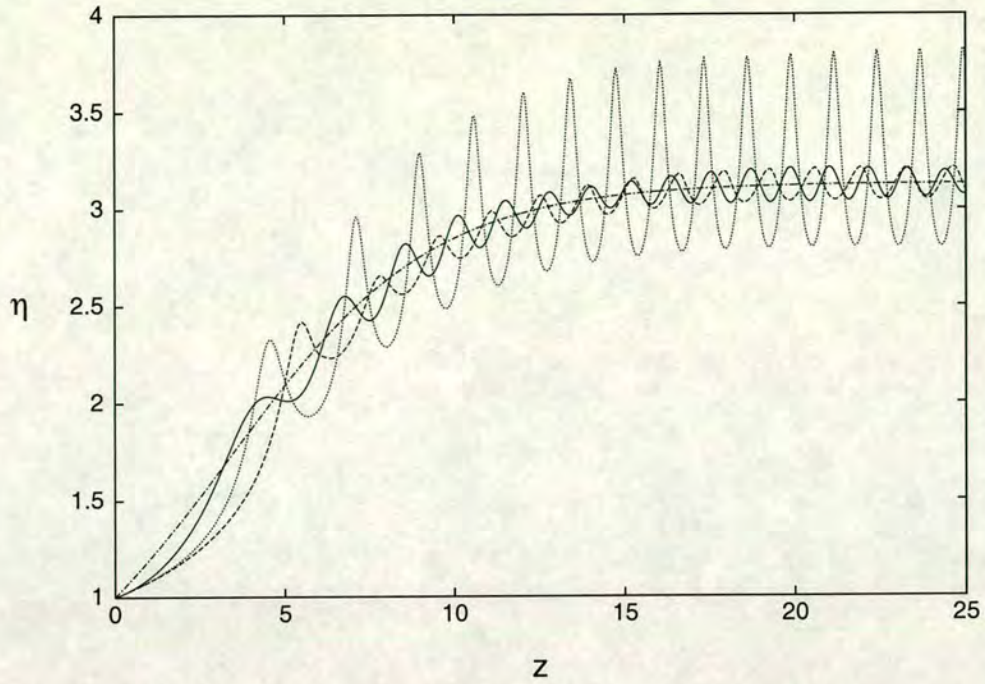

Figure 5.2: Amplitude η versus distance z: Comparison between approximate and numerical solutions for soliton boundary condition with $\eta = 1$, $w = 1$ and $V = 0$ with parameter values $\Omega = 0.1$, $\gamma = 0.03$ and $\sigma = -0.1$. Full numerical solution: — ; solution of approximate equations (5.39)–(5.45) with radiation: – – – – ; solution of approximate equations (5.39)–(5.45) without radiation: $\cdots$; solution of approximate equations (5.20) and (5.21): – - – - .

so that $\alpha = 0$, then the approximate equations (5.39)–(5.45) would not possess a steady state and there would be a persistent oscillation in η, w, and g about the state given by (5.62). As the amplitude and width of the pulse oscillate, dispersive radiation is generated in the shelf under the pulse, which is then amplified and filtered. The steady oscillations in the absence of radiation damping then represent a balance between the amplitude and width oscillations and the radiation in the shelf as mass and energy oscillate between the pulse and the shelf. The inclusion of the effect of the dispersive radiation shed as the pulse evolves is then vital in order to drive the system to settle to a steady state. In this regard, Mamyshev and Mollenauer [32] noted that full numerical solutions of the perturbed NLS equation (5.1) showed oscillations in the pulse amplitude which they attributed to the generation of radiation by the sliding and filtering.

Figure 5.2 shows the evolution of the pulse amplitude as given by the full numerical solution of the governing perturbed NLS equation (5.1), by the present approximate equations (5.39)–(5.45), both with and without radiation damping, and by the solution of the approximate equations (5.20) and (5.21) of [6, 26], for a case of stable pulse propagation, for which the inequality (5.66) holds. The above dimensionless parameters correspond to a dispersion length of $z_0 = 133$ km

and an amplifier filter spacing of $z_a = 285$ km, and so do not correspond to a physically realistic situation. However the figure is included in order to illustrate various aspects of the solution which are evident at these small parameter values.

It can be seen that the numerical amplitude shows an oscillation which is also present in the solution of the present approximate equations (5.39)–(5.45) with radiation loss and that there is excellent agreement between these two solutions. The main difference between the numerical and approximate solutions is a phase difference, which is expected as equations for the phase are of higher order than the modulation equations (5.39)–(5.45) [15, 16]. It can further be seen that the solution of the modulation equations (5.20) and (5.21) of [6, 26] does not oscillate and in fact gives the mean of the numerical oscillations. This is because their perturbed solution (5.19) has width w fixed to be the inverse amplitude $1/\eta$, so that the pulse cannot undergo the amplitude-width oscillations exhibited by the full numerical solutions of (5.1) and by the solutions of the present approximate equations (5.39)–(5.45). The final observation to be made about Figure 5.2 is that if the radiation damping in the approximate equations (5.39)–(5.45) is neglected (i.e. $\alpha = 0$), the approximate solution exhibits amplitude-width-shelf oscillations which do not settle to a steady state, as noted in the previous paragraph. The addition of loss due to dispersive radiation allows leakage from the shelf under the pulse so that the pulse can settle to a steady state, as noted in the previous paragraph. It can therefore be concluded that allowing the pulse amplitude and width to vary independently and the inclusion of radiative loss results in better agreement with the full numerical solution. Both of these effects were not included in the perturbation solutions of [6, 26].

Figure 5.3 shows the evolution of the pulse amplitude as given by the full numerical solution and by the solution of the present approximate equations for the same parameter values as Figure 5.2, but for a larger range of z. It can be seen that the numerical amplitude shows long term oscillations which are mirrored by the approximate solution. The approximate solution shows excellent agreement with the numerical solution both in terms of the final steady amplitude and the value of z at which the oscillations have basically died out.

Whereas Figures 5.2 and 5.3 do not correspond to a practical physical situation, Figure 5.4 does. The dimensionless filter and loss parameters from Figure 5.4 correspond to a dispersion length of $z_0 = 133$ km and a filter/amplifier spacing of $z_a = 38$ km. As the dispersion length is longer than the filter/amplifier spacing, the perturbed NLS equation (5.1) is physically valid. As can be seen from Figure 5.4, the solution of the approximate equations (5.39)–(5.45) is in good agreement with the full numerical solution of the perturbed NLS equation (5.1).

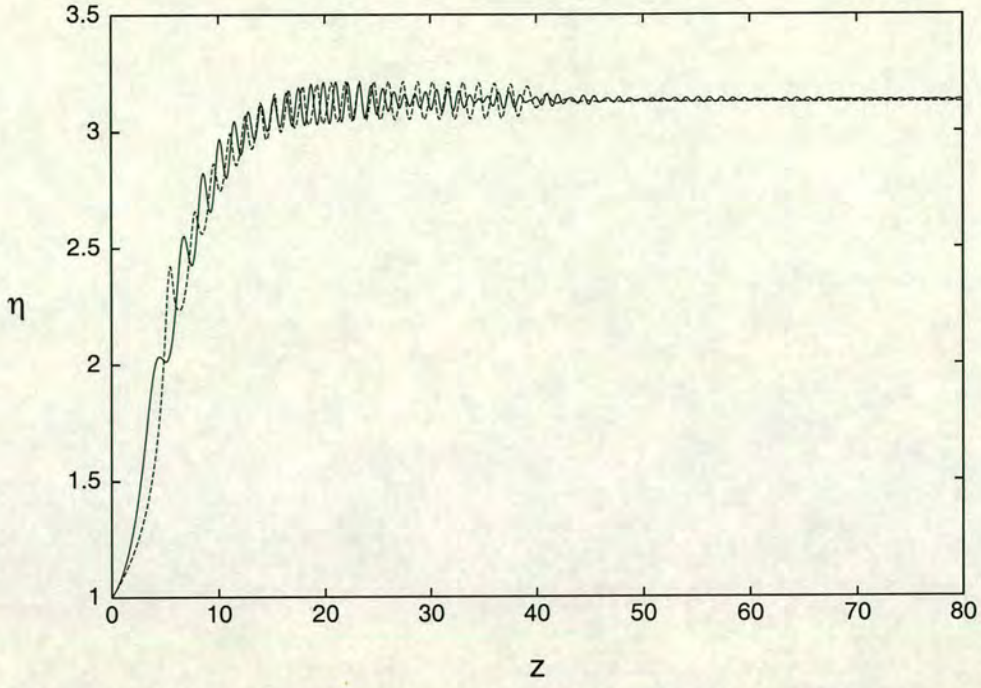

Figure 5.3: Amplitude η versus distance z: Comparison between approximate and numerical solutions for soliton boundary condition with $\eta = 1$, $w = 1$ and $V = 0$ with parameter values $\Omega = 0.1$, $\gamma = 0.03$ and $\sigma = -0.1$. Full numerical solution: — ; solution of approximate equations (5.39)–(5.45) with radiation: - - - - .

Again there is a phase difference between the two solutions for the same reasons outlined above. However the solution of the approximate equations (5.39)–(5.45) is superior to that given by the modulation equations (5.20) and (5.21) which do not reflect any of the dynamic evolutionary behaviour of the evolving pulse. It can also be seen from Figure 5.4 that the inclusion of radiation damping in the solution of the approximate equations (5.39)–(5.45) is essential for the pulse to decay to a steady soliton.

Let us now consider the evolution of a pulse in the absence of amplification. Figure 5.5 shows a comparison between the solutions of the present approximate equations (5.39)–(5.45), the solution of the approximate equations (5.20) and (5.21) of [6, 26, 29] and the full numerical solution of the perturbed NLS equation (5.1). The present approximate equations were solved both with and without the effect of shed dispersive radiation. The parameter values used were the same as those of Malomed and Tasgal [29], $\Omega = 0.1$, $\gamma = 0.09$ and $\sigma = 0.046$. The boundary pulse at $z = 0$ was taken as an NLS soliton with $\eta = 1$ and $w = 1$ and the initial velocity was $V = 0$. As can be seen from the figure, the solution of the present approximate equations is closer to the full numerical solution than the solution of the approximate equations of [6, 26, 29], especially for larger z. It can also be seen that for the NLS soliton boundary condition, the inclusion

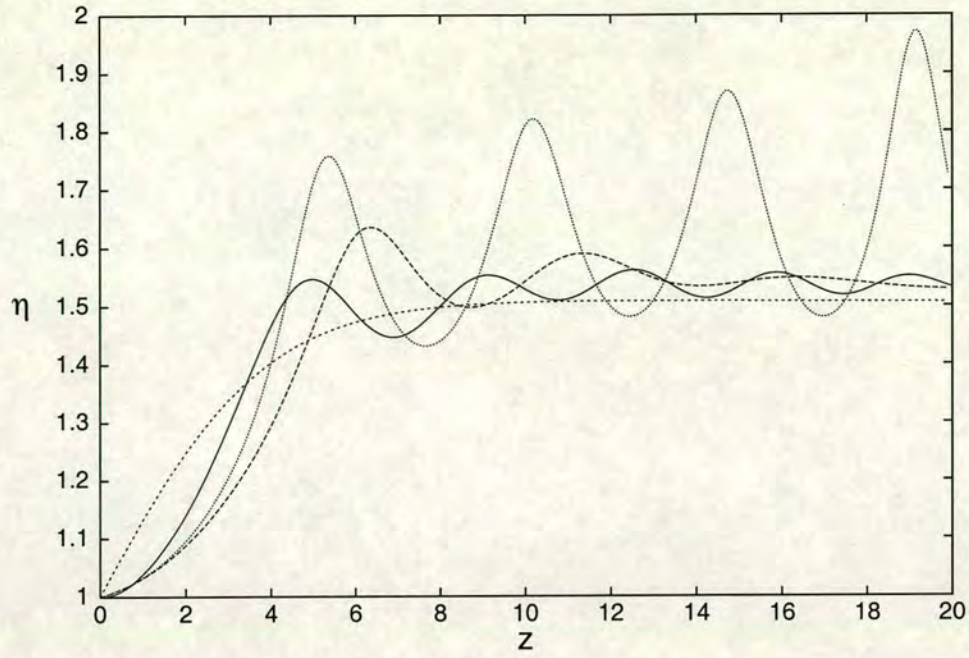

Figure 5.4: Amplitude η versus distance z: Comparison between approximate and numerical solutions for soliton boundary condition with $\eta = 1$, $w = 1$ and $V = 0$ with parameter values $\Omega = 0.15$, $\gamma = 0.1$ and $\sigma = -0.1$. Full numerical solution: — ; solution of approximate equations (5.39)–(5.45) with radiation: – – – – ; solution of approximate equations (5.39)–(5.45) without radiation: $\cdots$; solution of approximate equations (5.20) and (5.21): - - - .

of shed dispersive radiation makes little difference to the evolution of the pulse. This is because the non-zero loss σ quickly damps the dispersive radiation so that it has basically no effect on the evolution of the pulse. Indeed, the approximate solution is slightly closer to the full numerical solution when the effect of the shed dispersive radiation is neglected. This counterintuitive result is due to the approximations made in the derivation in Section 5.2 of the effect on the pulse of the shed dispersive radiation and again implies that the shed dispersive radiation can be neglected for non-zero fibre losses σ for a soliton boundary condition.

Figure 5.6 shows a comparison between the pulse velocity V as given by the approximate and numerical solutions for the same parameter values as that of Figure 5.5. This velocity comparison shows a marked difference between the approximate solution of the present work and that of [6, 26, 29]. It can be seen that the velocity as given by the approximate equations of [6, 26, 29] approaches a steady value, while the velocity as given by the present approximate equations continues to decrease as z increases, in agreement with the full numerical solution. In addition, the velocity as given by the approximate equations (5.39)–(5.45) is in good agreement with the numerical velocity. As for the amplitude comparison shown in Figure 5.5, the inclusion of shed radiation makes little difference to

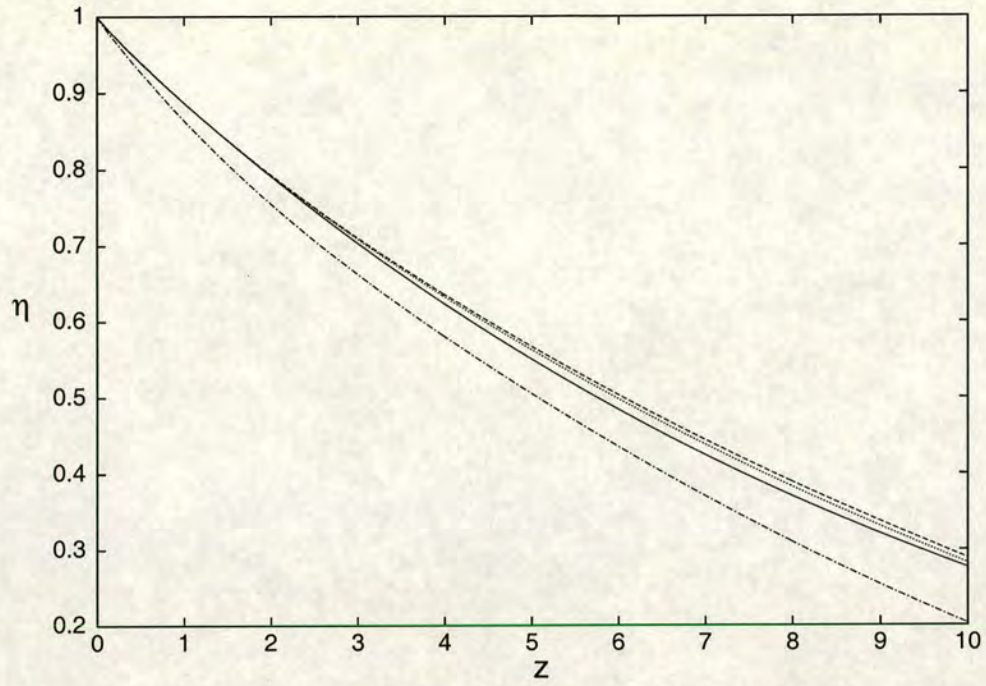

Figure 5.5: Amplitude η versus distance z: Comparison between approximate and numerical solutions for soliton boundary condition with $\eta = 1$, $w = 1$ and $V = 0$ with parameter values $\Omega = 0.1$, $\gamma = 0.09$ and $\sigma = 0.046$. Full numerical solution: — ; solution of approximate equations (5.39)–(5.45) with radiation: - - - - ; solution of approximate equations (5.39)–(5.45) without radiation: $\cdots$; solution of approximate equations (5.20) and (5.21): - - - - .

the approximate velocity due to the non-zero fibre loss σ damping the dispersive radiation.

As radiation loss makes little difference for NLS soliton boundary conditions, it cannot explain the difference between the solution of the approximate equations (5.39)–(5.45) and of the equations (5.20) and (5.21) of [6, 26, 29]. Therefore the only explanation for the difference must be in the trial function used. The trial function used by [6, 26, 29], (5.19), does not allow the pulse amplitude and width to vary independently. Rather, they are restricted to be inversely proportional, as in an NLS soliton. Figure 5.7 shows the product of amplitude and width ηw as given by the solution of the approximate equations (5.39)–(5.45) with radiation loss for the same parameter values as for Figures 5.2 and 5.3. Notice that the amplitude and width are clearly not inversely proportional, in contrast to the assumption made by [6, 26, 29]. The trial function used in the present work, (5.9), allows for independently varying pulse amplitude and width. As found previously in the case of amplification, this added degree of freedom results in better agreement with full numerical solutions.

Let us now examine the evolution of a non-NLS soliton boundary condition. As large loss and filter strength act as damping, killing off most dynamic, evolu-

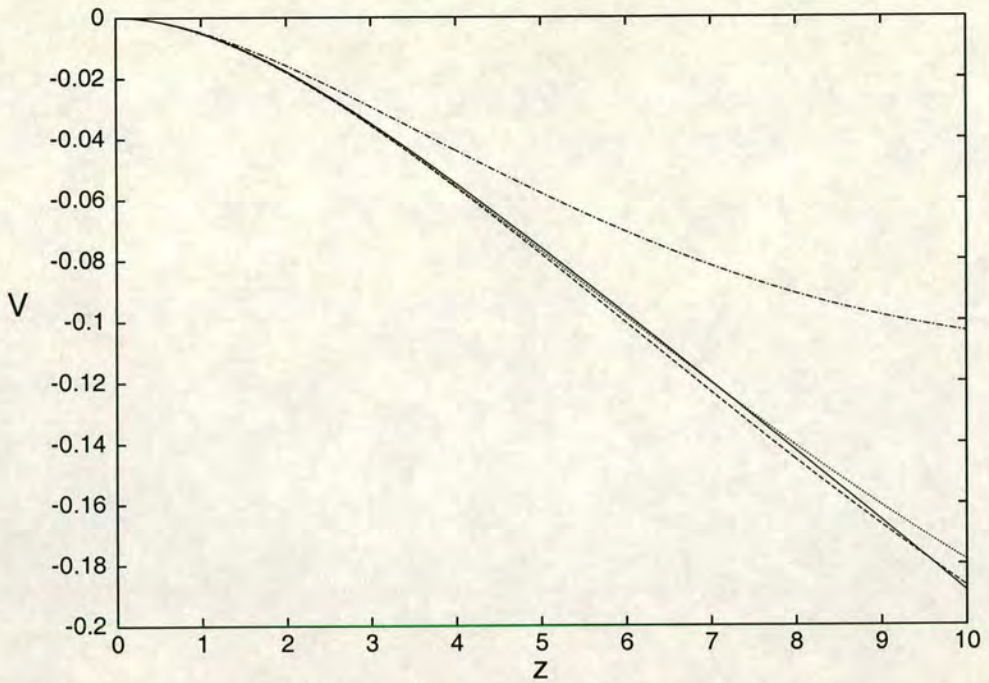

Figure 5.6: Velocity V versus distance z: Comparison between approximate and numerical solutions for soliton boundary condition with $\eta = 1$, $w = 1$ and $V = 0$ with parameter values $\Omega = 0.1$, $\gamma = 0.09$ and $\sigma = 0.046$. Full numerical solution: — ; solution of approximate equations (5.39)–(5.45) with radiation: - - - - ; solution of approximate equations (5.39)–(5.45) without radiation: $\cdots$; solution of approximate equations (5.20) and (5.21): - - - - .

tionary behaviour, we shall take small values for fibre loss σ and filter strength γ. Figure 5.8 shows a comparison between the pulse amplitude η as given by the solution of the present approximate equations (5.39)–(5.45), both with and without radiation damping, and by the full numerical solution of the perturbed NLS equation (5.1). The boundary condition is a non-NLS soliton pulse with $\eta = 1.25$ and $w = 1$ at $z = 0$. The initial velocity was taken as $V = 0.1$ and the parameter values $\sigma = 0$, $\gamma = 0.01$ and $\Omega = 0.1$ were chosen. The pulse is then propagating into a lossless fibre with an SFF, so that dispersive loss is expected to have an effect on the pulse evolution. No comparison was made with the solution of (5.20) and (5.21) as these approximate equations are valid only for an NLS soliton boundary condition. It can be seen from the amplitude comparison shown in Figure 5.8 that incorporating radiation loss gives an approximate amplitude in better agreement with the full numerical amplitude. The radiation loss acts as damping, without which the pulse amplitude is overestimated at every oscillation. There is again a phase difference and a period difference between the approximate and numerical amplitude oscillations. The phase difference is due to the assumption that the shelf forms instantaneously, while the period difference is due to the amplitude dependence of the oscillation period, noting that the numer-

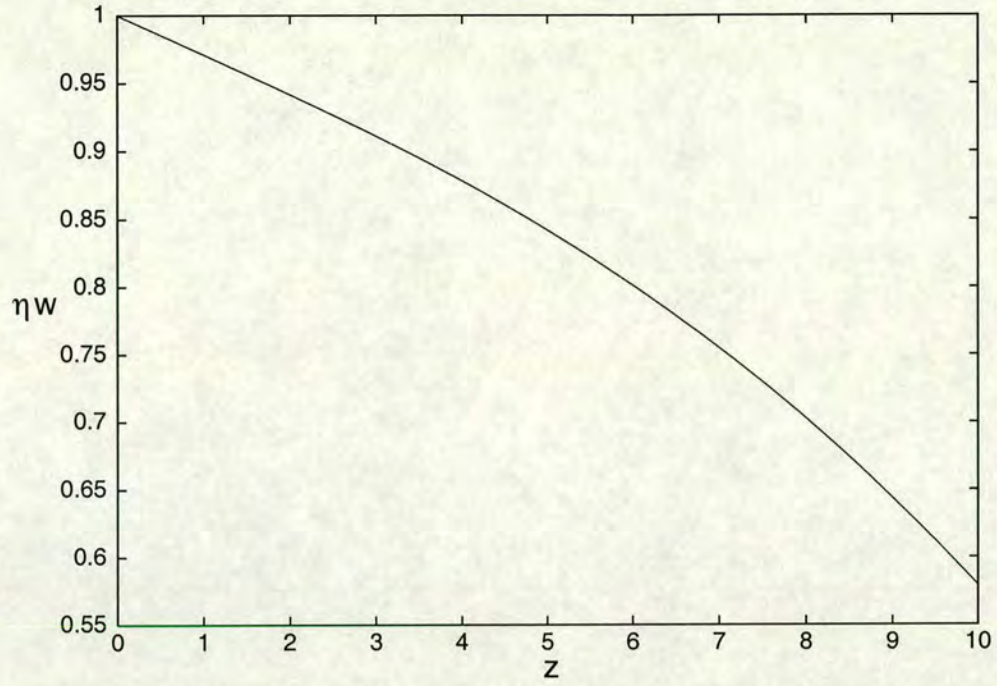

Figure 5.7: The product of amplitude and width ηw versus distance z as given by the approximate equations (5.39)–(5.45) with radiation for soliton boundary condition with $\eta = 1$, $w = 1$ and $V = 0$ and parameter values $\Omega = 0.1$, $\gamma = 0.09$ and $\sigma = 0.046$.

ical and approximate amplitudes are slightly different. Furthermore, the phase of the amplitude oscillation is a higher order effect, and while methods exist to determine equations for this phase [15, 16], these methods do not determine the initial phase, which is of importance here. In this regard, it should be noted that the amplitude of the phase oscillation is in good agreement with the numerical amplitude.

Figure 5.9 shows the velocity V of the pulse as given by the solution of the approximate equations (5.39)–(5.45), both with and without radiation damping, and by the full numerical solution of the perturbed NLS equation (5.1). The boundary and parameter values are as for Figure 5.8. It can be seen that the inclusion of radiative loss is necessary in order to obtain good agreement with the numerical solution, particularly for large z. As for the amplitude oscillations of Figure 5.8, there is again a phase and period difference between the numerical and approximate velocity oscillations for the same reasons.

Using the same parameter values as Malomed and Tasgal [29], Figure 5.10 shows a comparison between the pulse amplitude η as given by the solution of the present approximate equations (5.39)–(5.45), both with and without radiation loss, and by the full numerical solution of the perturbed NLS equation (5.1) for the non-NLS soliton boundary condition with $\eta = 1.25$, $w = 1$ and $V = 0.1$ at

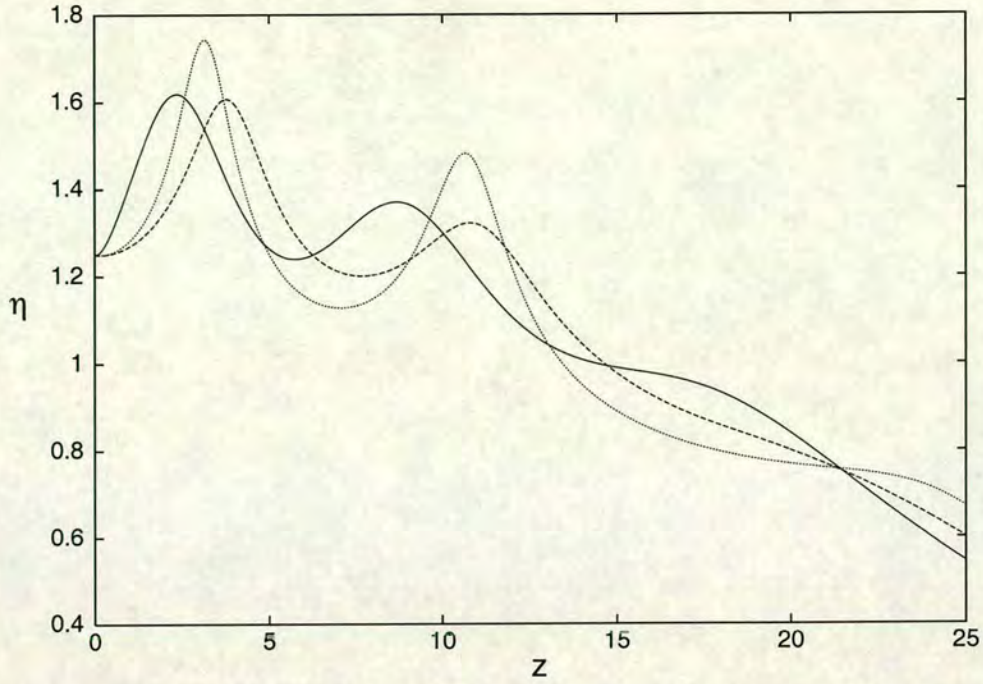

Figure 5.8: Amplitude η versus distance z: Comparison between approximate and numerical solutions for non-soliton boundary condition with $\eta = 1.25$, $w = 1$ and $V = 0.1$ with parameter values $\Omega = 0.1$, $\gamma = 0.01$ and $\sigma = 0.0$. Full numerical solution: — ; solution of approximate equations (5.39)–(5.45) with radiation: - - - - ; solution of approximate equations (5.39)–(5.45) without radiation: $\cdots$.

$z = 0$. The parameters used were $\Omega = 0.1$, $\gamma = 0.03$ and $\sigma = 0.005$ [29]. As for the comparison shown in Figure 5.5, adding radiation loss gives little change in the agreement with the full numerical solution except near the boundary $z = 0$. This is again due to the damping of the radiation by the fibre loss ($\sigma \neq 0$). It can also be seen that radiation loss over-estimates the amplitude damping near the boundary $z = 0$. This is not surprising as the radiation loss was derived for large z behaviour [22] (see Section 4.2). Without radiation loss, the amplitude oscillation has too large an amplitude near $z = 0$.

In conclusion it has been shown that for an accurate portrayal of pulse dynamics with SFF's and fibre loss, two things are necessary. Firstly, an independently varying amplitude and width and secondly, incorporating the effects of dispersive radiation into the evolution equations. Oscillations in the amplitude-width-shelf relation lead to oscillatory behaviour in the evolving pulse. To account for this oscillatory behaviour it is necessary to decouple the amplitude and width and account for the dispersive radiation on which the pulse sits. The perturbed inverse scattering analysis of [6] and the multiple scales analysis of [26, 29] assume a solution based upon an NLS soliton, with amplitude and width inversely proportional, and neglect the shelf of radiation upon which the pulse sits. As a

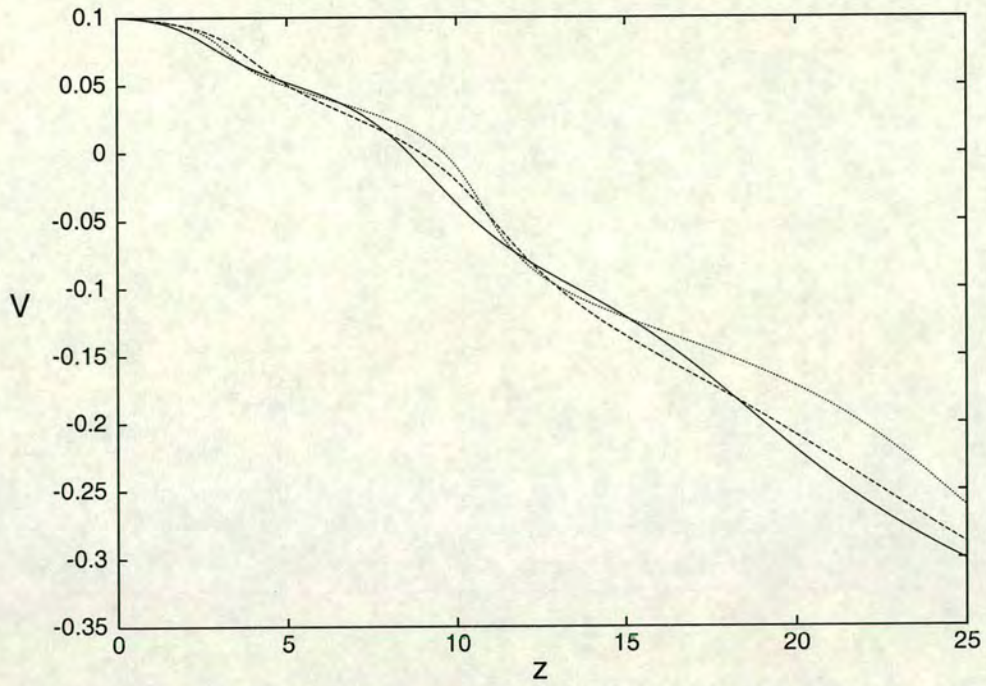

Figure 5.9: Velocity V versus distance z: Comparison between approximate and numerical solutions for non-soliton boundary condition with $\eta = 1.25$, $w = 1$ and $V = 0.1$ with parameter values $\Omega = 0.1$, $\gamma = 0.01$ and $\sigma = 0.0$. Full numerical solution: — ; solution of approximate equations (5.39)–(5.45) with radiation: – – – – ; solution of approximate equations (5.39)–(5.45) without radiation: $\cdots$.

result their equations monotonically evolve to a steady state missing out on the amplitude oscillations evident in full numerical solutions of (5.1). The effect of neglecting these factors can also be seen in the pulse velocity as shown in Figure 5.6. The equations of [26, 29] show the pulse velocity approaching a steady state value. This is not reflected in the full numerical solution which shows a pulse steadily accelerating. This is accurately reflected by the current evolution equations (5.14)–(5.18). Secondly, in order to damp the amplitude oscillations of the evolving pulse and drive it to a steady soliton, the effects of shed radiation must be accounted for as in the present work. No attempt is made to factor in the effects of the shed radiation on the evolving pulse, nor is it necessary as the evolution equations of [26, 29] monotonically evolve, missing out on much of the dynamic, evolutionary behaviour.

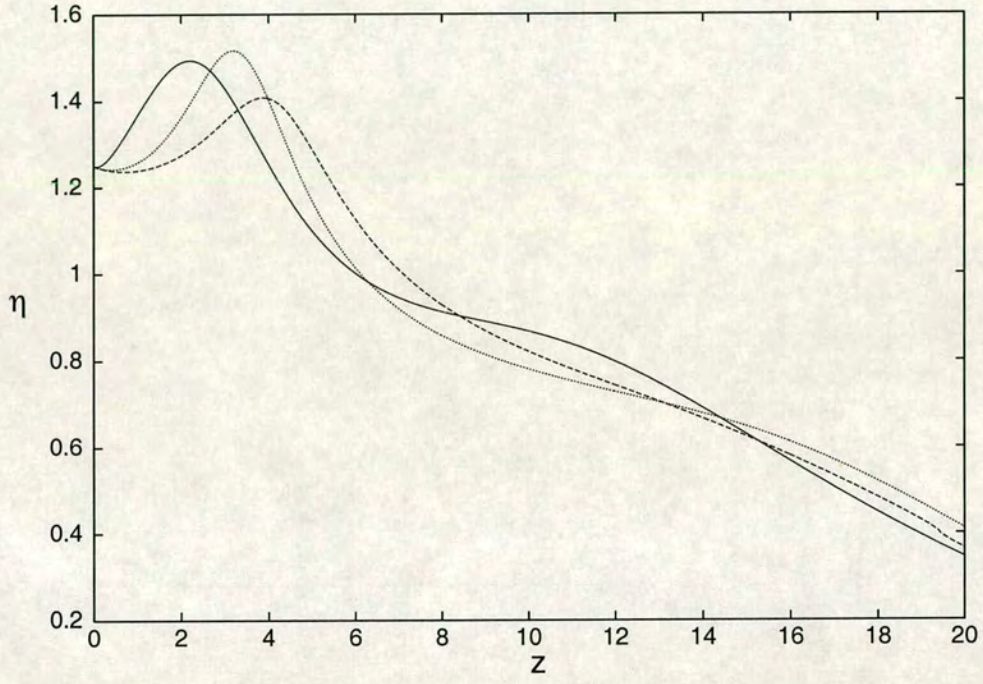

Figure 5.10: Amplitude η versus distance z: Comparison between approximate and numerical solutions for the non-soliton boundary condition with $\eta = 1.25$, $w = 1$ and $V = 0.1$ with parameter values $\Omega = 0.1$, $\gamma = 0.03$ and $\sigma = 0.005$. Full numerical solution: — ; solution of approximate equations (5.39)–(5.45), with radiation: – – – – ; solution of approximate equations (5.39)–(5.45), without radiation: $\cdots$.

Chapter 6

Fibre Compressor

With a soliton acting as an optical bit in a soliton-based fibre optic communication system, a major design objective would be to maximise the bit rate, or amount of information per second, which could be carried by the system. This can be achieved by narrowing the width of each individual soliton, thus fitting more solitons into a given length of fibre. This is the idea behind the fibre compressor. The term fibre compressor is used to describe a section of dispersion-decreasing fibre (DDF) whose dispersion decreases along its length. A soliton passing through a section of DDF will decrease in width and show a proportional increase in amplitude. Therefore using such a DDF, a train of solitons can be compressed, dramatically increasing data transfer rates.

Using DDF fibre to compress optical solitons was first proposed by Kuehl [27]. It was later demonstrated theoretically by Mamyshev and Chernikov [30] that very narrow, sub-picosecond pulses could be generated using DDF. However, it was not until the work of Bogatyrev *et al.* [5] that a practical method existed for the manufacture of suitable DDF's. Since then there has been numerous experimental validations of pulse compression by DDF's [8, 9, 10].

Another use of DDF is in the generation of solitons. It has been shown experimentally [31, 54] that passing a sinusoidal wave into a DDF will produce a periodic train of solitons. The dispersion profile of a DDF can either be composed of sections of constant dispersion, known as a discrete compressor, as in [10, 54], or be continuously varying along the length of the compressor [5, 8, 9]. Using both the soliton generation and pulse compression properties of a DDF, a sinusoidal wave input can be used to produce a train of solitons, which can then be compressed, ready for data transmission. This was the scenario studied by McKinnon *et al.* [34]. In that work, a Lagrangian method based on the work of Kath and Smyth [22] was used to study propagation in DDF's. This work was based on using a trial solution, with independently varying amplitude and width, in the Lagrangian for the NLS equation to obtain variational equations for

the wavetrain properties. Good agreement between the so-obtained approximate equations and full numerical solutions was found.

Besides getting an accurate representation of wavetrain evolution in DDF's, it is also of interest to find the dispersion profile of the DDF that will give maximum compression. This was also studied in [34] by utilising a multi-dimensional optimisation procedure to maximise the pulse amplitude, since increasing the amplitude decreases the width, thus leading to large data-transfer rates. The subject of this chapter is to extend the work of McKinnon *et al.* [34] by including the effect of fibre loss and radiation loss in the analysis. Two different analysis methods were utilised, one of which proved unsuccessful. However, for completeness, both methods will be discussed.

6.1 Approximate equations

As has been discussed previously, light travelling in a monomode, polarisation preserving, nonlinear optical fibre operating in the anomalous group-velocity regime is modelled by the NLS equation (1.1). If the dispersion is allowed to vary down the length of the fibre, the governing equation is the perturbed NLS equation

$$\mathrm{i}\frac{\partial u}{\partial z} + \frac{1}{2}\beta(z)\frac{\partial^2 u}{\partial t^2} + \Gamma(z)|u|^2 u = -\mathrm{i}\sigma u \tag{6.1}$$

in nondimensionalised form [20], where σ is the (linear) fibre loss (see Chapter 4). As before, u is the complex-valued envelope of the pulse, z is the normalised spatial variable along the length of the fibre and t is the normalised time in a frame of reference moving with the linear group velocity. The fibre is non-uniform, reflected in the fact that the dispersion coefficient β and nonlinear coefficient Γ are functions of the spatial variable z.

To study wavetrain evolution in DDF's, McKinnon *et al.* [34] used the Lagrangian method of Kath and Smyth [22]. When fibre loss is ignored, so that $\sigma = 0$, the NLS equation (6.1) possesses a Lagrangian. A trial solution based on a cnoidal wavetrain was substituted into the NLS Lagrangian and variations were then taken with respect to the wavetrain parameters to obtain ODE's for the evolution of these parameters. However, as the perturbed NLS equation (6.1) is not conservative, the Lagrangian method utilised in [34] cannot be used directly in the present work.

The first analysis method used to analyse the perturbed NLS equation (6.1) utilised conservation laws for this equation. This method is similar to that outlined in Section 2.1 for pulse evolution. However due to the algebraic complexity of the resulting ODE's, another method was investigated. This involved perform-

ing a transformation of the perturbed NLS equation (6.1), which reduced the equation to the unperturbed NLS equation of [34]. Based on this transformation, the approximate evolution equations of McKinnon *et al.* [34] can then be used to obtain approximate equations for wavetrain evolution for the perturbed NLS equation (6.1). Both of these methods will be discussed in turn.

Before discussing the techniques used to analyse evolving wavetrains, it will be useful to determine the form of the trial solution which will be used in the analysis. The scenario being studied is that in which a sinusoidal wave is used to create a train of compressed solitons. So the trial function must be able to mimic this evolutionary behaviour and must exhibit two unique traits. Firstly, the trial solution must incorporate an independently varying amplitude and width and a shelf of dispersive radiation as in (2.14) and (5.9) for pulse evolution. Secondly, the trial solution must be able to smoothly evolve from a sinusoidal input waveform to a train of solitons. The trial solution possessing both of these characteristics, and which was used in the study of McKinnon *et al.* [34] for the NLS equation, is

$$u = \left(\eta \operatorname{cn} \frac{t}{w} + \mathrm{i}g\right) \exp(\mathrm{i}\theta), \tag{6.2}$$

where $\operatorname{cn} x = cn(x|m)$ is the Jacobean elliptic cosine function of parameter m [1]. As $\operatorname{cn} x = \cos x$ when $m = 0$ and $\operatorname{cn} x = \operatorname{sech} x$ when $m = 1$, this trial solution displays the evolutionary behaviour desired. We also note that the trial solution includes the effect of the local long wavelength radiation through the parameter g, as in [4, 22]. The amplitude η, width w, phase θ and local radiation term g are all functions of z. The boundary condition, as assumed by McKinnon *et al.* [34], is a sinusoidal wave with amplitude A and frequency $1/W$

$$u(0,t) = A\cos(t/W). \tag{6.3}$$

In earlier chapters, the second term in the trial solution (6.2), corresponding to the radiation in the vicinity of a pulse, was assumed to hold in a region $-\ell/2 < t < \ell/2$ about the pulse. However, we are now dealing with a periodic wavetrain rather than a single, isolated pulse. To account for the periodic nature of the trial solution (6.2), McKinnon *et al.* [34] assumed that the radiation term holds in a region $-\mathrm{K}\,w < t < \mathrm{K}\,w$ about the pulse and is extended as an odd periodic function outside of this region. $\mathrm{K}(m)$ is the complete elliptic integral of the first kind [1] and the elliptic function $\operatorname{cn} x$ has period $4\,\mathrm{K}$. The radiation outside of the region $-\mathrm{K}\,w < t < \mathrm{K}\,w$, which is shed by an individual pulse, will be dealt with in a later section.

6.1.1 Conservation Equation Technique

For the perturbed NLS equation (6.1) the differential form of the conservation and moment equations (2.6)–(2.8) and (2.12) are modified to

$$\frac{\partial \rho}{\partial z} + \beta \frac{\partial J}{\partial t} = -2\sigma\rho, \tag{6.4}$$

$$\frac{\partial J}{\partial z} + \frac{\partial}{\partial t}\left[\beta\left(\rho^2 + E - \frac{1}{4}\rho_{tt}\right) - \frac{1}{2}\Gamma\rho^2\right] = -2\sigma J, \tag{6.5}$$

$$\begin{aligned}\frac{\partial}{\partial z}\left(\beta\left(E+\rho^2\right) - \Gamma\rho^2\right) + \frac{\partial}{\partial t}\Big[&\frac{\mathrm{i}}{2}\beta^2\left(u_t u_{tt}^* - u_t^* u_{tt}\right) \\ &- 2\beta\Gamma\rho J\Big] = 4\sigma\Gamma\rho^2 - 2\sigma\beta\left(E+\rho^2\right),\end{aligned} \tag{6.6}$$

$$\begin{aligned}\frac{\partial}{\partial z}tJ + \frac{\partial}{\partial t}\Big[&\beta tE + \beta t\rho^2 - \frac{1}{4}\beta t\rho_{tt} - \frac{1}{2}\Gamma\rho^2 \\ &+ \frac{1}{4}\beta\left(u^* u_t + u u_t^*\right)\Big] + \frac{1}{2}\Gamma\rho^2 - \beta E - \beta\rho^2 = -2\sigma tJ,\end{aligned} \tag{6.7}$$

where Γ and β are functions of z. Again these equations are conservation of mass, momentum, energy and moment of momentum respectively. Integrating these modified conservation and moment equations with respect to t over one period of the elliptic function $\operatorname{cn} x/w$, $-2\,\mathrm{K}\,w < t < 2\,\mathrm{K}\,w$, gives

$$\frac{\mathrm{d}}{\mathrm{d}z}\int_{-2\,\mathrm{K}\,w}^{2\,\mathrm{K}\,w} \rho\,\mathrm{d}t = -2\sigma\int_{-2\,\mathrm{K}\,w}^{2\,\mathrm{K}\,w} \rho\,\mathrm{d}t, \tag{6.8}$$

$$\frac{\mathrm{d}}{\mathrm{d}z}\int_{-2\,\mathrm{K}\,w}^{2\,\mathrm{K}\,w} J\,\mathrm{d}t = -2\sigma\int_{-2\,\mathrm{K}\,w}^{2\,\mathrm{K}\,w} J\,\mathrm{d}t, \tag{6.9}$$

$$\begin{aligned}\frac{\mathrm{d}}{\mathrm{d}z}\int_{-2\,\mathrm{K}\,w}^{2\,\mathrm{K}\,w} &\left(\beta|u_t|^2\,\mathrm{d}t - \Gamma\rho^2\right)\,\mathrm{d}t \\ &= 2\sigma\int_{-2\,\mathrm{K}\,w}^{2\,\mathrm{K}\,w}\left(2\Gamma\rho^2 - \beta|u_t|^2\right)\,\mathrm{d}t,\end{aligned} \tag{6.10}$$

$$\frac{\mathrm{d}}{\mathrm{d}z}\int_{-2\,\mathrm{K}\,w}^{2\,\mathrm{K}\,w} tJ\,\mathrm{d}t = \int_{-2\,\mathrm{K}\,w}^{2\,\mathrm{K}\,w}\left(\beta|u_t|^2 - \frac{1}{2}\Gamma\rho^2 - 2\sigma tJ\right)\,\mathrm{d}t. \tag{6.11}$$

Notice that the boundary condition (6.3) does not contain a t-dependent amplitude or phase, which means that the period P of the cnoidal wavetrain has

$$\mathrm{K}\,w = P = \frac{\pi}{2}W, \tag{6.12}$$

since $\mathrm{K}(0) = \pi/2$ is constant. Substituting the trial solution (6.2) into the conservation and moment equations (6.8)–(6.11) gives, after extensive algebra,

$$\frac{\mathrm{d}}{\mathrm{d}z}\left(\frac{\mathrm{E}-m_1\,\mathrm{K}}{m\,\mathrm{K}}\eta^2+g^2\right)=-2\sigma\left(\frac{\mathrm{E}-m_1\,\mathrm{K}}{m\,\mathrm{K}}\eta^2+g^2\right), \tag{6.13}$$

$$\begin{aligned}\frac{\mathrm{d}}{\mathrm{d}z}\left(\frac{2\eta g P\arcsin\left(\sqrt{m}\right)}{\mathrm{K}\sqrt{m}}\right)&=\frac{2\beta\eta^2\,\mathrm{K}}{3Pm}\left[(2m-1)\,\mathrm{E}+m_1\,\mathrm{K}\right]\\&\quad-\frac{\Gamma P\eta^4}{3\,\mathrm{K}\,m^2}\left[(2-3m)\,m_1\,\mathrm{K}+2\,(2m-1)\,\mathrm{E}\right]\\&\quad-\frac{2\Gamma\eta^2Pg^2}{\mathrm{K}\,m}\left(\mathrm{E}-m_1\,\mathrm{K}\right)-\frac{4\sigma\eta g P}{\mathrm{K}\sqrt{m}}\arcsin\left(\sqrt{m}\right),\end{aligned} \tag{6.14}$$

$$\begin{aligned}&\beta\frac{\mathrm{d}}{\mathrm{d}z}\left[\frac{\mathrm{K}\eta^2}{3Pm}\left((2m-1)\,\mathrm{E}+m_1\,\mathrm{K}\right)\right]\\&\quad-\Gamma\frac{\mathrm{d}}{\mathrm{d}z}\left[\frac{P\eta^4}{3\,\mathrm{K}\,m^2}\left((2-3m)\,m_1\,\mathrm{K}+2\,(2m-1)\,\mathrm{E}\right)+\frac{2\eta^2Pg^2}{\mathrm{K}\,m}\left(\mathrm{E}-m_1\,\mathrm{K}\right)\right]\\&\qquad=-2\sigma\left[\frac{\mathrm{K}\beta\eta^2}{3Pm}\left((2m-1)\,\mathrm{E}+m_1\,\mathrm{K}\right)\right]\\&\qquad\quad-\frac{4\Gamma\sigma\eta^4P}{3\,\mathrm{K}\,m^2}\left[(2-3m)\,m_1\,\mathrm{K}+2\,(2m-1)\,\mathrm{E}\right]\\&\qquad\qquad-\frac{8\Gamma\sigma\eta^2Pg^2}{\mathrm{K}\,m}\left(\mathrm{E}-m_1\,\mathrm{K}\right)\end{aligned} \tag{6.15}$$

where $m_1 = 1 - m$ is the complementary parameter and $\mathrm{E}(m)$ is the complete elliptic integral of the second kind [1]. As in the case of fibre loss in a uniform fibre, discussed in Chapter 4, the wavetrain can be taken to have zero velocity, and hence momentum, in a reference frame moving with the linear group velocity. This is reflected by the fact that the conservation of momentum equation (6.9) is identically satisfied by the trial solution (6.2).

What now remains is to perform the required differentiation in equations (6.13)–(6.15) to get them into a form ready for the approximate equation solver outlined in Section 3.2. While this was attempted for some time, the overwhelming complexity of the equations rendered much of the algebra virtually unworkable. As a result, another method was investigated to analyse the perturbed NLS equation (6.1).

6.1.2 Transformation Technique

While the conservation equation technique outlined in the previous section proved difficult, another method proved tractable. Let us perform the transformation

$$u = U(\xi, t)\mathrm{e}^{-\sigma z} \tag{6.16}$$

on the perturbed NLS equation (6.1), where

$$\xi = \frac{1 - \mathrm{e}^{-2\sigma z}}{2\sigma}. \tag{6.17}$$

The perturbed NLS equation (6.1) is then transformed to the NLS equation

$$\mathrm{i}U_\xi + \frac{1}{2}\tilde{\beta}U_{tt} + \Gamma|U|^2U = 0, \tag{6.18}$$

where

$$\tilde{\beta} = \beta \mathrm{e}^{2\sigma z}. \tag{6.19}$$

The transformed NLS equation (6.18) is the same equation, in the new variables, as that examined in the study of McKinnon *et al.* [34]. In that work, the NLS equation with variable dispersion was analysed using a Lagrangian technique. Specifically, the trial solution (6.2) was substituted into the Lagrangian for the NLS equation (6.18). Variations were then taken with respect to the wavetrain parameters, resulting in ODE's for these parameters. The Lagrangian for the NLS equation (6.18) is

$$L = \mathrm{i}(U^*U_\xi - UU_\xi^*) - \tilde{\beta}|U_t|^2 + \Gamma|U|^4, \tag{6.20}$$

where $*$ denotes the complex conjugate. Substituting the trial solution (6.2), suitably transformed as

$$U = \left(A \operatorname{cn}\frac{t}{w} + \mathrm{i}G\right)\exp(\mathrm{i}\theta), \tag{6.21}$$

into the Lagrangian (6.20), the averaged Lagrangian

$$\mathcal{L} = \int_{-2\mathrm{K}w}^{2\mathrm{K}w} L\,\mathrm{d}t = 2\int_{-\mathrm{K}w}^{\mathrm{K}w} L\,\mathrm{d}t \tag{6.22}$$

can be evaluated, on using symmetry. The averaged Lagrangian is therefore found to be

$$\begin{aligned}\frac{1}{2}\mathcal{L} = {} & \frac{2P}{\mathrm{K}}\frac{\arcsin(\sqrt{m})}{\sqrt{m}}(GA' - AG') - \frac{2P}{\mathrm{K}}\frac{\mathrm{E} - m_1\mathrm{K}}{m}A^2\theta' \\ & - \frac{P}{\mathrm{K}^2}\frac{\arcsin(\sqrt{m})}{\sqrt{m}}\frac{\mathrm{E} - m_1\mathrm{K}}{mm_1}AGm' - 2PG^2\theta' - \tilde{\beta}\frac{\mathrm{K}^2}{P}m_1A^2 \\ & + \tilde{\beta}\frac{\mathrm{K}}{P}\frac{(2m_1 - 1)\,\mathrm{E} + 2m_1\,\mathrm{K}}{3m}A^2 + \Gamma\frac{P}{\mathrm{K}}\frac{(3m_1 - 1)m_1\,\mathrm{K} + 2(1 - 2m_1)\,\mathrm{E}}{3m^2}A^4\end{aligned} \tag{6.23}$$

Taking variations of the averaged Lagrangian (6.23) with respect to the wavetrain parameters A, G, θ and m, noting that w is given by equation (6.12), we obtain

the variational equations describing wavetrain parameter evolution as

$$\frac{4P}{\mathrm{K}}\frac{\arcsin(\sqrt{m})}{\sqrt{m}}\frac{\mathrm{d}A}{\mathrm{d}\xi}+\frac{PA}{\mathrm{K}^2}\left(\frac{\mathrm{K}}{m\sqrt{m_1}}-\frac{\arcsin(\sqrt{m})}{\sqrt{m}}\frac{2\,\mathrm{E}-m_1\,\mathrm{K}}{mm_1}\right)\frac{\mathrm{d}m}{\mathrm{d}\xi}-4PG\frac{\mathrm{d}\theta}{\mathrm{d}\xi}=0, \tag{6.24}$$

$$\frac{4\arcsin(\sqrt{m})}{\sqrt{m}}\frac{\mathrm{d}G}{\mathrm{d}\xi}+\left(\frac{1}{m\sqrt{m_1}}-\frac{\arcsin(\sqrt{m})}{m\sqrt{m}}\right)G\frac{\mathrm{d}m}{\mathrm{d}\xi}+4\frac{\mathrm{E}-m_1\,\mathrm{K}}{m}A\frac{\mathrm{d}\theta}{\mathrm{d}\xi}=\frac{4}{3}\Gamma\frac{(3m_1-1)\,m_1\,\mathrm{K}+2\,(1-2m_1)\,\mathrm{E}}{m^2}A^3-2\tilde{\beta}\frac{\mathrm{K}^2}{P^2}\frac{m_1\,\mathrm{K}-(2m_1-1)\,\mathrm{E}}{3m}A, \tag{6.25}$$

$$\frac{2}{\mathrm{K}}\frac{\mathrm{E}-m_1\,\mathrm{K}}{m}A\frac{\mathrm{d}A}{\mathrm{d}\xi}+2G\frac{\mathrm{d}G}{\mathrm{d}\xi}-\frac{\mathrm{E}^2-m_1\,\mathrm{K}^2}{2m_1m^2\,\mathrm{K}^2}A^2\frac{\mathrm{d}m}{\mathrm{d}\xi}=0, \tag{6.26}$$

$$P\left(\sqrt{m_1}-m_1\frac{\arcsin(\sqrt{m})}{\sqrt{m}}\right)G\frac{\mathrm{d}A}{\mathrm{d}\xi}+\frac{P}{\mathrm{K}}\left[\frac{\arcsin(\sqrt{m})}{\sqrt{m}}\,(2\,\mathrm{E}-m_1\,\mathrm{K})-\mathrm{K}\sqrt{m_1}\right]A\frac{\mathrm{d}G}{\mathrm{d}\xi}+\frac{P}{\mathrm{K}}\frac{\mathrm{E}^2-m_1\,\mathrm{K}^2}{m}A^2\frac{\mathrm{d}\theta}{\mathrm{d}\xi}=\tilde{\beta}\frac{\mathrm{K}}{6P}\frac{\mathrm{E}^2+4m_1\,\mathrm{E}\,\mathrm{K}-2m_1\,\mathrm{E}^2-3m_1\,\mathrm{K}^2}{m}A^2-\Gamma\frac{P}{3\,\mathrm{K}}\frac{2m_1\,\mathrm{E}\,\mathrm{K}-3m_1^2\,\mathrm{K}^2-(1-2m_1)\,\mathrm{E}^2}{m^2}A^4, \tag{6.27}$$

after extensive algebraic manipulation and simplification. Notice that the above evolution equations contain θ, the phase. These equations were derived by taking variations of the averaged NLS Lagrangian and, as such, an equation for the phase is obtained, unlike for the conservation and moment equation approach.

Transforming back to the original variables using the transformations

$$A = \eta\mathrm{e}^{\sigma z}, \tag{6.28}$$

$$G = g\mathrm{e}^{\sigma z}, \tag{6.29}$$

$$\frac{\mathrm{d}}{\mathrm{d}\xi} = \mathrm{e}^{2\sigma z}\frac{\mathrm{d}}{\mathrm{d}z}, \tag{6.30}$$

the approximate evolution equations for the perturbed NLS equation (6.1) are

$$\frac{4P}{\mathrm{K}}\frac{\arcsin(\sqrt{m})}{\sqrt{m}}\frac{\mathrm{d}\eta}{\mathrm{d}z}+\frac{P\eta}{\mathrm{K}^2}\left(\frac{\mathrm{K}}{m\sqrt{m_1}}-\frac{\arcsin(\sqrt{m})}{\sqrt{m}}\frac{2\,\mathrm{E}-m_1\,\mathrm{K}}{mm_1}\right)\frac{\mathrm{d}m}{\mathrm{d}z}-4Pg\frac{\mathrm{d}\theta}{\mathrm{d}z}=-\frac{4P\sigma\eta}{\mathrm{K}}\frac{\arcsin(\sqrt{m})}{\sqrt{m}}, \tag{6.31}$$

$$\frac{4\arcsin(\sqrt{m})}{\sqrt{m}}\frac{\mathrm{d}g}{\mathrm{d}z}+\left(\frac{1}{m\sqrt{m_1}}-\frac{\arcsin(\sqrt{m})}{m\sqrt{m}}\right)g\frac{\mathrm{d}m}{\mathrm{d}z}$$
$$+4\frac{\mathrm{E}-m_1\,\mathrm{K}}{m}\eta\frac{\mathrm{d}\theta}{\mathrm{d}z}=\frac{4}{3}\Gamma\frac{(3m_1-1)\,m_1\,\mathrm{K}+2\,(1-2m_1)\,\mathrm{E}}{m^2}\eta^3$$
$$-2\beta\frac{\mathrm{K}^2}{P^2}\frac{m_1\,\mathrm{K}-(2m_1-1)\,\mathrm{E}}{3m}\eta-\frac{4\sigma g\arcsin(\sqrt{m})}{\sqrt{m}},\quad(6.32)$$

$$\frac{2}{\mathrm{K}}\frac{\mathrm{E}-m_1\,\mathrm{K}}{m}\eta\frac{\mathrm{d}\eta}{\mathrm{d}z}+2g\frac{\mathrm{d}g}{\mathrm{d}z}-\frac{\mathrm{E}^2-m_1\,\mathrm{K}^2}{2m_1m^2\,\mathrm{K}^2}\eta^2\frac{\mathrm{d}m}{\mathrm{d}z}=-\frac{2\sigma}{\mathrm{K}}\frac{\mathrm{E}-m_1\,\mathrm{K}}{m}\eta^2-2\sigma g^2,\quad(6.33)$$

$$P\left(\sqrt{m_1}-m_1\frac{\arcsin(\sqrt{m})}{\sqrt{m}}\right)g\frac{\mathrm{d}\eta}{\mathrm{d}z}$$
$$+\frac{P}{\mathrm{K}}\left[\frac{\arcsin(\sqrt{m})}{\sqrt{m}}\,(2\,\mathrm{E}-m_1\,\mathrm{K})-\mathrm{K}\sqrt{m_1}\right]\eta\frac{\mathrm{d}g}{\mathrm{d}z}$$
$$+\frac{P}{\mathrm{K}}\frac{\mathrm{E}^2-m_1\,\mathrm{K}^2}{m}\eta^2\frac{\mathrm{d}\theta}{\mathrm{d}z}$$
$$=\beta\frac{\mathrm{K}}{6P}\frac{\mathrm{E}^2+4m_1\,\mathrm{E}\,\mathrm{K}-2m_1\,\mathrm{E}^2-3m_1\,\mathrm{K}^2}{m}\eta^2$$
$$-\Gamma\frac{P}{3\,\mathrm{K}}\frac{2m_1\,\mathrm{E}\,\mathrm{K}-3m_1^2\,\mathrm{K}^2-(1-2m_1)\,\mathrm{E}^2}{m^2}\eta^4$$
$$-\sigma P\left(\sqrt{m_1}-m_1\frac{\arcsin(\sqrt{m})}{\sqrt{m}}\right)\eta g$$
$$-\frac{\sigma P}{\mathrm{K}}\left(\frac{\arcsin(\sqrt{m})}{\sqrt{m}}\,(2\,\mathrm{E}-m_1\,\mathrm{K})-\mathrm{K}\sqrt{m_1}\right)\eta g.\quad(6.34)$$

In calculating the right-hand side of equation (6.34) numerical difficulties can be encountered as the numerator and denominator of the first two terms vanish for small m. To overcome this, they are expanded as a Taylor series in m [1] as

$$\frac{2m_1\,\mathrm{E}\,\mathrm{K}-3m_1^2\,\mathrm{K}^2-(1-2m_1)\,\mathrm{E}^2}{m^2}=-\frac{3\pi^2m}{64}+O(m^2),\quad(6.35)$$
$$\frac{\mathrm{E}^2+4m_1\,\mathrm{E}\,\mathrm{K}-2m_1\,\mathrm{E}^2-3m_1\,\mathrm{K}^2}{m}=-\frac{3\pi^2m}{32}+O(m^2).\quad(6.36)$$

As the wavetrain, modelled by the above equations, travels along the DDF it will evolve from the sinusoidal input waveform (6.3) to a train of solitons. So as z increases, $m\to 1$ as $\mathrm{cn}\,z=\mathrm{sech}\,z$ when $m=1$. However the evolution equations (6.31)–(6.34) are singular as $m\to 1$ since $\mathrm{K}\to\infty$ as $m\to 1$ [1]. This singularity is due to the fact that the period P is constant, so that from (6.12), $w\to 0$ as $m\to 1$. This in turn is a reflection of the fact that a periodic wavetrain can never become an exact train of solitons since a soliton is an isolated wave on $-\infty<t<\infty$.

To overcome this singularity as $m \to 1$ McKinnon *et al.* [34] noted that as $m \to 1$, the trial solution (6.2) approaches the pulse solution

$$u = \eta \operatorname{sech} \frac{t}{w} \exp(\mathrm{i}\theta) + \mathrm{i}g \exp(\mathrm{i}\theta). \tag{6.37}$$

which is the same as that utilised in Chapter 4. Therefore as $m \to 1$ the approximate equations (6.31)–(6.34) must approach pulse equations similar to those of Chapter 4.

To obtain these pulse equations as $m \to 1$, we note that the transformations (6.16) and (6.17) can again be used to transform the NLS equation (6.1) with loss to the NLS equation (6.18). To obtain the approximate equations for the NLS equation (6.18), the pulse trial function

$$U = (A \operatorname{sech} \frac{t}{w} + \mathrm{i}G) \exp(\mathrm{i}\theta) \tag{6.38}$$

is substituted into the NLS Lagrangian (6.20), which is then averaged by integrating in t from $-\infty$ to ∞. Taking variations of this averaged Lagrangian results in the approximate equations

$$\frac{\mathrm{d}}{\mathrm{d}\xi}(Aw) = \frac{G\ell}{\pi}\left(\Gamma A^2 - \frac{\tilde{\beta}}{2w^2}\right), \tag{6.39}$$

$$\frac{\mathrm{d}G}{\mathrm{d}\xi} = -\frac{2A}{3\pi}\left(\Gamma A^2 - \tilde{\beta} w^{-2}\right), \tag{6.40}$$

$$\frac{\mathrm{d}\theta}{\mathrm{d}\xi} = \Gamma A^2 - \frac{\tilde{\beta}}{2w^2}, \tag{6.41}$$

$$\left(2\tilde{\beta}\frac{A}{w} - 8\Gamma A^3 w\right)\frac{\mathrm{d}A}{\mathrm{d}\xi} - \left(\tilde{\beta}\frac{A^2}{w^2} + 2\Gamma A^4\right)\frac{\mathrm{d}w}{\mathrm{d}\xi} = 0. \tag{6.42}$$

Transforming these evolution equations back to the original variables using the transformations (6.28)–(6.30), we obtain the equations

$$\frac{\mathrm{d}}{\mathrm{d}z}(\eta w) = \frac{g\ell}{\pi}\left(\eta^2 - \frac{\beta}{2w^2}\right) - \sigma\eta w, \tag{6.43}$$

$$\frac{\mathrm{d}g}{\mathrm{d}z} = -\frac{2\eta}{3\pi}\left(\eta^2 - \beta w^{-2}\right) - \sigma g, \tag{6.44}$$

$$\frac{\mathrm{d}\theta}{\mathrm{d}z} = \eta^2 - \frac{\beta}{2w^2}, \tag{6.45}$$

$$\left(2\beta\frac{\eta}{w} - 8\eta^3 w\right)\frac{\mathrm{d}\eta}{\mathrm{d}z} - \left(\beta\frac{\eta^2}{w^2} + 2\eta^4\right)\frac{\mathrm{d}w}{\mathrm{d}z} = 8\sigma\eta^4 w - 2\sigma\beta\frac{\eta^2}{w} \tag{6.46}$$

for the parameters of the pulse (6.37). It can be verified that the variational equations (6.31) to (6.34) for the cnoidal wavetrain reduce to these pulse equations

in the limit $m \to 1$. For a pulse, the shelf length ℓ can again be found by matching the frequency of oscillations of solutions of the approximate equations (6.43)–(6.46) near the fixed point $\eta = \hat{\kappa}$, $w = \hat{w}$, where $\hat{\kappa}^2\hat{w}^2 = \beta/\Gamma$, to the NLS soliton oscillation frequency, which gives

$$\ell = \frac{3\pi^2\sqrt{\beta}}{8\hat{\kappa}\sqrt{\Gamma}}, \tag{6.47}$$

where the fixed point $\hat{\kappa}$ is determined by

$$\hat{\kappa} = \left(2\sqrt{\frac{\Gamma}{\beta}}\eta^4 w - \sqrt{\frac{\beta}{\Gamma}}\frac{\eta^2}{w}\right)^{1/3}. \tag{6.48}$$

The steady amplitude $\hat{\kappa}$ was found from the energy conservation equation (6.46) with fibre loss $\sigma = 0$. In deriving ℓ, it has also been assumed that β and Γ are constant. If β and Γ are, however, slowly varying, it is assumed that the same expression will hold. A similar assumption was made in Chapters 4 and 5. The method used here and in Section 2.1 for determining $\hat{\kappa}$ will give the local value of $\hat{\kappa}$ that the pulse would achieve if the fibre loss was removed. With this value of ℓ, setting $\sigma = 0$ in (6.43)–(6.46) will give the approximate evolution equations for the NLS equation as found in [34].

Studying the evolution of the cnoidal wavetrain now involves numerically solving the approximate equations (6.31)–(6.34). As the wavetrain evolves, the modulus $m \to 1$, reflecting that the wavetrain is approaching a train of solitons. As m gets sufficiently close to 1, say $m = 0.9999$ at a distance $z = z_s$, we switch over to the pulse evolution equations (6.43)–(6.46) with the initial value of the pulse width w given by the period relation (6.12) as

$$w = \frac{P}{\mathrm{K}}. \tag{6.49}$$

After $z = z_s$ we must include the effects of the dispersive radiation shed away from the pulse in order for the solution of the approximate equations (6.43)–(6.46) to evolve to a steady pulse. The form of this radiation is dealt with in the next section. After the final point at which the dispersion changes , $z = z_f$, the fibre loss is removed. This has the effect of allowing the pulse train to settle down to a steady amplitude in the constant dispersion section in $z > z_f$. The lack of fibre loss can be interpreted as perfect amplification, meaning there is no net loss in the fibre.

6.2 Radiation Analysis

As mentioned in the last section, the effects of dispersive radiation are added after the switch is made to the soliton equations (6.43)–(6.46) at $z = z_s$ defined

by the value of z for which $m = 0.9999$. This point is generally close to the last dispersion point defined by $z = z_f$. The radiation integral which gives this radiation loss will be similar to that derived in Section 4.2 for the NLS equation with fibre loss. However, a radiation integral of this form is not suitable for use with the numerical optimiser. This is because the time required for a single numerical solution of the approximate equations is significantly increased when the radiation integral is included. This is not a problem for a single solution, but in the case of the optimised dispersion profiles, where hundreds of numerical solutions may be necessary, it proves prohibitive. Kath and Smyth [22] found an asymptotic expression for $z \to \infty$ to the radiation integral (2.36) based on the assumption that the radiation loss is dominated by the loss near $z = 0$. As this expression requires no numerical integration at every time-step, as for the integral (2.36), execution is very fast. However, a similar asymptotic expansion for a radiation integral incorporating fibre loss, as in (4.28) is not possible as the radiation loss is not dominated by the loss near $z = 0$. Rather in the fibre loss case radiation is lost throughout the evolution of the pulse, not necessarily near $z = 0$. However, as mentioned above, the point at which we switch to the pulse equations, $z = z_s$ is usually close to the last dispersion point defined by $z = z_f$. As the fibre loss is neglected after the final dispersion point, $z = z_f$, as discussed above, fibre loss only effects the radiation integral in a small region $z_s < z < z_f$. As such it seems reasonable to neglect the extra contribution due to the fibre loss in this small region. This will allow us to obtain a radiation integral for which an asymptotic approximation exists, thus making the inclusion of radiation damping in the optimiser a reasonable proposition.

Taking the perturbed variable coefficient NLS equation (6.1) and neglecting fibre loss, so that $\sigma = 0$, we obtain the NLS equation

$$\mathrm{i}u_z + \frac{1}{2}\beta u_{tt} + \Gamma|u|^2 u = 0. \tag{6.50}$$

Under the transformations

$$U = \sqrt{\frac{\beta}{\Gamma}}u, \tag{6.51}$$

$$Z = \beta(z - z_s), \tag{6.52}$$

this NLS equation then becomes

$$\mathrm{i}U_Z + \frac{1}{2}U_{tt} + |U|^2 U = 0. \tag{6.53}$$

This is the same equation, in the transformed variables Z and U, as that studied by Kath and Smyth [22] and also considered in Section 2.2. As such we may use

the radiation analysis of Section 2.2. Using a pulse trial function of the form of (6.38), the pulse parameter evolution equations, from Section 2.2 are

$$\frac{\mathrm{d}}{\mathrm{d}Z}(Aw) = \frac{GL}{\pi}\left(A^2 - \frac{1}{2}w^{-2}\right) \tag{6.54}$$

$$\frac{\mathrm{d}G}{\mathrm{d}Z} = \frac{2}{3\pi}\frac{A}{w^2}\left(1 - A^2w^2\right) - 2\hat{\alpha}G \tag{6.55}$$

$$\frac{\mathrm{d}\theta}{\mathrm{d}Z} = A^2 - \frac{1}{2}w^{-2}, \tag{6.56}$$

$$\left(2\frac{A}{w} - 8A^3w\right)\frac{\mathrm{d}A}{\mathrm{d}Z} - \left(\frac{A^2}{w^2} + 2A^4\right)\frac{\mathrm{d}w}{\mathrm{d}Z} = 0. \tag{6.57}$$

where

$$\hat{\alpha} = \frac{3K}{8}\frac{1}{R}\frac{\mathrm{d}}{\mathrm{d}Z}\int_0^Z \frac{R}{\sqrt{\pi\left(Z-\tau\right)}}\,\mathrm{d}\tau. \tag{6.58}$$

Energy conservation gives that the steady state, K, is given by

$$K = \left(2A^4w - \frac{A^2}{w}\right)^{1/3} \tag{6.59}$$

and the shelf width L is given, as before, by

$$L = \frac{3\pi^2}{8K}. \tag{6.60}$$

From the results of Section 2.2, the shelf height at the edge of the shelf, R, is given by

$$R^2 = \frac{3K}{8}\left(2A^2w - 2K + \frac{3\pi^2}{8K}G^2\right). \tag{6.61}$$

Transforming back to the original variables via

$$A = \sqrt{\frac{\Gamma}{\beta}}\,\eta, \tag{6.62}$$

$$G = \sqrt{\frac{\Gamma}{\beta}}\,g, \tag{6.63}$$

$$Z = \beta(z - z_s), \tag{6.64}$$

these expressions become

$$K = \sqrt{\frac{\Gamma}{\beta}}\left(2\sqrt{\frac{\Gamma}{\beta}}\eta^4 w - \sqrt{\frac{\beta}{\Gamma}}\frac{\eta^2}{w}\right)^{1/3} = \sqrt{\frac{\Gamma}{\beta}}\,\hat{\kappa} \tag{6.65}$$

and

$$R^2 = \frac{\Gamma}{\beta}\frac{3\hat{\kappa}}{8}\sqrt{\frac{\Gamma}{\beta}}\left[2\eta^2 w - 2\sqrt{\frac{\beta}{\Gamma}}\hat{\kappa} + \sqrt{\frac{\beta}{\Gamma}}\frac{3\pi^2}{8\hat{\kappa}}g^2\right] = \frac{\Gamma}{\beta}r^2. \tag{6.66}$$

In the above two equations, the steady amplitude $\hat{\kappa}$ and the radiation height at the edge of the shelf r are the same expressions as in McKinnon *et al.* [34]. The shelf width L is the same as that given by equation (6.47). The expression for the radiation integral, $\hat{\alpha}$, becomes

$$\hat{\alpha} = \frac{3\hat{\kappa}}{8}\frac{\sqrt{\Gamma}}{r}\frac{1}{\beta}\frac{\mathrm{d}}{\mathrm{d}z}\int_0^{\beta(z-z_s)} \frac{r}{\sqrt{\pi\beta}\sqrt{[\beta(z-z_s)-\tau]}}\,\mathrm{d}\tau \tag{6.67}$$

in the original variables. Introducing the new variable of integration $y = \tau/\beta$, the radiation integral (6.67) simplifies to

$$\hat{\alpha} = \frac{3\hat{\kappa}}{8}\frac{\sqrt{\Gamma}}{r(y)}\frac{1}{\beta}\frac{\mathrm{d}}{\mathrm{d}z}\int_0^{z-z_s} \frac{r}{\sqrt{\pi\,(z-z_s-y)}}\,\mathrm{d}y. \tag{6.68}$$

The final step is to transform pulse evolution equations (6.54)–(6.56) back to the original variables to get

$$\frac{\mathrm{d}}{\mathrm{d}z}(\eta w) = \frac{g\ell}{\pi}\left(\Gamma\eta^2 - \frac{\beta}{2w^2}\right), \tag{6.69}$$

$$\frac{\mathrm{d}g}{\mathrm{d}z} = -\frac{2\eta}{3\pi}\left(\Gamma\eta^2 - \beta w^{-2}\right) - 2\hat{\alpha}\beta g, \tag{6.70}$$

$$\frac{\mathrm{d}\psi}{\mathrm{d}z} = \Gamma\eta^2 - \frac{\beta}{2w^2}, \tag{6.71}$$

with the loss coefficient $\hat{\alpha}$ given by equation (6.68).

Due to the large number of numerical integrations required when the optimisation of the pulse compression is performed, it is of significant importance to make the individual numerical integrations of the approximate equations as quick as possible. Keeping this in mind, the radiation integral $\hat{\alpha}$ in equation (6.68) for g is a potential problem. At each distance step in a numerical integration, the integral in (6.68) must be calculated over all the distance $z - z_s$. In other words, as the integration progresses and z increases, the numerical integration becomes progressively slower. For a small number of integrations this is not a problem. However, for a large number of individual integrations over the fibre length, as for dispersion optimisation, the calculations of the integral in (6.68) can render the optimisation impractical. To avoid this problem, Kath and Smyth [22] found an asymptotic approximation for the integral in (6.68) when this integral is dominated by r near $z = z_s$. Using this asymptotic expression, equation (6.58) becomes

$$\hat{\alpha} = \frac{3K}{8}\frac{R}{R(z_s)\sqrt{\pi Z}}. \tag{6.72}$$

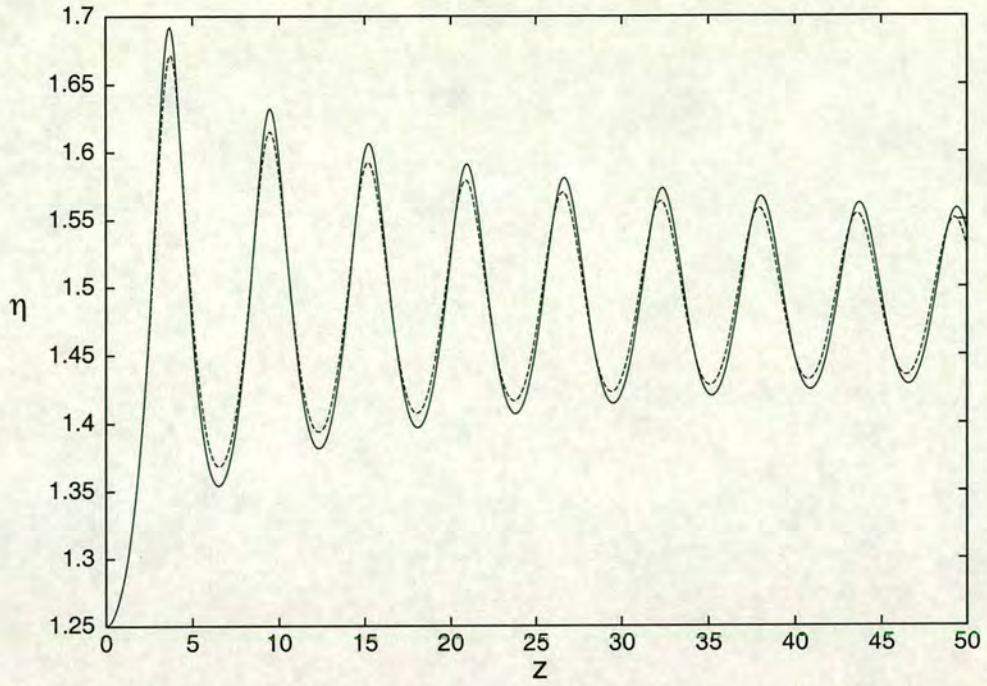

Figure 6.1: Amplitude η versus distance z: Comparison between approximate solutions for non-soliton boundary condition with $\eta = 1.25$, $w = 1$. Solution of approximate equations (6.43)–(6.46) with (6.58): — ; solution of approximate equations (6.43)–(6.46) with (6.72): - - - -

Transforming this expression back to the original variables, we obtain

$$\hat{\alpha} = \frac{3\hat{\kappa}}{8}\frac{\Gamma}{\beta}\frac{r}{R(z_s)\sqrt{\pi\beta(z - z_s)}}, \tag{6.73}$$

where $R(z_s)$ is given by (6.66) evaluated at the distance at which the wavetrain is approximated by a train of solitons, i.e. when $m = 0.9999$. The approximation (6.72) to the true radiation integral (6.58) is in general quite accurate. Figure 6.1 shows a comparison between the solution of the approximate equations (6.69)–(6.71), with constant dispersion $\beta = 1.0$ using the two different radiation expressions (6.72) and (6.68). The initial condition is a soliton-like pulse with $\eta = 1.25$ and $w = 1$. As can be seen in the figure, there is very little difference between the two solutions. The radiation given by (6.72), is slightly over-estimated in comparison to the full expression (6.68), but overall, there is very little difference. So, in the interest of keeping numerical computation times to a minimum, it seems reasonable to use the asymptotic expression (6.73) as an estimate of the radiation.

Another possible solution to the problem of long integration times would be to split the radiation integral into two regions. In the first region, defined as $z_s < z < z_f$ from the point at which radiation is just included up to the final dispersion point, the radiation could be evaluated using the full radiation integral

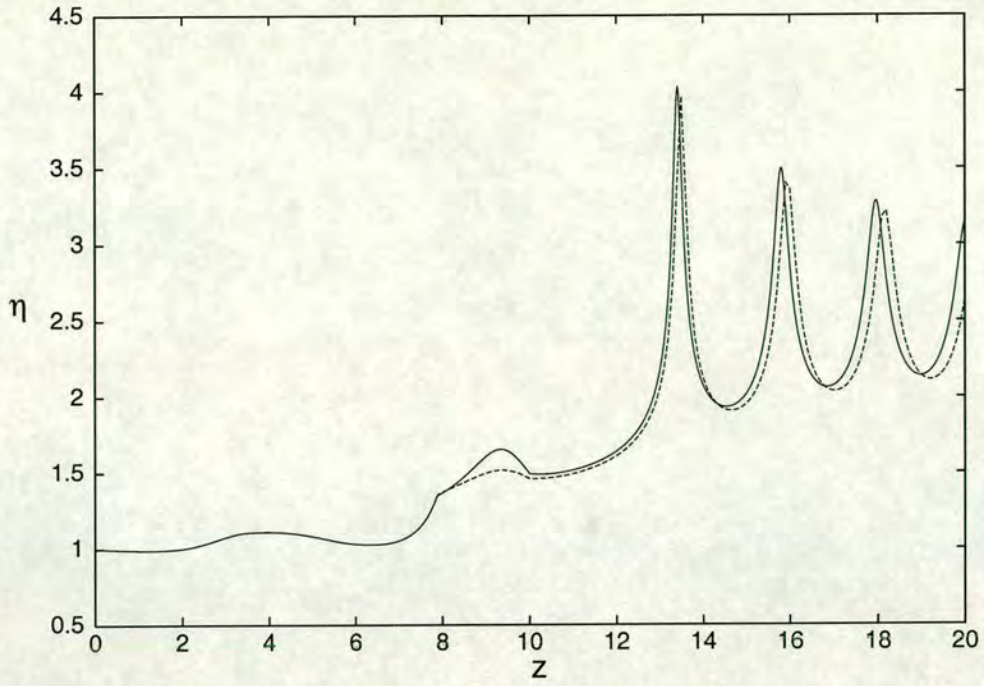

Figure 6.2: Amplitude η versus distance z: Comparison between approximate solutions over a randomly varying decreasing dispersion profile of length 10 km with fibre loss $\sigma = 0.03$. Solution of approximate equations (6.43)–(6.46) using asymptotic radiation approximation (6.73) over entire range: — ; solution of approximate equations (6.43)–(6.46) using full radiation approximation (6.68) for $z_s < z < z_f$ and asymptotic approximation (6.73) for $z > z_f$: – – – –

(6.68). In the second region, defined by $z > z_f$ after the final dispersion point, the asymptotic approximation (6.73) could be used. As the region $z_s < z < z_f$ is usually quite small, the time required for the integration of (6.68) may be reasonable. Figure 6.2 shows a comparison between a simulation using the above described radiation analysis method and one in which the asymptotic approximation (6.73) is used over the entire applicable range $z > z_s$. As can be seen in Figure 6.2 there is very little difference between the two methods beyond a small phase shift. Worth mentioning are the two small kinks seen in the numerical solutions at approximately $z = 8$ and $z = 10$. The first corresponds to the point $z = z_s$, where the switch to soliton equations is made. The second point corresponds to $z = z_f$, the final dispersion point in the fibre. With this information, and considering the increased time required to perform the numerical integration required by (6.68), it still seems reasonable to use the asymptotic approximation (6.73) over the entire range of integration $z > z_s$.

To summarise, the equations governing the evolution of a sinusoidal input wave to a train of compressed solitons consists of two sets. The first govern the evolution of the input wave to a train of compressed soliton-like pulses based

upon the wavetrain trial solution (6.2) and are

$$\begin{aligned}\frac{4P}{\mathrm{K}}\frac{\arcsin(\sqrt{m})}{\sqrt{m}}\frac{\mathrm{d}\eta}{\mathrm{d}z}+\frac{P\eta}{\mathrm{K}^2}\left(\frac{\mathrm{K}}{m\sqrt{m_1}}-\frac{\arcsin(\sqrt{m})}{\sqrt{m}}\frac{2\,\mathrm{E}-m_1\,\mathrm{K}}{mm_1}\right)\frac{\mathrm{d}m}{\mathrm{d}z}\\ -4Pg\frac{\mathrm{d}\psi}{\mathrm{d}t}=-\frac{4P\sigma\eta}{\mathrm{K}}\frac{\arcsin(\sqrt{m})}{\sqrt{m}},\end{aligned}\tag{6.74}$$

$$\begin{aligned}\frac{4\arcsin(\sqrt{m})}{\sqrt{m}}\frac{\mathrm{d}g}{\mathrm{d}z}+\left(\frac{1}{m\sqrt{m_1}}-\frac{\arcsin(\sqrt{m})}{m\sqrt{m}}\right)g\frac{\mathrm{d}m}{\mathrm{d}z}\\ +4\frac{\mathrm{E}-m_1\,\mathrm{K}}{m}\eta\frac{\mathrm{d}\psi}{\mathrm{d}z}=\frac{4}{3}\Gamma\frac{(3m_1-1)\,m_1\,\mathrm{K}+2\,(1-2m_1)\,\mathrm{E}}{m^2}\eta^3\\ -2\beta\frac{\mathrm{K}^2}{P^2}\frac{m_1\,\mathrm{K}-(2m_1-1)\,\mathrm{E}}{3m}\eta-\frac{4\sigma g\arcsin(\sqrt{m})}{\sqrt{m}},\end{aligned}\tag{6.75}$$

$$\frac{2}{\mathrm{K}}\frac{\mathrm{E}-m_1\,\mathrm{K}}{m}\eta\frac{\mathrm{d}\eta}{\mathrm{d}z}+2g\frac{\mathrm{d}g}{\mathrm{d}z}-\frac{\mathrm{E}^2-m_1\,\mathrm{K}^2}{2m_1m^2\,\mathrm{K}^2}\eta^2\frac{\mathrm{d}m}{\mathrm{d}z}=-\frac{2\sigma}{\mathrm{K}}\frac{\mathrm{E}-m_1\,\mathrm{K}}{m}\eta^2-2\sigma g^2,\tag{6.76}$$

$$\begin{aligned}P\left(\sqrt{m_1}-m_1\frac{\arcsin(\sqrt{m})}{\sqrt{m}}\right)g\frac{\mathrm{d}\eta}{\mathrm{d}z}\\ +\frac{P}{\mathrm{K}}\left[\frac{\arcsin(\sqrt{m})}{\sqrt{m}}\,(2\,\mathrm{E}-m_1\,\mathrm{K})-\mathrm{K}\sqrt{m_1}\right]\eta\frac{\mathrm{d}g}{\mathrm{d}z}\\ +\frac{P}{\mathrm{K}}\frac{\mathrm{E}^2-m_1\,\mathrm{K}^2}{m}\eta^2\frac{\mathrm{d}\psi}{\mathrm{d}z}\\ =\beta\frac{\mathrm{K}}{6P}\frac{\mathrm{E}^2+4m_1\,\mathrm{E}\,\mathrm{K}-2m_1\,\mathrm{E}^2-3m_1\,\mathrm{K}^2}{m}\eta^2\\ -\Gamma\frac{P}{3\,\mathrm{K}}\frac{2m_1\,\mathrm{E}\,\mathrm{K}-3m_1^2\,\mathrm{K}^2-(1-2m_1)\,\mathrm{E}^2}{m^2}\eta^4\\ -\sigma P\left(\sqrt{m_1}-m_1\frac{\arcsin(\sqrt{m})}{\sqrt{m}}\right)\eta g\\ -\frac{\sigma P}{\mathrm{K}}\left(\frac{\arcsin(\sqrt{m})}{\sqrt{m}}\,(2\,\mathrm{E}-m_1\,\mathrm{K})-\mathrm{K}\sqrt{m_1}\right)\eta g.\end{aligned}\tag{6.77}$$

When the wavetrain very nearly approximates a train of solitons, i.e. when $m = 0.9999$, we switch to the second set of evolution equations based upon the pulse trial solution (6.37)

$$\frac{\mathrm{d}}{\mathrm{d}z}(\eta w) = \frac{g\ell}{\pi}\left(\Gamma\eta^2-\frac{\beta}{2w^2}\right)-\sigma\eta w,\tag{6.78}$$

$$\frac{\mathrm{d}g}{\mathrm{d}z} = -\frac{2\eta}{3\pi}\left(\Gamma\eta^2-\beta w^{-2}\right)-\sigma g-2\hat{\alpha}\beta g,\tag{6.79}$$

$$\frac{\mathrm{d}\psi}{\mathrm{d}z} = \Gamma\eta^2-\frac{\beta}{2w^2},\tag{6.80}$$

$$\left(2\beta\frac{\eta}{w}-8\Gamma\eta^3w\right)\frac{\mathrm{d}\eta}{\mathrm{d}z}-\left(\beta\frac{\eta^2}{w^2}+2\Gamma\eta^4\right)\frac{\mathrm{d}w}{\mathrm{d}z}=8\sigma\Gamma\eta^4w-2\sigma\beta\frac{\eta^2}{w},\tag{6.81}$$

$$\hat{\alpha} = \frac{3\hat{\kappa}}{8}\frac{\sqrt{\Gamma}}{r}\frac{1}{\beta}\frac{\mathrm{d}}{\mathrm{d}z}\int_0^{z-z_s}\frac{r}{\sqrt{\pi\,(z-z_s-y)}}\,\mathrm{d}y, \tag{6.82}$$

where

$$\ell = \frac{3\pi^2\sqrt{\beta}}{8\hat{\kappa}\sqrt{\Gamma}}, \tag{6.83}$$

and

$$\hat{\kappa} = \left(2\sqrt{\frac{\Gamma}{\beta}}\eta^4 w - \sqrt{\frac{\beta}{\Gamma}}\frac{\eta^2}{w}\right)^{1/3}. \tag{6.84}$$

When $z > z_f$, the pulse is in the constant dispersion section of the fibre for which $\beta = \beta(z_f)$. Here amplification is assumed to balance loss so that the pulse train settles to a train of steady solitons. This is done by setting $\sigma = 0$ in the pulse evolution equations (6.78)–(6.81). The shelf height, r, in the above expressions is the same as that of McKinnon *et al.* [34] and $\hat{\kappa}$ is given by equation (6.84).

To facilitate faster numerical integration, the radiation integral term in (6.82) is replaced by

$$A = \frac{3\hat{\kappa}}{8}\frac{\Gamma}{\beta}\frac{r}{R(z_s)\sqrt{\pi\beta(z-z_s)}}, \tag{6.85}$$

where

$$R^2 = \frac{\Gamma}{\beta}\frac{3\hat{\kappa}}{8}\sqrt{\frac{\Gamma}{\beta}}\left(2\eta^2 w - 2\sqrt{\frac{\beta}{\Gamma}}\hat{\kappa} + \sqrt{\frac{\beta}{\Gamma}}\frac{3\pi^2}{8\hat{\kappa}}g^2\right) = \frac{\Gamma}{\beta}r^2. \tag{6.86}$$

$R(z_s)$ is obtained by evaluating this expression at the change-over point $z = z_s$.

6.3 Optimisation

This section describes the optimisation procedure used to maximise pulse compression in a section of DDF. As was mentioned in the previous section, the fibre has variable dispersion in the region $0 \leq z \leq z_f$. For $z > z_f$, the fibre has constant dispersion. The optimisation procedure aims to find the form of the dispersion profile $\beta(z)$ for which the pulse has maximum compression after passing through the DDF. As we are forming NLS soliton-like pulses, the amplitude and width are inversely related, so maximum compression translates to maximum amplitude, which is the variable the optimisation is based upon.

In this study, two distinct types of dispersion profiles were examined; discrete and continuous fibre compressors. In a discrete fibre compressor, the fibre is composed of sections of fibre with constant dispersion. The optimisation procedure

then aims to achieve maximum pulse amplitude for $z > z_f$ by varying the lengths and dispersion of each individual section. A continuous fibre compressor has dispersion which varies continuously along the DDF. The optimisation is performed by varying the dispersion at a fixed number of variable points along the DDF. To determine the continuous dispersion profile a cubic spline is then fitted through these points at which the dispersion is known.

Ideally, one would use the perturbed NLS equation (6.1) directly for optimisation purposes. However, with numerical integration times on the order of an hour per run, this is not practical for use with an optimiser for which hundreds of individual runs may be necessary. For this reason, the approximate equations derived in section 6.1.2, augmented by the radiation analysis of section 6.2, were used. Using the asymptotic approximation (6.85) to the radiation integral (6.82), the run times were generally less than 30 seconds each, making the approximate equations reasonable to use with the optimiser. As has been seen in previous Chapters, the solution of the approximate equations are generally in good agreement with the direct numerical solution of the original NLS equations, and so the compromise of using the approximate equations seems a reasonable one.

The end result of the optimisation should be a train of highly compressed solitons which have shed little dispersive radiation. In order to achieve this McKinnon *et al.* [34] chose an optimisation function that optimised the pulse amplitude with various penalties for the production of dispersive radiation. As well as the production of dispersive radiation, there is another potential problem with compressing pulses. This problem is that if the dispersion in the fibre is too low, the amplitude of the pulses can become very large and the pulses can split into two or more solitons. In the work of McKinnon *et al.* [34] this was avoided by setting a minimum dispersion $\beta = \beta_{\min}$. In that work the dispersion in the final section $z > z_f$, was set to this minimum value $\beta = \beta_{\min}$. With this information McKinnon *et al.* [34] chose to maximise

$$f = a_f - \left(\sum_{i=1}^{n} \left\{ R r_i + R_Q \left[\max(0, r_i - \hat{r}) \right]^2 \right\} + a_{\text{pen}} \log \left(\frac{5\alpha}{a_f} - 4 \right) \right), \tag{6.87}$$

where

$$\alpha = \sum_{i=1}^{n} |a_i - a_{i-1}|, \; a_0 = 0. \tag{6.88}$$

Here a_f is the final steady amplitude of the solitons given by

$$a_f^3 = 2\sqrt{\frac{\Gamma}{\beta_{\min}}}\, a^4 w - \sqrt{\frac{\beta_{\min}}{\Gamma}} \frac{a^2}{w}. \tag{6.89}$$

Again $\beta_{\min}$ was the preordained minimum possible dispersion. The radiation height at the edge of the shelf r is given by equation (6.66) as

$$r^2 = \frac{3\hat{\kappa}}{8}\sqrt{\frac{\Gamma}{\beta}}\left(2a^2 w - 2\sqrt{\frac{\beta}{\Gamma}}\,\hat{\kappa} + \sqrt{\frac{\beta}{\Gamma}}\frac{3\pi^2}{8\hat{\kappa}}g^2\right). \tag{6.90}$$

The r_i in equation (6.87) is the radiation height as given by (6.90) at the ith space step in the Runge-Kutta integration of the approximate equations of section 6.1.2. The shed dispersive radiation was not included for the wavetrain trial solution (6.2), so $r_i = 0$ when this wavetrain solution is used.

The first penalty in equation (6.87), Rr_i, is a linear penalty on the amount of dispersive radiation produced, as given by r_i. If the amount of radiation exceeds some set limit $r_i > \hat{r}$, the quadratic penalty $R_Q\left[\max(0, r_i - \hat{r})\right]^2$ activates in an effort to quickly drive down the amount of dispersive radiation begin produced. The third penalty in (6.87) is a penalty on the amount of variation in successive pulse amplitudes. This penalty ensures the result is a train of smooth, stable solitons in the uniform section $z > z_f$. The coefficients 5 and 4 in this expression were found, by trial and error, to produce a smooth soliton train without imposing too much of a restriction on the oscillatory nature of the pulses. While various values were tried for the penalty strengths, the work in this thesis used [34] $R = 10$, $R_Q = 200$, $\hat{r} = 0.025$, and $a_{\text{pen}} = 1$.

As mentioned above, in the work of McKinnon *et al.* [34] a minimum dispersion was set to avoid the pulse splitting into two or more pulses. The minimum dispersions, $\beta(z_f) = 0.05$ for the discrete case and $\beta(z_f) = 0.001$ for the continuous case, were found by performing a large number of numerical simulations and observing at what value of $\beta(z_f)$ the pulse would split. However the current optimisation work utilised the results of Chapter 5. In Section 5.3.3, it was found, by performing an energy and mass analysis on the evolving pulses, that a soliton would split into two solitons if $\eta w > 1.702$ at some point. As a result this was initially used as the criterion for a soliton splitting. Specifically it was included in the optimisation procedure by monitoring the product ηw throughout the numerical simulation. If at any point this product exceeded 1.702, that particular simulation was abandoned and a large penalty was subtracted from the predicted steady-state amplitude a_f in place of the three penalties discussed above.

Not included in the above optimisation function (6.87) are penalties for producing physically impossible situations. These include such situations as negative dispersion values and disordered spatial points. For example, in a fibre compressor with five sections, $z_3 > z_4$ is impossible. However, the optimising routine may produce such spurious results and so penalties must be included to discourage

these. In the case of a physically impossible situation arising the solution of the approximate equations is not necessary, and in some cases impossible. This is handled in a similar fashion to that of pulse splitting discussed above. To stop physically impossible results, a large penalty is assumed and subtracted from a_f in place of the three penalties discussed above, in which case

$$f = a_f - \sum_{i=1}^{n} R_i P_i, \tag{6.91}$$

where R_i is the penalty factor for a particular physically unrealisable situation P_i.

The actual optimisation procedure used is the Nelder-Mead method [25, 46], as discussed in Section 3.3. As discussed in that section, the function to be optimised, (6.87), is not differentiable and also contains discontinuities. These arise for a number of reasons, the main being the switch to the soliton equations at $m = 0.9999$. Also the numerical algorithms used to calculate the elliptic integrals in the approximate equations contain convergence loops which are executed a different number of times depending on the parameters. As a result there may be a small discontinuity at the point at which there is a change in the number of times a loop is executed. A discrete dispersion profile also introduces discontinuities at the boundaries between regions of differing dispersion. All these factors preclude the use of an optimisation routine based on local gradient information. As the Nelder-Mead method only uses function evaluations, and not gradient information, it is an ideal routine for this problem. As discussed in Section 3.3, the numerical routine has been modified to avoid the stagnation reported by [33] to which the Nelder-Mead method is susceptible.

6.4 Results

In this section numerical solutions of the approximate equations (6.74)–(6.77) and (6.78)–(6.81) are compared with full numerical solutions of the perturbed NLS equation (6.1). The approximate equations (6.74)–(6.77) and (6.78)–(6.81) were solved using the method of Section 3.2. The perturbed NLS equation (6.1) was solved numerically using the method described in Section 3.1.

6.4.1 Modifications to Full Numerical Code

The procedure for numerically solving the perturbed NLS equation (6.1) is similar to that described in Section 5.3.1 for the NLS equation governing sliding frequency filters. As in that case, the constituent NLS is a variable coefficient equation.

Following the method of Section 3.1, we write the NLS equation incorporating variable dispersion and nonlinear coefficient, fibre loss and absorbing boundaries as

$$\mathrm{i}\frac{\partial u}{\partial z} + \frac{1}{2}\beta(z)\frac{\partial^2 u}{\partial t^2} + \Gamma(z)|u|^2 u + \mathrm{i}\theta(t)u = -\mathrm{i}\sigma u. \tag{6.92}$$

Fourier transforming equation (6.92) we obtain

$$\frac{\mathrm{d}\hat{u}}{\mathrm{d}z} + \frac{\mathrm{i}}{2}\beta(z)\omega^2\hat{u} = \mathrm{i}F\left\{\Gamma(z)|u|^2 u\right\} - F\left\{\theta(t)u\right\} - \sigma\hat{u}, \tag{6.93}$$

where F denotes the Fourier transform. Taking the lower limit of integration as the previous space point z for the calculation of u at $z+\Delta z$, the integrating factor for the half space step $\Delta z/2$ is then $\exp(\lambda\Delta z/2)$, where

$$\lambda = \frac{\mathrm{i}}{2}\beta(z)\omega^2 + \sigma \tag{6.94}$$

on evaluating the integral to first order. At $z = z_f$, the distance at which the pulse is in the constant dispersion section of the fibre, fibre loss is turned off, so that $\sigma = 0$, modifying λ to

$$\lambda = \frac{\mathrm{i}}{2}\beta(z_f)\omega^2. \tag{6.95}$$

6.4.2 Modification to Approximate Code

The radiation integral (6.82) is the same as that discussed in Section 3.2, so no changes to the numerical technique are necessary. However, as the radiation integral must be evaluated from $y = 0$ to $y = z - z_s$ at each individual time-step, the numerical evaluation of the integral becomes progressively slower. To keep each individual numerical solution of the approximate equations relatively short, the approximation (6.85) to the radiation integral is used in its place. As this expression requires no numerical integration, execution is extremely quick.

6.4.3 Numerical Results

In this section the approximate evolution equations (6.74)–(6.77) are solved using the Runge-Kutta technique discussed in Section 3.2. When $m = 0.9999$ the wave-train is assumed to be a train of solitons and equations (6.78)–(6.81) are solved using the same Runge-Kutta method. The value of m at which we switch from the equations based on the Jacobian elliptic trial function (6.2) to the equations based on the pulse trial function (6.37) was varied. It was found that some difference in the resulting pulse evolution occurred. This is to be expected in that making the change-over point smaller, say $m = 0.99$, means that the switch to

the soliton equations happens earlier. Likewise, larger m delays this switch for longer. As the Jacobian elliptic cosine function cn approaches sech as $m \to 1$, it is reasonable to delay this change-over for as long as possible. This means making the change-over value of m as near 1 as possible. However as the equations are being solved numerically, there is a limit, determined by the step-size Δz, as to how close to 1 we may set this change-over point since $m < 1$ and $\mathrm{K}(m) \to \infty$ as $m \to \infty$. Making it too close to 1 means that when m is close to 1 it would be possible to step over the value $m = 1$ into a region in which the Jacobian elliptic function cn is not defined. Various values of the change-over point going up from $m = 0.99$ were tried. It was found that values larger than $m = 0.9999$ would occasionally cause numerical difficulty in the sense discussed above, and so $m = 0.9999$ was chosen as the change-over point.

The solution of the approximate equations were then compared with full numerical solutions of (6.1) using the method of Section 3.1 with the modifications of Section 6.4.1. These comparisons were carried out for both continuous and discrete dispersion profiles of varying lengths. In all the following numerical solutions the input wave is

$$u(0,t) = \cos t \tag{6.96}$$

and the dispersion is normalised so that $\beta = 1.0$ at $z = 0$.

6.4.3.1 Discrete Dispersion Profiles

We will start by examining discrete dispersion profiles. For discrete dispersion profiles the fibre was split into six regions of constant dispersion. The optimiser varied the length and dispersion of each section by varying the pair $(z_i, \beta_i), i = 1, \ldots, 6$. The Nelder-Mead algorithm could have easily been modified to account for varying Γ, the nonlinear coefficient, but this would double the number of vertices in the Nelder-Mead simplex, thus increasing computation time. As this work is primarily concerned with the effect of decreasing dispersion on pulse evolution, the effect of varying Γ was ignored. This is done by setting $\Gamma = 1$. The profile end points were fixed at $(z_1, \beta_1) = (0, 1)$ and $(z_6, \beta_6) = (15, 0.01)$ in the first instance. The final dispersion point β_6 was fixed at 0.01 even though it could be allowed to vary freely as application of penalties based on the condition $\eta w > 1.7$ should prevent any pulse splitting. However, β_6 was fixed at 0.01 for two reasons. Firstly, it was useful to have a fixed minimum dispersion across a large range of DDF lengths. This allows a comparison in the amount of compression available to varying lengths of DDF over the same range of dispersion variation. Secondly, the work of McKinnon *et al.* [34] fixed the final dispersion point for discrete DDF's at

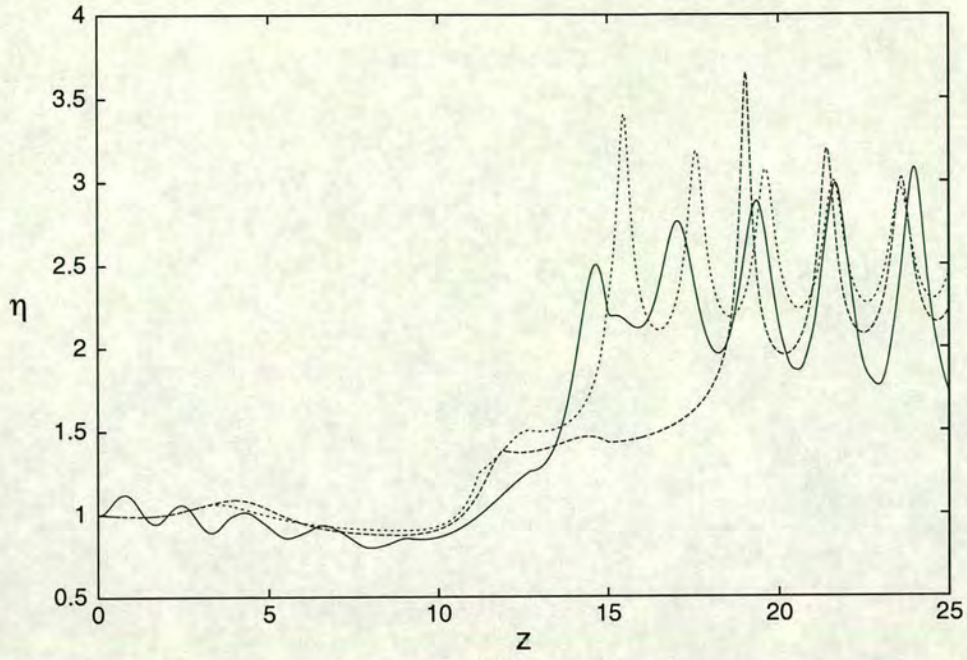

Figure 6.3: Pulse amplitude η versus distance z for a discrete compressor of length 15 km. Dispersion parameters are given in Table 6.1. Full numerical solution of (6.1): — ; solution of approximate equations with initial profile: - - - - ; solution of approximate equations with optimised profile: $\cdots$.

Table 6.1: Optimised dispersion parameters for a compressor of length 15 km.

Initial Dispersion Parameters		Optimised Dispersion Parameters	
z_i	β_i	z_i	β_i
3.0	0.7	3.88876922	0.71157971
6.0	0.5	6.53057431	0.66029753
9.0	0.2	9.19158189	0.09307016
12.0	0.1	12.72807288	0.01598908
15.0	0.01	15.0	0.01

$\beta_6 = 0.05$ and noted that anything below this value could produce pulse splitting. However not all dispersion parameter combinations in which the final dispersion point is below 0.05 will produce pulse splitting. This is illustrated by the current work in which the inclusion of the pulse splitting condition $\eta w > 1.702$ allows us to use a smaller final dispersion without pulse splitting occurring. In other words, not all dispersion parameter combinations with $\beta_6 = 0.01$ will produce stable pulse trains, however optimising the function (6.87) with the condition $\eta w > 1.702$ ensures a stable, compressed pulse train is produced. The fibre loss was set to $\sigma = 0.03$, which means a length $z = 1$ corresponds to a dispersion distance of $z_0 = 1$ km. So in this case we are examining a discrete fibre compressor 15 km in length.

As can be seen from Figure 6.3 the comparison between the approximate and

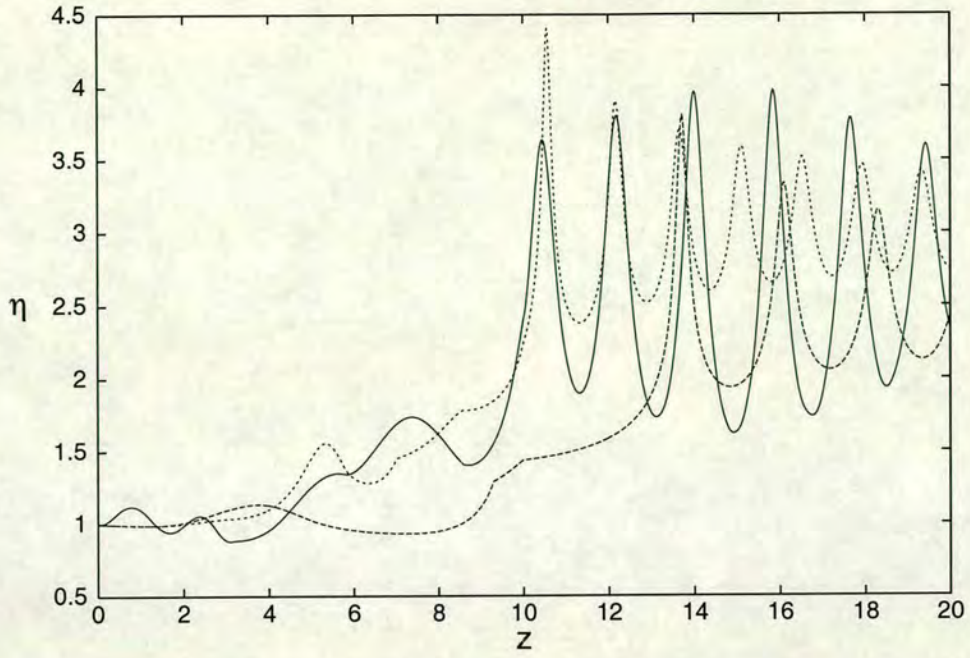

Figure 6.4: Pulse amplitude η versus distance z for a discrete compressor of length 10 km. Dispersion parameters are given in Table 6.2. Full numerical solution of (6.1): — ; solution of approximate equations with initial profile: - - - - ; solution of approximate equations with optimised profile: $\cdots$.

full numerical solutions, with the optimised dispersion profiles, is good. The relevant dispersion parameters are listed in Table 6.1. The final optimised pulse train however exhibits reasonably large amplitude oscillations, which makes this a less than ideal soliton train as it must shed a correspondingly large amount of radiation to evolve to a steady state. However it is instructive to examine the resulting pulses more closely. Firstly we note that the pulse train for the optimised dispersion profile is superior to that for the initial profile in a number of respects. The steady-state amplitude for the optimised dispersion profile is $\eta_f = 3.103$, while the initial profile gives $\eta_f = 2.658$. By itself, the increase in amplitude is not enough to say that the optimised profile is somehow better than the initial. It is perfectly possible to choose a dispersion profile which will give a larger steady state amplitude. However it may also produce more dispersive radiation, or exhibit larger amplitude oscillations. Both of these factors were considered in the choice of the optimisation function (6.87). So an optimum pulse train in this case is one in which there is some pulse compression, relative to the initial dispersion profile, with a minimum of dispersive radiation and amplitude oscillations. The optimised dispersion profile of Figure 6.3 satisfies these criteria. In addition to the increased pulse compression discussed above, the dispersive radiation has been decreased. The amount of dispersive radiation shed by the

Table 6.2: Optimised dispersion parameters for a compressor of length 10 km.

Initial Dispersion Parameters		Optimised Dispersion Parameters	
z_i	β_i	z_i	β_i
1.5	0.8	2.26447663	1.20742390
3.0	0.6	3.18126347	0.25295495
5.0	0.4	5.79028096	0.10147737
7.5	0.1	8.58691828	0.01653631
10.0	0.01	10.0	0.01

pulse is measured by r. As the amount of this radiation propagating away from the pulse is governed by r, a smaller r means less dispersive radiation. The initial dispersion profile produced a maximum r of 0.33 while the optimised dispersion profile produced a maximum r of 0.21. Comparing the amount of amplitude oscillation qualitatively, we can see the pulse formed in the optimised dispersion profile exhibits smaller amplitude oscillations than the pulse derived from the initial profile. Notice also the effect of including the shed dispersive radiation in the evolution equations (6.78)–(6.81). Doing so dampens successive amplitude oscillations in the uniform section of fibre in $z > 15$, forcing the pulse to a steady state. Taken together, these three factors indicate that the optimised pulse is superior to the initial.

Figure 6.4 shows a similar comparison, this time with compressor length 10 km. The dispersion parameters are listed in Table 6.2. The comparison between the approximate and full numerical solutions is good, but not of the same quality as in Figure 6.3. The amplitude oscillations of the full numerical solution are larger than in the approximate solution, but the steady state is nearly the same. Comparing the approximate solution with an optimised profile to that with the initial profile shows an immediate improvement. The steady state pulse amplitude with the optimised profile is $\eta_f = 4.34$, compared to $\eta_f = 2.56$ for the initial profile. In addition, the maximum shelf height for the optimised case is $r = 0.29$ versus $r = 0.37$ for the initial case. So a significant amount of compression has been achieved along with less background radiation. Both of the approximate solutions appear to exhibit similar amounts of amplitude oscillations so that it would appear that the optimised profile has not decreased the amount of oscillation. However, taking into account the improvement in compression and background radiation, and noticing that the amount of amplitude oscillation is not excessive, it is fairly easy to say that the optimised profile is superior to the initial one.

Decreasing the compressor length again to 5 km, we get the results shown in Figure 6.5. The optimised dispersion parameters are listed in Table 6.3. Here

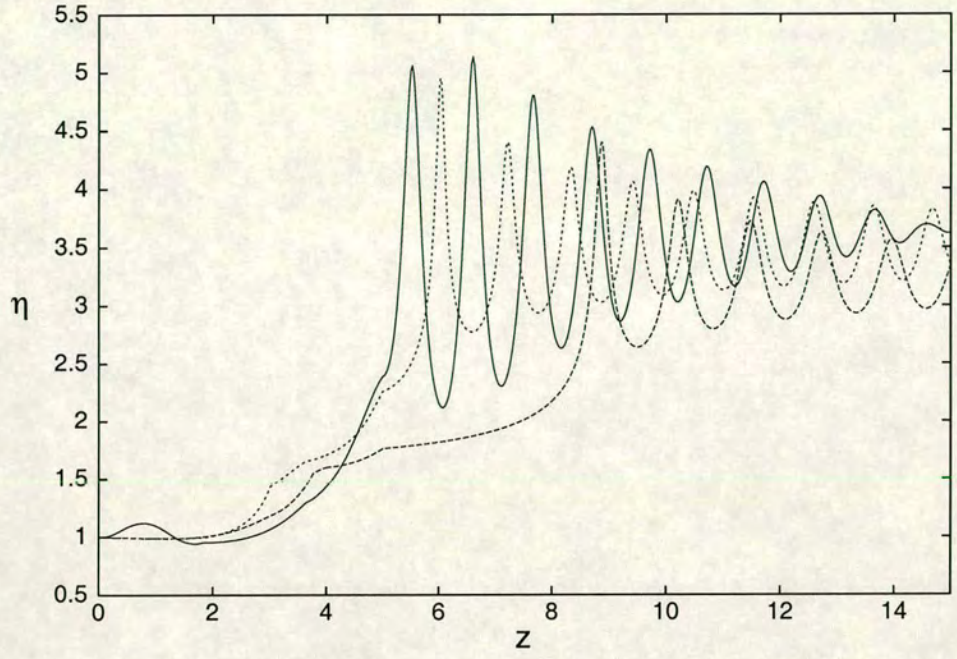

Figure 6.5: Pulse amplitude η versus distance z for a discrete compressor of length 5 km. Dispersion parameters are given in Table 6.3. Full numerical solution of (6.1): — ; solution of approximate equations with initial profile: – – – – ; solution of approximate equations with optimised profile: $\cdots$.

Table 6.3: Optimised dispersion parameters for a compressor of length 5 km.

Initial Dispersion Parameters		Optimised Dispersion Parameters	
z_i	β_i	z_i	β_i
1.5	0.7	1.82899996	1.23930512
2.0	0.5	1.82906274	0.14069769
3.0	0.2	3.63548774	0.06695649
4.0	0.1	4.02582994	0.05640979
5.0	0.01	5.0	0.01

the comparison between the approximate and full numerical solutions for the optimised dispersion profile is very good. Notice that the amplitude oscillations rapidly decay, giving a smooth steady train of solitons. In this case the inclusion of dispersive radiation in the solution of the approximate equations is vital for an accurate determination of the pulse evolution. Comparing the solution of the approximate equations for the initial and optimised dispersion profiles, we can see that the final steady amplitude for the optimised fibre has increased. The steady state amplitude for the optimised fibre is $\eta_f = 3.67$, compared with $\eta_f = 3.27$ for the initial fibre. While this is a fairly modest gain in compression, examining the background radiation provides more information. The maximum value of r for the initial dispersion profile was $r = 0.54$, while the maximum value for the optimised dispersion profile was $r = 0.25$, a significant reduction. Further, examining the amplitude oscillations for the initial and optimised dispersion profiles, it appears that the pulse for the initial profile may actually have smaller initial oscillations than the pulse for the optimised dispersion profile. However, as in the previous example shown in Figure 6.4, it is not necessary to improve all aspects of the pulse for it to be optimised. Rather the value of the function (6.87) must be increased. This could involve a significant decrease in one penalty followed by a small increase in another. However the net result is a pulse which meets the criteria of being compressed, having low background radiation and having reasonably small amplitude oscillations.

For shorter compressor lengths it becomes increasingly difficult to find possible optimised profiles. For a shorter fibre compressor, the initial pulse must shed a large amount of dispersive radiation in a short distance. This contrasts with longer fibre compressors for which the pulse can evolve slowly over a longer distance. The radiation which is forced out of the initial wave in forming a train of solitons finds its way into the constant dispersion section of the fibre, where it travels with the train of solitons. This large amount of shed radiation makes it difficult to optimise the dispersion profile, as the optimising function (6.87) includes penalties for this radiation. Because of this, it proved difficult to find optimised profiles with $\beta_6 = 0.01$. Raising the value of this final dispersion point to $\beta_6 = 0.1$ helped in that not as much dispersive radiation had to be shed for the pulse to evolve to a steady state. As a result there were more possible optimised solutions with low values of r.

Figure 6.6 shows a comparison for a compressor length of 2.5 km with the optimised dispersion parameters listed in Table 6.4. The most interesting thing about the results is that the soliton train formed for the optimised profile has a smaller steady state amplitude than the pulse train formed for the initial profile.

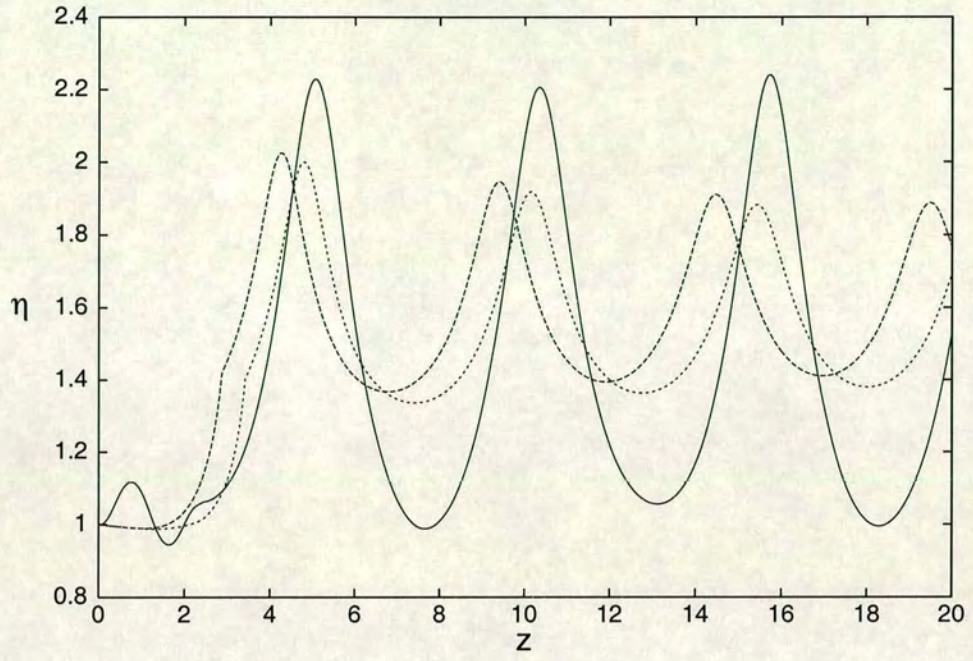

Figure 6.6: Pulse amplitude η versus distance z for a discrete compressor of length 2.5 km. Dispersion parameters are given in Table 6.4. Full numerical solution of (6.1): — ; solution of approximate equations with initial profile: – – – – ; solution of approximate equations with optimised profile: $\cdots$.

Table 6.4: Optimised dispersion parameters for a compressor of length 2.5 km.

Initial Dispersion Parameters		Optimised Dispersion Parameters	
z_i	β_i	z_i	β_i
1.0	0.9	0.01304148	1.02459761
1.3	0.7	2.23849044	0.84367563
1.6	0.4	2.29882413	0.62809954
1.9	0.2	2.44729244	0.18070287
2.5	0.1	2.5	0.1

The steady state amplitude has decreased from $\eta_f = 1.69$ to $\eta_f = 1.66$ in going from the initial to the optimised profile. Also, examining the maximum radiation height r, we find $r = 0.133$ for the initial profile and $r = 0.134$ for the optimised profile. Again this goes against what is expected in the optimisation process, i.e. lower r and higher amplitude. However, examining this case more closely confirms that the optimisation has succeeded. Firstly, remember that the optimisation function (6.87) has penalties based upon a summation of radiation values, rather than a single maximum value. The initial value of the optimising function was $f = -19.24$. As the initial steady state amplitude was only $\eta_f = 1.69$, this means a significant total of penalties must have been subtracted. The value of the optimising function for the optimum dispersion profile is $f = -17.84$. While there is very little difference in the steady state amplitudes, and from examining Figure 6.6 there appears to be very little difference in the amplitude oscillations, we can say that the improvement has come from a decrease in the total amount of dispersive radiation produced. Specifically, the maximum radiation height has increased for the optimum dispersion profile, but the total sum of radiation produced has decreased, as expected for the optimising function. So in some sense our optimised profile produces a cleaner, less noisy train of solitons.

Examining these large negative values of the optimised function also confirmed the reasons given previously for the relative difficulty in finding optimised profiles for shorter dispersion lengths. For the 10 km fibre compressor, shown in Figure 6.4, the value of the optimised function went from $f = -3$ for the initial profile to about $f = 3$ for the final profile. Compared to the optimised value of $f = -19.24$ for the 2.5 km fibre compressor, it confirms the hypothesis that large amounts of shed radiation are produced very quickly when wavetrains evolve in short fibre compressors. This makes it increasingly difficult to find optimised profiles as this radiation forms a penalty in the optimised function (6.87). Also, as reported in [22], the interaction between the shelf of radiation under the pulses, measured by g, and the pulse itself leads to the amplitude oscillations seen in the previous figures. Large values of g, which in turn imply large values of r will lead to large amplitude oscillations, which again is a penalty in the optimising function (6.87).

From the above examples for discrete fibre compressors of different lengths a few conclusions may be drawn. Firstly, compressors of longer length seem to produce pulse trains with large amplitude oscillations, even for the optimised case, as seen in Figures 6.3 and 6.4. This is not a major limitation however, as in practice, fibre compressors are not this long. Making the fibre compressor too short, however, can introduce difficulties as well, as seen in Figure 6.6. As the pulse evolves and is compressed over a very short distance, large amounts of disper-

sive radiation are produced. In order to find optimised profiles with a reasonable amount of dispersive radiation it is necessary to increase the minimum dispersion of the fibre. However this comes at the expense of having a less compressed final pulse train and the resulting pulse train also exhibits large and slowly decaying amplitude oscillations. In between these two extremes it appears that discrete fibre compressors with lengths on the order of $3-5$ km provide the best compromise between practicality and performance. For example, as was seen in Figure 6.5, a steady compressed pulse train with little shed dispersive radiation is easily produced in a 5 km fibre compressor.

6.4.3.2 Continuous Dispersion Profiles

For a continuous dispersion profile DDF, six knots (z_i, β_i) where chosen, with initial dispersion $(z_1, \beta_1) = (0, 1)$ and final dispersion $(z_6, \beta_6) = (15.0, 0.01)$ in the first instance, as in the discrete case. A cubic spline was fitted through these knots to model the continuous variation and the optimisation code then varied the dispersion at and position of these knots.

Notice that the final dispersion point β_6 is set to 0.01 as in the discrete dispersion profile case. In McKinnon *et al.* [34] it was shown that the final dispersion point in a continuously varying fibre compressor could be lowered to $\beta_6 = 0.001$ before pulse splitting would occur. Keeping this in mind the final dispersion point was chosen as $\beta_6 = 0.01$ for two reasons. Firstly, while pulse splitting does not occur when the final dispersion point is set to $\beta_6 = 0.001$, very large steady state amplitudes result.

Table 6.5: Optimised dispersion parameters for a compressor of length 15 km.

z_i	β_i
1.77429513	1.23030355
3.06805498	0.33543980
4.67864727	0.10842196
4.94704047	0.08793691
7.5	0.000947200

Figure 6.7 shows just such a situation. In this case the final dispersion point β_6 has been unconstrained. Again the optimising function (6.87) contains the pulse splitting condition $\eta w > 1.702$. Notice that the final dispersion point in Table 6.5 has decreased slightly below 0.001 with no resulting pulse splitting. However, there are problems with obtaining such highly compressed pulse trains. With a large amplitude increase comes a proportionally large decrease in pulse width. For narrow pulses, higher order effects become important and these effects have not been accounted for in the present analysis. So the relevance of the full numerical

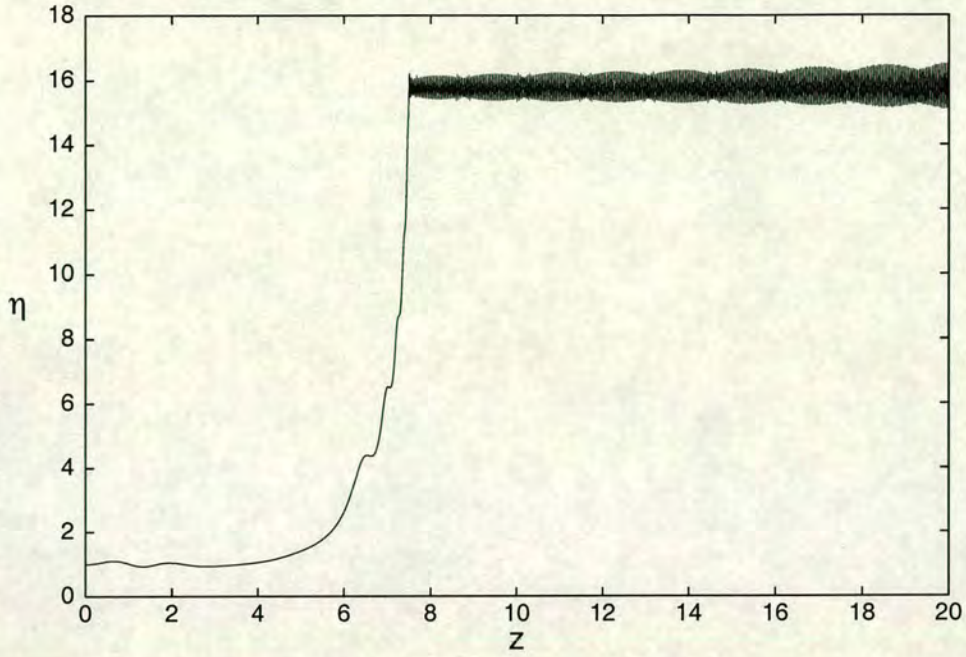

Figure 6.7: Pulse amplitude η versus distance z for a continuous compressor of length 7.5 km from full numerical solution. Dispersion parameters are given in Table 6.5.

solution to practical situations for such large pulse amplitudes is questionable. Also, to obtain the full numerical solution for very large steady state amplitudes it is necessary to discretise the t-direction with very small time-steps. As the pulses have very narrow widths, the pulse dynamics occur on a very short time-scale and so require a correspondingly small time-step to capture this fast t behaviour. This means that the full numerical solutions can become impractically slow. On the available computing resources, individual simulations can take over 20 hours for very narrow pulse simulations.

The other advantage to setting the final dispersion to the same value as for the discrete compressor case was that it was then possible to make comparisons between the discrete and continuous compressors for the same dispersion ranges. Comparisons between the amount of compression and the quality of the resulting pulse trains for discrete and continuous fibre compressors are then possible.

Figure 6.8 shows a comparison between the approximate solution for the initial and optimised profiles and the full numerical solution for the optimised profile for a DDF of length 15 km. There is a large difference between the approximate and full numerical solutions in the region of uniform fibre that was not present for the discrete dispersion profiles. In an effort to find out the reasons for this large difference for the continuous dispersion profile, a comparison was made between the approximate and full numerical solutions for a DDF with the dispersion pa-

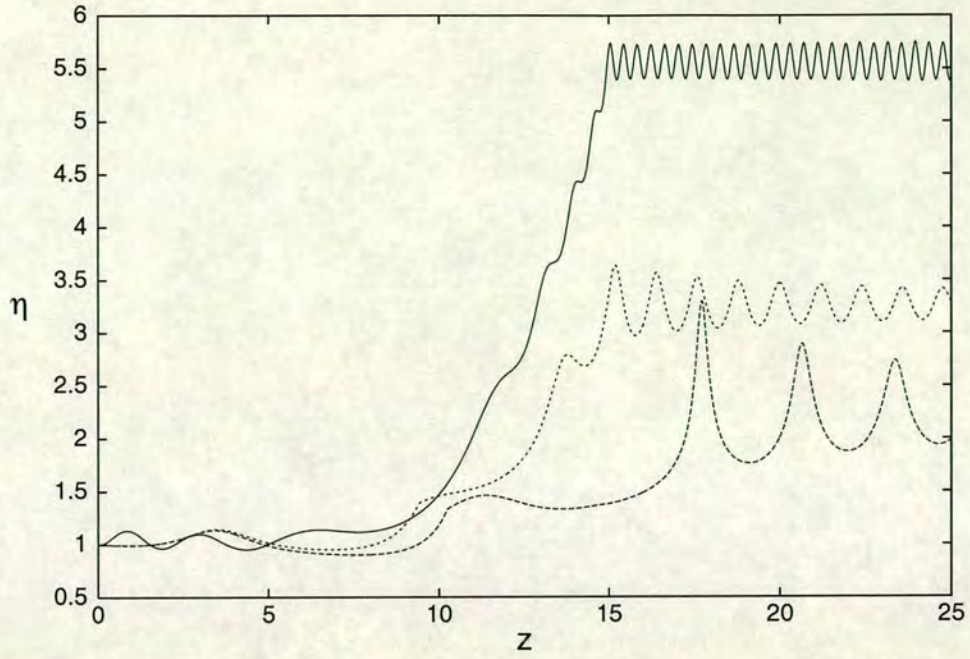

Figure 6.8: Pulse amplitude η versus distance z for a continuous compressor of length 15 km. Dispersion parameters are given in Table 6.6. Full numerical solution of (6.1): — ; solution of approximate equations with initial profile: – – – – ; solution of approximate equations with optimised profile: $\cdots$.

Table 6.6: Optimised dispersion parameters for a compressor of length 15 km.

Initial Dispersion Parameters		Optimised Dispersion Parameters	
z_i	β_i	z_i	β_i
3.0	0.7	3.38569415	0.63379736
6.0	0.5	6.73283102	0.33296195
9.0	0.2	9.75155672	0.13267236
12.0	0.1	12.00284250	0.04695441
15.0	0.01	15.0	0.01

rameters of Table 6.6 in the absence of fibre loss, so that $\sigma = 0$. The results of this comparison are shown in Figure 6.9. Notice that while there is still a difference between the amplitudes in the uniform section of fibre, the comparison is much better than for the loss case of Figure 6.8.

To examine this discrepancy further, let us examine a fibre compressor with continuously varying dispersion over 10 km, so that $(z_6, \beta_6) = (10.0, 0.01)$. This comparison is shown in Figure 6.10 based on the optimised dispersion parameters listed in Table 6.7. While the comparison is slightly better than that of Figure 6.8, there is still a large difference in the pulse amplitudes in the uniform section of the fibre between the approximate and full numerical solutions. Again this difference was not present in the results for the equivalent discrete fibre compressor. Figure 6.11 shows a comparison between the approximate and full numerical solutions

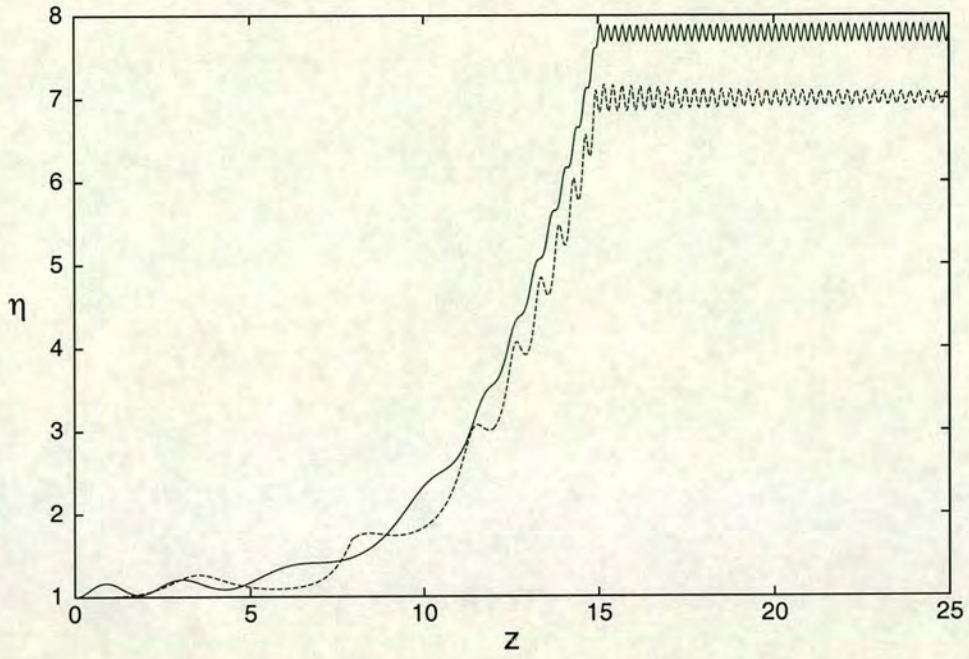

Figure 6.9: Pulse amplitude η versus distance z for a continuous compressor of length 15 km with zero fibre loss. Dispersion parameters are given in Table 6.6. Full numerical solution of (6.1): — ; solution of approximate equations: - - - -

Table 6.7: Optimised dispersion parameters for a compressor of length 10 km.

Initial Dispersion Parameters		Optimised Dispersion Parameters	
z_i	β_i	z_i	β_i
1.5	0.7	1.51319555	1.16731600
3.0	0.5	3.80480860	0.31161317
5.0	0.2	5.13947772	0.17252798
7.5	0.1	6.72955973	0.08692482
10.0	0.01	10.0	0.01

using the optimised parameters of Table 6.7, but neglecting fibre loss, so that $\sigma = 0$. As for the similar lossless case of Figure 6.9 the comparisons is very good in this lossless case, with very little difference between the amplitudes in the uniform section of the fibre. The comparisons of Figures 6.8–6.11 imply that the modelling of fibre loss in the approximate equations is responsible for the disagreement between the approximate and numerical solutions. However comparing the results of Figures 6.8 and 6.10 it can be seen that this effect is not uniform for fibre compressors of different length as the difference between the approximate and numerical solutions increases as the fibre compressor increases in length. To verify this conjecture, let us examine a 5 km continuous DDF, so that $(z_6, \beta_6) = (5.0, 0.01)$.

Figure 6.12 shows this comparison. It can immediately be seen that the agree-

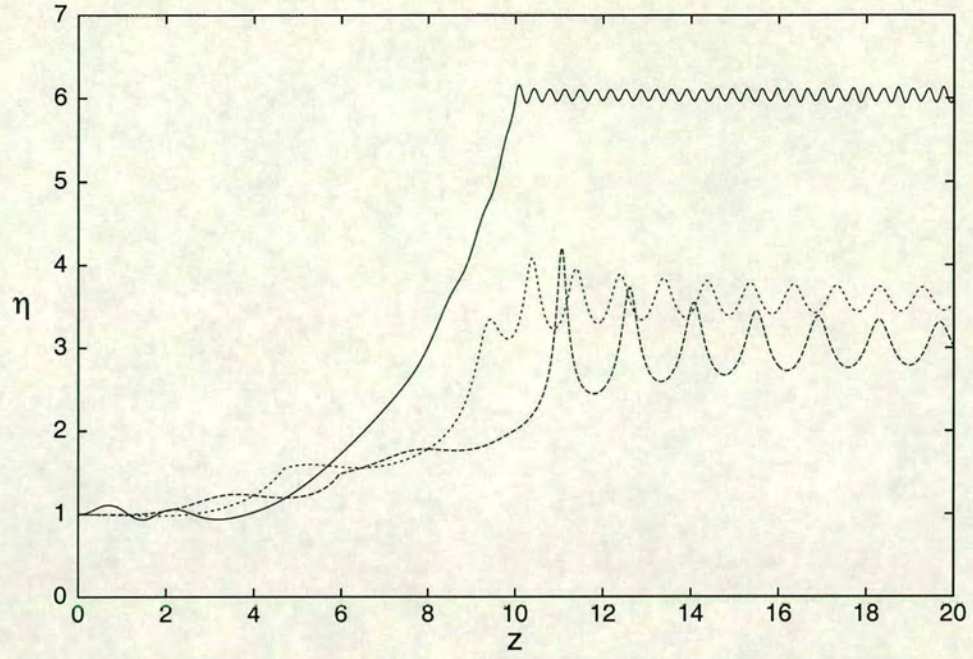

Figure 6.10: Pulse amplitude η versus distance z for a continuous compressor of length 10 km. Dispersion parameters are given in Table 6.7. Full numerical solution of (6.1): — ; solution of approximate equations with initial profile: – – – – ; solution of approximate equations with optimised profile: $\cdots$.

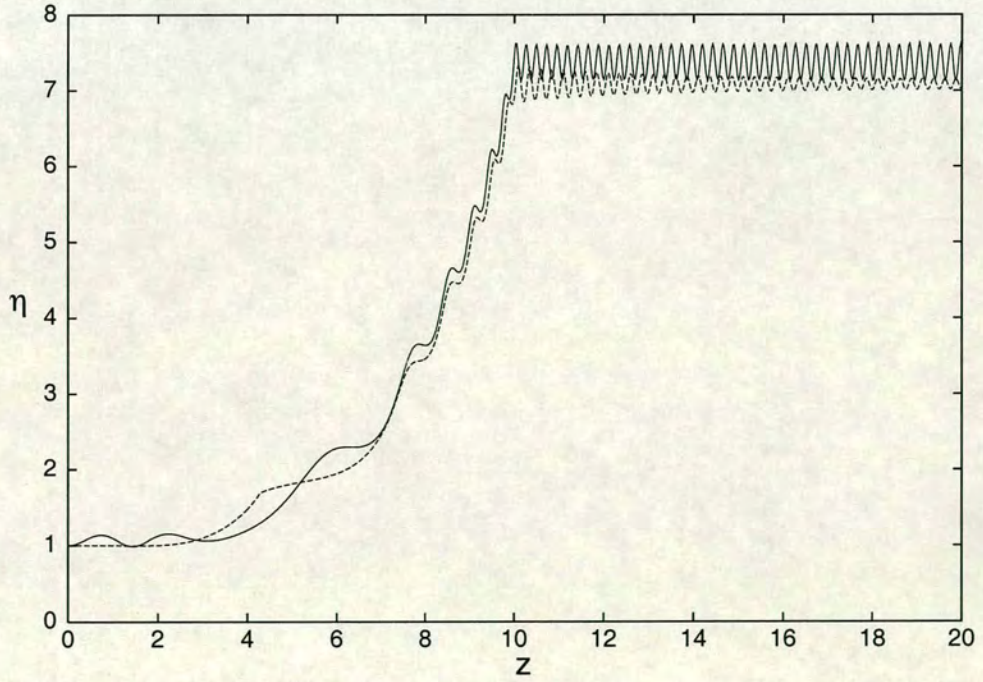

Figure 6.11: Pulse amplitude η versus distance z for a continuous compressor of length 10 km with zero fibre loss. Dispersion parameters are given in Table 6.7. Full numerical solution of (6.1): — ; solution of approximate equations: – – – –

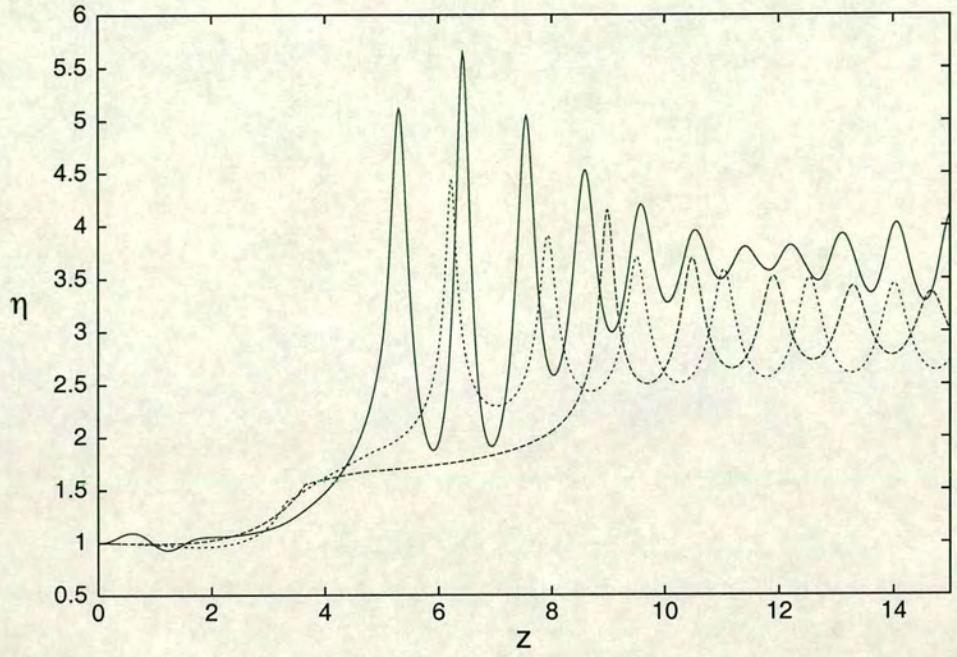

Figure 6.12: Pulse amplitude η versus distance z for a continuous compressor of length 5 km. Dispersion parameters are given in Table 6.8. Full numerical solution of (6.1): — ; solution of approximate equations with initial profile: – – – – ; solution of approximate equations with optimised profile: $\cdots$.

Table 6.8: Optimised dispersion parameters for a compressor of length 5 km.

Initial Dispersion Parameters		Optimised Dispersion Parameters	
z_i	β_i	z_i	β_i
1.5	0.8	1.76804928	1.00864200
2.0	0.6	2.01259291	0.66161478
3.0	0.3	3.73214458	0.21306244
4.0	0.1	4.74725867	0.11159053
5.0	0.01	5.0	0.01

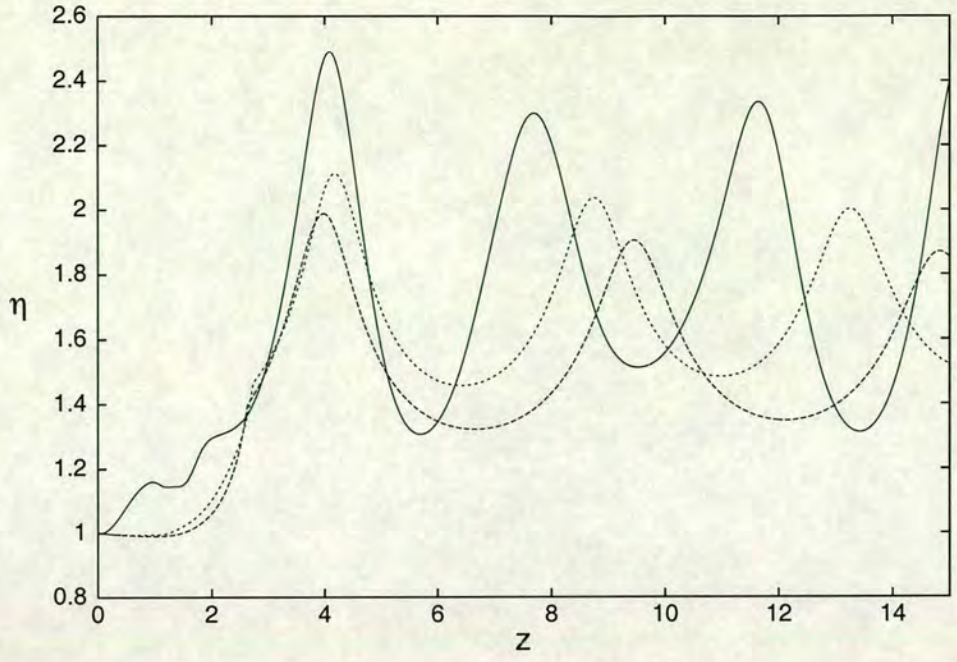

Figure 6.13: Pulse amplitude η versus distance z for a continuous compressor of length 2.5 km. Dispersion parameters are given in Table 6.9. Full numerical solution of (6.1): — ; solution of approximate equations with initial profile: – – – – ; solution of approximate equations with optimised profile: $\cdots$.

ment between the full numerical and approximate solutions, for the optimised profile, is much better than for the previous continuous dispersion profile DDF comparisons. This suggests that there is some cumulative error building up over distance in the continuous dispersion profile case when fibre loss is included that has not been accounted for. However, as much of the experimental work [8, 39] dealing with dispersion-decreasing fibre has used shorter compressor lengths (usually less than 5 km), this is not of great practical concern.

However this is not to say that shorter continuous compressor lengths uniformly produce better pulse compression. As was seen Figure in 6.6, which was for a discrete compressor of length 2.5 km, short compressors are prone to producing pulses which have a large amounts of amplitude oscillation and background radiation. This is due to the wavetrain being forced to a train of compressed solitons over a very short distance, so that large amounts of radiation are shed very quickly. This leads to a relatively low quality compressed soliton train.

This drawback of short pulse compressors is reflected in Figure 6.13, which shows the comparison between the full numerical solution of (6.1) and the solutions of the approximate equations for the initial and optimised dispersion profile for a DDF of length 2.5 km. Notice that in Table 6.9 the last dispersion point has been fixed at $(z_6, \beta_6) = (2.5, 0.1)$, as in Table 6.4. This is in contrast to the

Table 6.9: Optimised dispersion parameters for a compressor of length 2.5 km.

Initial Dispersion Parameters		Optimised Dispersion Parameters	
z_i	β_i	z_i	β_i
1.0	0.9	1.01379438	0.90494855
1.3	0.7	1.03603132	0.91429825
1.5	0.35	1.16333298	0.41231258
1.9	0.2	1.58321347	0.21095415
2.5	0.1	2.5	0.1

other comparisons for the longer compressor lengths, for which $\beta_6 = 0.01$. The reason for this is that when $\beta_6 = 0.01$ in a compressor of length 2.5 km it was very difficult, due to the large amounts of dispersive radiation produced, for the optimiser to find steady, optimised pulse train solutions. Setting $\beta_6 = 0.1$ lessened this problem at the expense of having less compression in the final soliton train. As can be seen in Figure 6.13 the comparison between the full numerical and approximate solutions is reasonable. They both have approximately the same amplitude oscillation mean (i.e. final steady state) but the full numerical solution exhibits larger and more persistent amplitude oscillations, as in Figures 6.4, 6.5, 6.6 and 6.12. The optimiser was started with several different initial dispersion variations in an effort to find a soliton train with smaller amplitude oscillations, but all the profiles obtained from the optimiser resembled that seen in Figure 6.13.

As for the discrete compressor of Section 6.4.3.1, the best comparisons and optimised pulse trains came from compressors with lengths in the region of $3 - 5$ km. In the continuous case, the comparison between the full numerical and approximate solutions over longer lengths, that is DDF's of between 10 and 15 km, were not good. However, as these lengths probably are not practical for use in a real system, this is not of immediate concern. At the other extreme, shorter fibre compressors produced the same difficulties as their discrete counterparts. Namely, the dispersion point of the uniform fibre must be increased to ward off the generation of excessive dispersive radiation. In doing so however, the final pulse compression is compromised.

Overall, across all the comparisons presented in this chapter, a general conclusion is that discrete dispersion profiles provide better agreement between the full numerical and approximate solutions in the presence of fibre loss. The continuous compressor comparisons do get better as the compressor length is shortened; however, making the compressor too short presents its own set of problems. A possible reason for the discrepancy in the continuous compressor comparisons may be found in the phase of the two solutions. This phase difference between

the numerical and approximate solutions was discussed in Section 2.2. A small phase difference between the approximate and full numerical solutions means that when the pulse reaches the final dispersion point in the fibre, where $\beta = \beta_6$, the two solutions could be very similar, except for a phase shift. This could result in the approximate pulse being at a slightly different point in its evolution when it reaches the uniform fibre in $z > z_6$, which then results in its amplitude evolution in the uniform fibre being different to that of the full numerical solution.

Another possible factor in the difference between the full numerical and approximate solutions for the continuous dispersion compressors may be found in the analysis of the dispersive radiation. As previously discussed in Section 6.2, an asymptotic approximate (6.85) was used to the true radiation integral (6.82). Now as can be seen in Figure 6.1, there is very little change in the pulse evolution if this asymptotic approximation is used in normal, constant dispersion fibres. However the fibre compressors, particularly the continuous version, can produce significant amounts of dispersive radiation. As the integrand of the radiation integral is proportional to r, the radiation height at the edge of the shelf, large amounts of radiation will produce a large value for the radiation integral. Under these circumstances it is possible that the full radiation integral (6.82) may be necessary for an accurate description of dispersive radiation effects on pulse evolution. However, as we are examining pulse compressors producing soliton trains with large amplitudes, and so large changes of amplitude, a small space step is necessary in the solution of the approximate equations. This small space step can produce long computation times in numerically evaluating the integral (6.82) using the method outlined in Section 2.2. As a result, a parallel implementation of the code may be needed when the full radiation integral is used in the optimisation routine.

The optimisation routine could also be based on the full numerical solution of the NLS equation (6.1). This was discussed in the work of McKinnon *et al.* [34]. While an implementation of the full numerical code in the optimiser is probably unrealistic, even in a parallel implementation, it would be possible to use the approximate equations in the optimiser to refine the initial dispersion profile. This refined profile could then be used as an initial profile for the optimisation routine based on the full numerical solution of (6.1). The idea is that much of the initial work in finding a dispersion profile in the vicinity of a region of optimal dispersion could be done relatively quickly with the approximate equations. Optimisation with the full numerical solution could then be used to fine-tune and finish off the optimisation problem. With a parallel version of the optimised code this does seem possible.

Chapter 7

Conclusions

Inverse scattering theory shows that an initial pulse in a nonlinear optical fibre will evolve to a finite number of solitons, the soliton being the steady state waveform for nonlinear optical fibres. The evolution occurs in a complicated, dynamic fashion which can be seen both experimentally and in numerical solutions of the constituent equations. Due to the nonlinear stability of solitons in the face of perturbations and fibre loss, they have been proposed as the information carriers in next generation fibre optic networks. As the solitons travel the network they lose energy due to fibre loss and so this loss must be compensated for in some fashion. In addition, filtering may be necessary to reduce the harmful effects of dispersive background radiation in the system.

These fibre effects and optical devices are modelled by adding perturbing terms to the right hand side of the NLS equation (1.1). As analytical solutions for these perturbed NLS equations are not known, approximate and computational techniques are utilised to study pulse evolution in these systems. This was the subject of this thesis. Specifically, we have presented an analysis of pulse evolution in nonlinear optical fibres under the influence of fibre loss and optical devices including sliding-frequency filters, discrete amplifiers and fibre compression via dispersion-decreasing fibres. The analysis method was based upon using conserved quantities of the NLS equation to derive evolution equations for the pulse parameters. As found by Kath and Smyth [22] the choice of trial function substituted into the above conservation equations is very important. Using the same trial function (2.14) as Kath and Smyth [22] consisting of independently varying amplitude and width and a shelf of dispersive radiation in the vicinity of the pulse, evolution equations were obtained for the pulse parameters. By analysing the linearised NLS equation, expressions are obtained for the shed radiation which can then be coupled to the parameter evolution equations. These evolution equations were then solved using a fourth-order Runge-Kutta method with a numerical technique employed for the integration of the singular radia-

tion integral. These approximate solutions are then compared to full numerical solutions of the particular perturbed NLS equation. These numerical solutions were obtained using a pseudo-spectral method with exponential space-stepping in Fourier space. The agreement between the solution of the approximate equations and the full numerical solutions of the NLS equations were in general good.

7.1 Usefulness of Analysis Method

In Chapter 4 we examined the effect of fibre loss and discrete amplification on evolving pulses. As this has been extensively studied in the past it is primarily included to test the limits of the analysis technique. Doing so it was shown that radiation damping is very important for small values of fibre loss. Without the radiation damping the solution of the approximate equations was not in agreement with full numerical solutions. However adding the radiation damping gave very good agreement. For larger values of fibre loss the radiation damping became less important. This is because the large fibre loss overwhelmed most of the evolutionary dynamics in the evolving pulse including the amplitude oscillations. As such there was little difference between the approximate solutions with and without radiation damping. Adding periodic amplification proved to be problematic over long distances. This is because the amplifier would amplify the solution at periodic intervals as the pulse travelled down the fibre. Any difference between the approximate and full numerical solutions was then magnified by this amplification.

Examining sliding-frequency filters in Chapter 5 proved the usefulness of the approximate method. As the radiation is continuously amplified and filtered, the radiation plays a crucial role not only in pulse evolution, but also in the behaviour of the steady state pulse which originates from the boundary conditions. It was particularly seen in this chapter how the inclusion of the independently varying amplitude and width and the effects of dispersive radiation in the vicinity of and away from the pulse are necessary for the accurate determination of evolutionary behaviour. Decoupling the amplitude and width allowed for small variations in their inverse relationship. These oscillations are due to mass and energy being transferred between the pulse and shelf of radiation upon which the pulse sits. Without the effect of shed radiation being included in the pulse parameter evolution equations, this mass and energy, being trapped in the pulse, will oscillate between the pulse and shelf indefinitely. However including the effects of the shed radiation allows the pulse to settle to a steady soliton state as seen in full numerical solutions.

This analysis also allowed for a simpler approximation to the upper energy bound corresponding to the generation of a second soliton from the dispersive radiation. The upper bound as given by Burtsev and Kaup [6] is

$$\mathrm{Re}\,[g(k=0,z)] \leq \frac{\pi}{2} \tag{7.1}$$

where g is is the amplitude of the dispersive waves. The expression $\mathrm{Re}\,[g(k=0,z)]$ was interpreted as a correction to the area of the soliton. Hence as long as the correction never exceeded the value $\pi/2$ the soliton would not have enough mass and energy to form a second soliton. The inequality discussed in this work given by $\eta w > 1.702$, where η is the pulse amplitude and w is the width, was found from an analysis of the mass and energy of the soliton and that required to form a second. This expression is physically clearer and seems to be a more straightforward condition on stability. As discussed in Chapter 5 it has been shown from inverse scattering that for a boundary condition $u = \eta \,\mathrm{sech}\, t$, a second soliton will form for $\eta > 1.5$. This is in good agreement with the value given by the current work of $\eta > 1.702$.

The fibre compressor comparisons of Chapter 6 showed a variety of pulse behaviours. The original analysis method, utilising conservation and moment equations derived from the perturbed NLS equation (6.1), proved to be unsuccessful. This was because of the extraordinary complexity of the resulting algebra which came about from the use of elliptic functions in the trial function (6.2). However, with a fortunate change of variables, it was possible to transform the perturbed NLS equation (6.1) to the unperturbed NLS equation (6.18) of McKinnon *et al.* [34]. Hence their expressions for pulse parameter evolution, suitably transformed back to the original variables, could then be used. A variety of compressor lengths were examined ranging from 2.5 to 15 km over both discrete and continuous dispersion profiles. Using the approximate evolution equations derived from the variable transformation, it was possible to use the Nelder-Mead optimisation method to maximise pulse compression.

The comparison between the approximate evolution equations and the full numerical solutions of the NLS equation describing the system over the discrete dispersion profiles were in general good. The approximate equations correctly predicted the steady state amplitude of the pulse train and accurately mimicked the decaying amplitude oscillations. While the comparisons over the entire range of sampled lengths were good, those resulting from shorter compressor lengths produced superior quality pulse trains. Pulse trains produced over compressors of lengths 10 and 15 km produced pulse trains with large amplitude oscillations. Decreasing the compressor lengths tended to increase the agreement between nu-

merical solutions of the approximate equations and the perturbed NLS equation. Also, the resulting amplitude oscillations were reasonably small and rapidly decayed due to shed radiation, producing high quality compressed soliton trains. However shortening the compressor beyond a certain threshold was not beneficial and in fact seriously degraded the resulting pulse trains as was seen in Figure 6.6 showing a comparison over a 2.5 km discrete compressor. This appears to result from compressing the pulse train over a short distance thus producing large amounts of dispersive radiation in a small area. This dispersive radiation is built up under the soliton. While this happens in all the compressor situations, the large amounts of radiation produced in a short distance for short compressors produces extremely large amplitude oscillations. This can be partially remedied by increasing the final dispersion point β_f. However doing so means less compression in the final pulse train.

Comparisons over the continuous compressors proved more problematic. The comparison between the approximate and full numerical solutions over longer compressor lengths (10 and 15 km) show large discrepancies in the final steady state amplitude of the pulses. While these longer compressors are not necessarily physically realistic it is still cause for concern. The discrepancy in the steady state of the approximate and full numerical solutions decreased with compressor length. Decreasing the compressor length too much however (less than 3 km) caused the same difficulties as in the discrete case. Namely, large amounts of dispersive radiation interacting with the pulse caused large amplitude oscillations. One possible reason for the discrepancy may be found in the phase. The determination of the phase in the approximate equations is a higher-order effect and is not predicted by the first order analysis presented here. In the previous work with fibre loss and sliding-frequency filters this has not been a problem. However phase differences here may be more important. This is because two wave forms, identical except for a phase shift, will be increased by different amounts at the final dispersion point β_f. This would produce pulse trains with different steady state amplitudes. As discussed in Chapter 6 a more accurate determination of the phase could be determined by using the full numerical solution of the perturbed NLS equation. However, being prohibitively slow, it may be possible to use the full numerical solution at the end of the optimisation near a point of maximum compression.

Overall the work of this thesis has shown that for an accurate portrayal of pulse evolution in nonlinear optical fibres two things are necessary. Firstly, a trial solution incorporating independently varying amplitude and width. Secondly, some account of radiation in the vicinity of and away from the pulse must be

taken. Decoupling the amplitude and width, and including the effect of radiation in the vicinity of the pulse, allows for the dynamic, oscillatory behaviour seen in full numerical solutions of the NLS equation. Incorporating shed dispersive radiation away from the pulses allows for the decay of these amplitude oscillations and allows for the pulse to settle to a steady soliton. The trial solution used in this work (2.14) incorporates both of these factors.

7.2 Future Work

There are many possibilities for future work based upon the results of this thesis. An obvious possible extension would be to include analysis of higher-order effects in the NLS equation (1.1). These include effects such as higher-order linear and nonlinear dispersion and Raman gain. While the effect of these terms are negligible for solitons of width greater than 10 ps [20] they become significant over long distances or for subpicosecond solitons. As both long distance communication systems and subpicosecond solitons will figure into future fibre optic networks understanding of the effect of higher-order terms is crucial. As the higher-order terms are incorporated into the NLS equation (1.1) as small perturbations, the analysis method used in this thesis would provide an ideal means for their analysis.

A more accurate determination of the phase of the approximate equations derived via the conservation and moment equation technique is another avenue for possible future work. While phase information was not crucial for the work, the lack of it proved detrimental in the fibre compressor analysis as discussed above. As the determination of the phase is a higher order effect, the current analysis method does not determine equations for the phase. The phase of the shelf of radiation under the soliton was assumed constant initially in order to facilitate the radiation analysis. However this is not true as the phase undergoes a transient evolution to a steady state. It may be possible to more accurately recover phase information by a careful numerical study of the radiation conservation equation (2.31). This more accurate initial phase information may improve the overall phase comparison and would be particularly useful for fibre compressor analysis.

As was discussed in Chapter 6 another possible method to improve the results of the fibre compressor comparisons would be to utilise the full numerical solution in at least some of the optimisation. As an accurate determination of phase is possible with the full numerical solution this would provide the phase information necessary. However due to the long simulation times necessary for the full numerical simulation, a complete optimisation based on it would be prohibitive.

However, using the approximate evolution equations to move the dispersion profile to the vicinity of a point of maximum pulse compression would significantly reduce computational time. The optimisation could then be completed with the full numerical solution.

Bibliography

[1] Milton Abramowitz and Irene A. Stegun, editors. *Handbook of Mathematical Functions.* Dover Publications, Inc., 1972.

[2] Govind P. Agrawal. *Nonlinear Fiber Optics.* Academic Press, Inc., San Diego, 1989.

[3] D. Anderson. Variational approach to non-linear pulse-propogation in optical fibers. *Physical Review A*, 27(6):3135–3145, 1983.

[4] Jason J. Beech-Brandt and Noel F. Smyth. Pulse evolution in nonlinear optical fibers with sliding-frequency filters. *Physical Review E*, 63(5-2):056604, May 2001.

[5] V. A. Bogatyrev, M. M. Bubnov, E. M. Dianov, A. S. Kurkov, P. V. Mamyshev, A. M. Prokohorov, S. D. Rumyantsev, V. A. Semenov, S. L. Semenov, A. A. Sysoliatin, S. V. Chernikov, A. N. Guryanov, G. G. Devyatykh, and S. I. Miroshnichenko. A singe-mode fiber with chromatic dispersion varying along the length. *Journal of Lightwave Technology*, 9(5):561–566, May 1991.

[6] S. Burtsev and D. J. Kaup. Effective control of a soliton by sliding-frequency guiding filters. *Journal of the Optical Society of America B*, 14(3):627–635, March 1997.

[7] T. F. Chan and T. Kerkhoven. Fourier methods with extended stability intervals for the Korteweg-de Vries equation. *SIAM Journal on Numerical Analysis*, 22(3):441–454, 1985.

[8] S. V. Chernikov, E. M. Dianov, D. J. Richardson, and D. N. Payne. Soliton pulse compression in dispersion-decreasing fiber. *Optics Letters*, 18(7):476–478, April 1993.

[9] S. V. Chernikov and P. V. Mamyshev. Femtosecond soliton propagation in fibers with slowly decreasing dispersion. *Journal of the Optical Society of America B - Optical Physics*, 8(8):1633–1641, August 1991.

[10] S. V. Chernikov, J. R. Taylor, and R. Kashyap. Integrated all-optical fiber source of multigigahertz soliton pulse train. *Electronics Letters*, 29(20):1788–1789, September 1993.

[11] B. Fornberg and G. B. Whitham. A numerical and theoretical study of certain nonlinear wave phenomena. *Philosophical Transactions of the Royal Society of London, Series A*, 289:373–404, May 1978.

[12] Bengt Fornberg and Tobin A. Driscoll. A fast spectral algorithm for nonlinear wave equations with linear dispersion. *Journal of Computational Physics*, 155(2):456–467, November 1999.

[13] I. M. Gelfand and S. V. Fomin. *Calculus of Variations*. Prentice-Hall, Englewood Cliffs, USA, 1963.

[14] J. P. Gordon and H. A. Haus. Random walk of coherently amplified solitons in optical fiber transmission. *Optics Letters*, 11(10):665–667, October 1986.

[15] Richard Haberman. The modulated phase shift for weakly dissipated nonlinear oscillatory waves of the Korteweg-de Vries type. *Studies in Applied Mathematics*, 78(1):73–90, February 1988.

[16] Richard Haberman. Phase shift modulations for stable, oscillatory, travelling, strongly nonlinear waves. *Studies in Applied Mathematics*, 84(1):57–69, January 1991.

[17] A. Hasegawa. Amplification and reshaping of optical solitons in a glass fibre - IV: Use of the stimulated Raman process. *Optics Letters*, 8(12):650–652, 1983.

[18] A. Hasegawa and F. D. Tappert. Transmission of stationary nonlinear optical pulses in dispersive dielectric fibres. I. Anomalous dispersion. *Applied Physics Letters*, 23(1):142–144, August 1973.

[19] Akira Hasegawa. *Optical Solitons in Fibres*, volume 116 of *Springer Tracts in Modern Physics*. Springer-Verlag, Berlin, 1989.

[20] Akira Hasegawa and Yuji Kodama. *Solitons in Optical Communications*. Number 7 in Oxford series in optical and imaging sciences. Clarendon Press, Oxford, 1995.

[21] F. If, P. Berg, P. L. Christiansen, and O. Skovgaard. Split-step spectral method for nonlinear Schrödinger equation with absorbing boundaries. *Journal of Computational Physics*, 72(2):501–503, October 1987.

[22] William L. Kath and Noel F. Smyth. Soliton evolution and radiation loss for the nonlinear Schrödinger equation. *Physical Review E*, 51(2):1484–1492, February 1995.

[23] D. J. Kaup and A. C. Newell. Solitons as particles, oscillators, and in slowly changing media: A singular perturbation theory. *Proceedings of the Royal Society of London, Series A*, 361:413–446, 1978.

[24] C. T. Kelley. Detection and remediation of stagnation in the Nelder-Mead algorithm using a sufficient decrease condition. *SIAM Journal on Optimization*, 10(1):43–55, November 1999.

[25] C. T. Kelley. *Iterative Methods for Optimization.* Society for Industrial and Applied Mathematics, Philadelphia, 1999.

[26] Y. Kodama and S. Wabnitz. Analysis of soliton stability and interactions with sliding filters. *Optics Letters*, 19(3):162–164, February 1994.

[27] H. H. Kuehl. Solitons on an axially nonuniform optical fiber. *Journal of the Optical Society of America B - Optical Physics*, 5(3):709–713, March 1988.

[28] B. A. Malomed and Y. S. Kivshar. Dynamics of solitons in nearly integrable systems. *Reviews of Modern Physics*, 61(4):763–915, October 1989.

[29] Boris A. Malomed and Richard S. Tasgal. Matching intrapulse self-frequency shift to sliding-frequency filters for transmission of narrow solitons. *Journal of the Optical Society of America B*, 15(1):162–170, January 1998.

[30] P. V. Mamyshev and S. V. Chernikov. Ultrashort pulse propagation in optical fibers. *Optics Letters*, 15(19):1076–1078, October 1990.

[31] P. V. Mamyshev, S. V. Chernikov, and E. M. Dianov. Generation of fundamental soliton trains for high-bit-rate optical fiber communication lines. *IEEE Journal of Quantum Electronics*, 27(10):2347–2355, October 1991.

[32] P. V. Mamyshev and L. F. Mollenauer. Stability of soliton propagation with sliding-frequency guiding filters. *Optics Letters*, 19(24):2083–2085, December 1994.

[33] K. I. M. McKinnon. Convergence of the Nelder-Mead simplex method to a nonstationary point. *SIAM Journal on Optimization*, 9(1):148–158, December 1998.

[34] Ken I. M. McKinnon, Noel F. Smyth, and Annette L. Worthy. Optimization of soliton amplitude in dispersion-decreasing nonlinear optical fibers. *Journal of the Optical Society of America B*, 16(3):441–447, March 1999.

[35] R. J. Mears, L. Reekie, I. M. Jauncey, and D. N. Payne. Low noise Erbium-doped fibre amplifer operating at 1.54μm. *Electronics Letters*, 23(19):1026–1028, September 1987.

[36] A. Mecozzi, J. D. Moores, H. A. Haus, and Y. Lai. Soliton transmission control. *Optics Letters*, 16(23):1841–1843, 1991.

[37] Micheal J. Miksis and L. Ting. A numerical method for long time solutions of integro-differential systems in multiphase flow. *Computers & Fluids*, 16(3):327–340, 1988.

[38] Paul A. Milewski and Esteban G. Tabak. A pseudospecral procedure for the solution of nonlinear wave equations with examples from free-surface flows. *SIAM Journal on Scientific Computing*, 21(3):1102–1114, December 1999.

[39] L. F. Mollenauer. Solitons in optical fibres and the soliton laser. *Philosophical Transactions of the Royal Society of London Series A-Mathematical, Physical and Engineering Sciences*, 315(1533):437–450, 1985.

[40] L. F. Mollenauer and D. M. Bloom. Colour-centre laser generates picosecond pulses and several watts cw over the 1.24–1.45μm range. *Optics Letters*, 4(8):247–249, August 1979.

[41] L. F. Mollenauer, J. P. Gordon, and S. G. Evangelides. The sliding-frequency guiding filter: An improved form of soliton jitter control. *Optics Letters*, 17(22):1575–1577, November 1992.

[42] L. F. Mollenauer and K. Smith. Demonstration of soliton transmission over more than 4000 km in fiber with loss periodically compensated by Raman gain. *Optics Letters*, 13(8):675–677, August 1988.

[43] L. F. Mollenauer, R. H. Stolen, and J. P. Gordon. Experimental observation of picosecond pulse narrowing and solitons in optical fibres. *Physical Review Letters*, 45(13):1095–1098, September 1980.

[44] L. F. Mollenauer, R. H. Stolen, and M. N. Islam. Experimental demonstration of soliton propagation in long fibers: Loss compensated by Raman gain. *Optics Letters*, 10(5):229–231, 1985.

[45] M. Nakazawa, K. Suzuki, and Y. Kimura. 20-GHz soliton amplification and transmission with Er^{3+}-doped fibre repeater pumped by GaInAsP laser diode. *Optics Letters*, 14(19):1065–1067, October 1989.

[46] J. A. Nelder and R. Mead. A simplex method for function optimization. *Computer Journal*, 7:308–313, 1965.

[47] Alan C. Newell. *Solitons in Mathematics and Physics.* Number 48 in CBMS-NSF Regional Conference Series in Applied Mathematics. Society for Industrial and Applied Mathematics, Philadelphia, 1985.

[48] Alan C. Newell and Jerome V. Moloney. *Nonlinear Optics.* Addison-Wesley Publishing Company, Redwood City, California, 1992.

[49] William H. Press, Saul A. Teukolsky, William T. Vetterling, and Brain P. Flannery. *Numerical Recipes in FORTRAN: The Art of Scientific Computing.* Cambridge University Press, Cambridge, second edition, 1992.

[50] Junkichi Satsuma and Nobuo Yajima. Initial value problems of one-dimensional self-modulation of nonlinear waves in dispersive media. *Supplement of the Progress of Theoretical Physics*, 55:284–306, 1974.

[51] Noel F. Smyth and William L. Kath. Radiative losses due to pulse interactions in birefringent nonlinear optical fibers. *Physical Review E*, 63(3-2):036614, March 2001.

[52] Noel F. Smyth and Adrian H. Pincombe. Effect of radiative loss on pulses in periodically inhomogenous birefringent optical fibers. *Physical Review E*, 57(6):7231–7238, June 1998.

[53] Noel F. Smyth and Annette L. Worthy. Dispersive radiation and nonlinear twin-core fibers. *Journal of the Optical Society of America B*, 14(10):2610–2617, October 1997.

[54] E. A. Swanson and S. R. Chinn. 40-GHz pulse train generation using soliton compression of a Mach-Zehnder modulator output. *IEEE Photonics Technology Letters*, 7(1):114–116, January 1995.

[55] G. R. Walsh. *Methods of Optimization.* John Wiley & Sons Ltd., New York, 1975.

[56] G. B. Whitham. *Linear and Nonlinear Waves.* John Wiley & Sons, Inc., New York, 1999.

[57] V. E. Zakharov and A. B. Shabat. Exact theory of two-dimensional self-focusing and one-dimensional self-modulation of waves in nonlinear media. *Soviet Physics JETP*, 34:62–69, 1972.